

AD611406



NOLTR 63-264

A STUDY OF THE WATER-ENTRY CAVITY

COPY	2	OF	3	<i>vmc</i>
HARD COPY	\$ . 3. 00			
MICROFICHE	\$ . 0. 75			

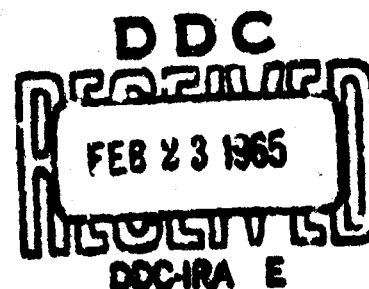
*75-p*

NOL

4 DECEMBER 1963

UNITED STATES NAVAL ORDNANCE LABORATORY, WHITE OAK, MARYLAND

NOLTR 63-264



ARCHIVE COPY

---

## NOTICE

Requests for additional copies by Agencies of the Department of Defense, their contractors, and other Government agencies should be directed to:

Defense Documentation Center (DDC)  
Cameron Station  
Alexandria, Virginia

Department of Defense contractors who have established DDC services or have their 'need-to-know' certified by the cognizant military agency of their project or contract should also request copies from DDC.

All other persons and organizations should apply to:

U. S. Department of Commerce  
Office of Technical Services  
Washington 25, D. C.

---

UNCLASSIFIED  
NOLTR 63-264

Ballistics Research Report 121

A STUDY OF THE WATER-ENTRY CAVITY

Prepared by:  
Albert May and William R. Hoover

ABSTRACT: For missiles producing clean cavities after water entry the cavity development is shown by theory to depend significantly only on: entry angle, an effective mass, and a Froude number based on the nose-flat diameter. A method is outlined for estimating pressures in closed, almost-steady cavities, from cavity geometry.

Data from application of these methods to water-entry records of models are given. Influence of effective mass was small. The pressures in steady cavities were estimated as 0.5 to 1.3 atmospheres.

PUBLISHED MARCH 1965

U. S. NAVAL ORDNANCE LABORATORY  
WHITE OAK, MARYLAND

NOLTR 63-264

4 December 1963

A STUDY OF THE WATER-ENTRY CAVITY

This report has been compiled under the authorization of WEPTASK RRRE-04-022-002.

The report is for information only and is not to be used as a basis for action.

Several persons made major contributions to this research. The authors wish especially to express their appreciation to Mr. Jacob Berezow for carrying out a large part of the data reduction, and to Mr. John L. Baldwin who conducted the water-entry model program from which most of the experimental data were obtained.

R. E. ODENING  
Captain, USN  
Commander

*A E Seigel*  
A. E. SEIGEL  
By direction

# NOLTR 63-264

## CONTENTS

	Page
LIST OF ILLUSTRATIONS. . . . .	1v
LIST OF SYMBOLS. . . . .	v
Chapter 1: DEVELOPMENT OF TECHNIQUES FOR CAVITY STUDY	
FIRST ANALYSIS METHOD: A CORRELATION TECHNIQUE. . . .	1
Introduction. . . . .	1
Non-Dimensional Parameters and Equations. . . . .	3
SECOND ANALYSIS METHOD: CAVITY-PRESSURE ESTIMATION. .	5
Chapter 2: APPLICATION OF THE TECHNIQUES. . . . .	7
Data Reduction. . . . .	8
Discussion of Cavity Behavior . . . . .	10
Cavity Collapse. . . . .	12
The Universal Curves . . . . .	13
Analysis of Cavity Dimensions and Events. . . . .	14
Maximum Cavity Diameter. . . . .	15
Time of Pullaway . . . . .	15
Cavity Length. . . . .	17
Cavity Volume. . . . .	17
Cavity Collapse. . . . .	18
The Detached Bubble. . . . .	19
Cavity Pressure. . . . .	21
Recapitulation and Conclusions. . . . .	22
REFERENCES . . . . .	24
Table 1. . . . .	25

ILLUSTRATIONS

Figure	Title
1	Water Entry of Right Cylinder
2	Cavity with "Almost Steady" Flow
3	Variation of Dimensions of Steady Cavity with Cavitation Number
4	Experimental Parameters of Available Water-Entry Tests
5	Gun Mount
6	Arrangement of Cameras and Lights
7	Photographs of Water-Entry Cavity
8	Dependence of Cavity Development on Conditions of Test
9	Cavity Development - Round 124
10	Cavity Development - Round 131
11	Cavity Development - Round 142
12	Cavity Development - Rounds 159 and 169
13	Cavity Development - Rounds 172 and 180
14	Cavity Development - Rounds 186 and 187
15	Cavity Development - Rounds 189 and 190
16	Cavity Development - Rounds 205 and 228
17	Type of Cavity Collapse
18	The "Universal" S/M versus T/M Graph
19	The "Universal" V versus T/M Graph
20	Contours of Maximum Cavity Diameter
21	Variation of Cavity Diameter after Entry (M=11)
22	Variation of Cavity Diameter after Entry (M=69)
23	Contours of Time of Pullaway of Cavity from Water Surface
24	Contours of Maximum Cavity Length
25	Variation of Cavity Length after Entry (M=11)
26	Variation of Cavity Length after Entry (M=69)
27	Contours of Maximum Cavity Volume
28	Variation of Cavity Volume after Entry (M=11)
29	Variation of Cavity Volume after Entry (M=69)
30	Contours of Time after Entry when Cavity Length is Half the Distance Traveled
31	Contours of Cavity Length which is Half the Distance Traveled
32	Sketches from Round 208
33	Sketches from Round 158
34	Sketches from Round 156
35	Sketches from Round 148
36	Sketches from Round 91
37	Sketches from Round 193
38	Sketches from Round 94
39	Maximum-Volume Contours for Detached Bubble
40	Pressure Contours for "Almost Steady" Cavities

NOLTR 63-264

LIST OF SYMBOLS

- A =  $\pi/10\alpha$  (capital alpha)
- $C_D$  drag coefficient of missile (usually while generating a cavity) based on maximum body diameter, D
- d diameter of missile-nose truncation (actual or equivalent)
- D maximum body diameter of missile
- $D_M$  maximum cavity diameter
- F Froude number based on truncation diameter;  $F = v_0 / (gd)^{1/2}$
- g acceleration of gravity
- L cavity length
- m mass of missile
- M "effective mass";  $M = m/d^3 \rho$
- $p_0$  ambient pressure at missile depth
- $p_c$  pressure in cavity
- s path length measured from water impact
- S dimensionless path length;  $S = s/d$
- t time from water impact
- T dimensionless time;  $T = tv_0/d$
- v instantaneous speed of missile
- $v_0$  missile speed at water impact
- V dimensionless missile speed;  $V = v/v_0$
- $\alpha$  retardation coefficient;  $\alpha = -(dv/dt)/v^2 = \pi \rho C_D D^2 / 8m$
- $\theta_0$  water-entry angle, measured from horizontal
- $\rho$  mass density of water
- $\sigma$  cavitation number;  $\sigma = \frac{p_0 - p_c}{\frac{1}{2} \rho v^2}$

## Chapter 1

### DEVELOPMENT OF TECHNIQUES FOR CAVITY STUDY FIRST ANALYSIS METHOD: A CORRELATION TECHNIQUE

#### INTRODUCTION

The behavior of a missile when it enters water from air is strongly influenced by the development of an air-filled cavity about it (ref. (1) and (2)), which subjects the missile to a series of changing environments. These environments can be predicted only if detailed information is available concerning the cavity configuration and history.

The general features of cavity development may be summarized as follows. The cavity is generated by a lateral displacement of the water by the nose of the missile, and air rushes in behind to fill it. Later the cavity closes off at the water surface while it is still growing, and the pressure in the cavity tends to decrease. The cavity then moves away from the water surface, portions of it may be separated off by "closures" or "seals," and the part of the cavity attached to the missile suffers a continuing attrition.

In general, the cavity development may be expected to depend on the nose shape of the missile. This development could be studied experimentally for any particular nose configuration, but unfortunately an infinity of shapes is possible. The simplification of this problem is the purpose of the present correlation technique. This correlation had its origin in the observation that missiles designed for water entry are generally truncated by a plane perpendicular to the axis of the missile. Because of this "nose-flat," the flow which forms the cavity wall leaves the nose of the missile abruptly, and this flow pattern is generally conducive to the generation of a well-formed cavity and to a stable behavior.

The present study will be restricted to water entries which are accompanied by well-formed cavities. It will be assumed that the trajectory is reasonably straight and that the cavity is large enough to envelop the missile completely. The missile must not tumble, but its afterbody may have occasional contacts with the cavity wall if these contacts are not too violent.

The purpose of the present report is to describe a method for systematizing the treatment of cavity growth so that all missiles can be regarded as belonging to a single

family, no matter what the nose shape may be, provided that the entry is well-behaved and a clean cavity is produced. Parts of this method were described in reference (3).

The right cylinder will be taken as the basic configuration of the correlation technique. Figure 1 shows that the cavity flow about a right cylinder does not wet any portion of such a missile appreciably except the flat portion of the nose during the "cavity running" following water entry. Evidently the flow from such a nose is not influenced by the after-shape of the missile, but only by the size of the nose truncation, and the speed, mass, and entry angle of the missile. A similar statement may be made concerning missiles with smaller nose flats if there is no appreciable wetting of the rest of the nose.

Many missiles which generate clean cavities at water entry have much more wetting of the nose than is assumed above. This is true of spherical and ogival noses, for example, and also of truncated noses which have flats which are too small to produce a completely detached flow. All such missiles may be treated in the same way as the right cylinder by ascribing to each an "equivalent nose-flat diameter." The equivalence is based on the observation (experimentally verified in reference (1)) that missiles with the same mass and speed, and the same drag force, generate cavities which are reasonably identical in shape (except, perhaps, very near the nose). Accordingly, a missile with ogival nose will be regarded as equivalent to a right cylinder (or a missile with some other sufficiently truncated nose) of equal mass, and with the same drag force at the same speed. A sphere which has a cavity drag coefficient of 0.3 is equivalent to a right cylinder ( $C_D=0.8$ ) of the same mass, whose cross-sectional area is three-eighths that of the sphere.

Noses whose truncations are too small to prevent wetting of the rest of the nose will have some increase in drag coefficient due to this wetting. If this increase is appreciable, such noses should be equated to right cylinders (or adequately truncated noses) with the same drag force.

In general, a water entry may be influenced by many parameters such as Froude number, Reynolds number, Mach number, missile mass, entry angle, transverse moment of inertia, and the position of the center of gravity. We shall assume that only three dimensionless parameters have a significant effect on the behavior of the missile or on the shape of the cavity during its formation. These are:

a. "Effective mass" =  $M = m/\rho d^3$

b. Froude number =  $F = v_o / (gd)^{\frac{1}{2}}$

c. Entry angle =  $\theta_o$ .

Both the effective mass and the Froude number are related to the diameter of the nose-flat (real or equivalent) since this is the only length of significance during the impact phase. The effective mass is the ratio of the missile's mass to the mass of a cube of water whose edge is the diameter of the flat.

Many considerations determine and limit the validity of the assumption that only these parameters are significant.

a. Mach number in air will affect the cavity pressure at high entry speeds. Later cavity pressures, however, will depend principally on the conditions which exist when the cavity closes at the water surface, and at the time of surface closure the missile speed will have dropped far below the entry speed.

b. Reynolds number has not been found to have appreciable importance for cavity formation.

c. Change of the gas pressure above the water without a density change (as required by the scaling laws) has been shown experimentally (ref. (1) and (2)) to have small effect on cavity behavior, although the effect on whip may be relatively large (ref. (4)).

d. Moment of inertia and center-of-gravity position need not be regarded explicitly if it is assumed that the missile behaves stably at water entry.

e. The neglecting of accidental angles of pitch and yaw which the model may have at water impact, and the corresponding angular velocities, is also largely justified by our limitation to trajectories for which the behavior is reasonably stable.

#### NON-DIMENSIONAL PARAMETERS AND EQUATIONS

Because  $C_D=0.8$  for a right cylinder during cavity generation, we shall assume that

$$C_D = 0.8d^2/v^2 \quad (1)$$

for a truncated body with nose-flat diameter  $d$ , if the flow separates cleanly.

Missile speed, time, and path length may be non-dimensionalized:

$$V = v/v_0; \quad T = tv_0/d; \quad S = s/d \quad (2)$$

Here, unit length is taken as the truncation diameter, unit time is the time  $(d/v_0)$  required for the missile to travel a distance equal to the truncation diameter at the entry speed, and unit speed is the speed at entry. By use of the non-dimensionalized quantities of equation (2), the equations of motion

$$v = v_0 e^{-\alpha s}; \quad 1/v = 1/v_0 + \alpha t; \quad \text{and} \quad \alpha s = \ln(v_0 \alpha t + 1), \quad (3)$$

which apply to a missile acted on by only a drag force, can be written in the form

$$1/V = 1 + AT = e^{AS} \quad (4)$$

where  $A = \pi/10 M$ , so that  $AT$  and  $AS$  are respectively proportional to  $T/M$  and  $S/M$ .

It will be seen that the equations (4) are "universal equations" in the sense that each of the three can be represented by a single graph of  $V$  versus  $S/M$ ,  $V$  versus  $T/M$ , or  $S/M$  versus  $T/M$ . Each should be applicable to missiles entering water with any values of the experimental parameters within the overall limitations of this study. Deviations will be observed when the effect of transverse forces and gravity become significant, or when  $C_D$  changes. It is easily seen that two right cylinders of different diameters will have the same accelerations after water entry if their Froude numbers and effective masses are the same, with the acceleration in ordinary units or in the non-dimensional units of equation (2). Missiles with other nose shapes may be compared similarly if their values of  $P$  and  $M$  are based on "equivalent nose-flat diameters" derived from their drag coefficients.

## SECOND ANALYSIS METHOD: CAVITY-PRESSURE ESTIMATION

Very little has been published concerning the pressure in the water-entry cavity, although one measurement was reported in reference 5, and the general features of the pressure changes to be expected have been discussed (ref. (1)).

Some time after water entry, when the cavity length has decreased to, perhaps, twice the missile length, high-speed motion pictures frequently show that the missile travels for a short distance in an ellipsoidal cavity which has the appearance of a rigid ellipsoidal missile moving through the water. Such a cavity is shown in figure 2. Although this "almost-steady" motion persists for a short time only, the cavity is unmistakably similar to the vented cavities which have been studied in the water tunnel. It appears probable that the flow at this time will approximate the flow about an obstacle in the water tunnel, and this should make it possible to estimate the pressure in the cavity.

Reichardt (ref. (6)) studied the shapes of cavities produced in the water tunnel behind disks when air was fed into the cavity to reduce the cavitation number. This investigation was later extended by Rouse and McNown (ref. (7)) and by Eisenberg and Pond (ref. (8)). They found that the ratio of maximum cavity diameter to disk diameter and the ratio of cavity length (twice the distance from the disk to the maximum diameter) to disk diameter, are uniquely related to the cavitation number.

Figure 3 shows the variation with cavitation number,  $\sigma$ , of the non-dimensionalized maximum diameter and length of the cavity ( $D_M/d$  and  $L/d$ ), where  $d$  is the disk diameter. The measurement of one of these quantities for an "almost-steady" cavity permits the evaluation of

$$\sigma = \frac{P_0 - P_c}{\frac{1}{2} \rho v^2} \quad (4)$$

by use of figure 3. The pressure in the cavity,  $p_c$ , is easily found since all other quantities in equation (4) are available. If both the length and diameter of the cavity are known, two determinations of the pressure are possible. If the two values agree well, the cavity is presumably of the proper shape and is suited to the evaluation of  $\sigma$ .

Experimental values of  $\sigma$  (discussed in Chapter 2) were actually obtained from the volume of the cavity. The reason for this and the method are as follows. If different values

of  $\sigma$  are obtained from measured values of  $D_M/d$  and  $L/d$ , one can get a mean value in various ways. If the cavity is longer and thinner or shorter and fatter than the steady-state cavity, it seems probable that the cavity volume would be more nearly invariant with time than the linear cavity dimensions. It was assumed that the cavity is a prolate ellipsoid and values of volume, calculated from the data of references (6), (7), and (8) are plotted in figure 3. For ease of calculation the volume is expressed as  $D_M^2 L/d^3$ . This value times  $\pi/6 = 0.5236$  gives the value which would be obtained from an expression of the form  $\frac{4}{3} \pi a b^2$ .

Based on the comparison of almost-steady entry cavities with those observed in the water tunnel, some general deductions can be made relating to the pressures to be expected in small closed cavities. It should be noted first that cavities with  $\sigma > 0.2$  can hardly be of interest, since their lengths (Fig. 3) would be less than 6.5 times the diameter of the nose flat.

Near the water surface a missile must be traveling at about 100 feet per second to generate a cavity with  $\sigma = 0.2$  if it contains only water vapor. The speed required would increase as the square root either of the ambient pressure or of  $1/\sigma$ . At a depth of 34 feet a missile traveling at 100 feet per second could generate a cavity with  $\sigma = 0.2$  only if the pressure in the cavity were one atmosphere.

## Chapter 2

## APPLICATION OF THE TECHNIQUES

The correlation technique described in Chapter 1 has been applied to high-speed motion pictures which were obtained during an earlier water-entry model program in support of missile development. Records were available from about 200 water entries, but, for various reasons, many of the rounds were not suitable for this analysis. Only 59 rounds were given a complete analysis, although some data are included from many other rounds.

Nearly all of the models used had truncated noses with flats ranging from 0.275 to 1.00 times the full missile diameter. Behind the truncation, in many cases, was a conical or ogival surface, and sometimes the flow wetted this surface slightly.

Most of the models had body diameters of 1.570 inches and were not provided with fins. Accordingly, they were not hydrodynamically stable but all of the rounds included in the study had reasonably straight trajectories and had a pseudo-stability, usually because of guidance by the cavity wall, at least during the portion of the trajectory analyzed. Eight of the entries were of models with body diameters of approximately 1 inch and with cruciform fins. Data for the 59 rounds which were given a complete analysis are listed in Table 1. Entry speeds for these rounds ranged from 321 to 1600 feet per second and the angles of entry were between 45 and 70 degrees from the horizontal. Figure 4 is a plot on Froude number ( $F$ ) versus effective mass ( $M$ ) coordinates, indicating the values of  $F$  and  $M$  for each of the completely analyzed rounds by an encircled point, and for the other rounds used, by a simple point.

A large amount of information was presented for spheres in reference (1). Some of the data obtained in that study will be compared with the present analysis although the entry angle was  $90^\circ$  (vertical) instead of the 45 to 70 degrees of the present study. The effective mass of a sphere is  $M=2.280k$ , where  $k$  is the specific gravity. It does not depend on the diameter of the sphere. For a steel sphere  $M=17.7$  approximately.

The photographic records used in the present analysis were obtained from Fairchild high-speed cameras operating at speeds between about 2100 and 6800 frames per second. The

models were launched from a 40-mm smooth-bore powder gun into the Undersea Weapons Tank at NOL. This tank is a vertical cylinder, 100 feet deep and 50 feet in diameter. The adjustable gun mount is shown in figure 5.

Photographic lights and cameras were mounted on parallel triangular trusses as shown in figure 6. The truss in the foreground carried the two cameras in waterproof housings. The other truss supported the lights. These were unprotected incandescent bulbs designed for underwater use only. In front of the lights was a nylon diffusing screen. Elastic ropes were tightly stretched, one or two feet apart along the line of fire, to serve as a reference grid. The trusses pivoted about a common axis which was the same as that of the gun mount, and were fastened together at their further ends. In operation the gun was adjusted to the desired entry angle, and the trusses were oriented so that the line of fire was approximately along the center of the truss system and grid network.

Enlargements of sample frames from the high-speed photographs taken with the "first" and "second" cameras are shown in figure 7. The first camera gave a record of approximately the first ten feet of the trajectory after water entry. The second camera included a section of the trajectory about 13 to 23 feet from the entry point.

#### DATA REDUCTION

The use of automatic film-reading equipment was found unsatisfactory because of variations, from frame to frame, in the position of the image on the film area.

Time calibration of the frames was obtained from 1000-cycle timing marks printed on the film. Frames from the motion pictures were projected onto white paper; the nose positions were marked on the paper and the frame numbers were recorded, starting at water entry. The distances of the nose along the trajectory were then entered on punched cards and the distance-time data were machine-fitted to the cubic  $t = as^3 + bs^2 + cs + d$  for each camera separately. During this operation the machine printed out the horizontal and vertical coordinates of the nose position, its distance along the trajectory, the time, the speed, the acceleration, and the frame number. The accuracy of the position-time data was not adequate to permit satisfactory determinations of the drag coefficient.

Graphs of the position-time data were next plotted separately for the two cameras, and the two graphs were then "fitted." The fitting consisted in the determination of the time interval between the two camera records, since the timing marks on the two films were not synchronized and the position data did not overlap. The two graphs were so positioned by trial that they could be faired together by adding an intermediate curve. To improve the accuracy of this operation three determinations were made by fitting separately, graphs of distance, speed, and reciprocal speed, and comparing the time intervals resulting.

Before the adoption of the technique just described, several other methods were attempted, using other fitting equations, and fitting the data from both cameras to one equation. These methods were abandoned because of the poor quality of the fit obtained.

After the overall relation between distance and time was available, the distance-time curve was drawn to large scale on cross-section paper. Several frames in turn were then projected and traced on the paper containing the distance-time graph. The magnification was adjusted to agree with the distance scale on the plot, and the center line of the cavity was located at the proper time position. A graph was then drawn of the position of the upper or base end of the cavity. Figures 8 to 16 are samples of the sketches just described. Usually many more outlines were drawn than are shown on the sketches included in this report. In addition to the omission of some outlines to avoid confusion, some of the cavity outlines were modified slightly in one respect. It must be remembered that all of the entries were oblique. The angle between the cavity axis and the surface was approximately the entry angle, and the base of the cavity was oblique until the cavity had pulled away from the surface. Because the variation of entry angle has been disregarded, some of the cavity bases have been drawn as though the cavities had circular symmetry near the base.

Most cavity dimension data were obtained from the drawings just described. Cavity volume was obtained by approximating the cavity as a number of right circular cylinders.

Figure 8 is intended to show the pattern of cavity development behavior over the range of experimental parameters analyzed in the present study. It has been assumed that the cavity development can be correlated with only three parameters: the effective mass,  $M$ ; a Froude number,  $F$ ; and the angle of entry,  $\theta_0$ .

No correlation with the angle of entry was found. The angle might be expected to affect the size of the cavity by changing the time at which the surface seal occurs, and the size and collapse behavior through the different hydrostatic pressure due to depth at various angles. Undoubtedly, small effects of angle were present in the data analyzed, and large effects would be expected under some conditions of large angle variation. No intensive search for effects of angle were made.

In the sketches of figures 9 to 16 the upper graphs give the position of the nose of the missile; the ordinate being the distance traveled from water impact. This traveling was oblique to the water surface. Although the abscissa serves as a reference line for measurement of the distances after entry, the distances given are not those from the water surface because of the obliquity. When the water surface is drawn in, it is shown separately for each cavity outline as an oblique line closing the rear end of the cavity and making an angle with the abscissa. Some of the cavity outlines have been squared off at the water surface.

The lower curve on each of the contour graphs shows the position of the base of the cavity. This lower end of the cavity in the drawings is the upper end in the actual water entry. The vertical distance between the upper and lower curves gives the cavity length.

#### DISCUSSION OF CAVITY BEHAVIOR

Figure 8 is set up on F-M coordinate axes with plots for 13 rounds positioned at approximately the F and M values of each water entry. Figures 9 to 16 present the same graphs in larger size.

Some comments will be made in this section of the trends which can be observed on figure 8 but explanations of these trends will generally be reserved until later when contour plots and graphs of cavity data will be discussed.

The lowest values of M on figure 8 ( $M=11$ ) are given by the three rounds at the left of the figure. A small value of M means, of course, that the missile had small mass for a given nose-flat diameter. These rounds with  $M=11$  were right cylinders. All had the same low mass and rapid deceleration and they behaved similarly. Each cavity grew carrot-shaped and closed at the water surface, and shortly thereafter a deep closure or deep seal occurred. Just before or after this seal, the cavity pulled away slightly from the surface.

These deep closures, which occurred at points, will be called "point closures" in this report. They represent a cavity collapse caused by the hydrostatic pressure due to depth outside the cavity and a lowered pressure within the cavity because of the cavity expansion following surface closure. As the Froude number increases (higher speed), deep closure and pullaway from the surface are later, and the cavities become fatter. The upper (nose position) curves of the three rounds shown with  $M=11$  are almost identical, as is predicted by equation (4). This means that the non-dimensional distances traveled were identical. The actual distances were also the same because the unit length (the nose-flat diameter) was the same, but trajectory points were not reached at the same times. At higher Froude numbers, the time unit is smaller, giving smaller actual time intervals. This is due, of course, to the higher speeds of travel.

Each column ( $M=\text{constant}$ ) in figure 8 also contains identical distance-time (upper) graphs for the missile nose. As  $M$  increases, the curves become higher because of the smaller deceleration.

There is a discontinuity in the cavity length when deep closure occurs, because cavity length is interpreted to mean the length of the cavity attached to the missile. At a point closure the length decreases from the full cavity length to the length which remains attached.

If we proceed from the lower left-hand corner of figure 8 in the direction of increasing  $M$ , greater changes of behavior are observed. The point closure which was observed for Round 169 ( $M=11$ ,  $F=290$ ) does not occur with Round 190 ( $M=69$ ,  $F=211$ ). In the former round the cavity remained intact until the point closure occurred and then was divided into two portions. In Round 190 the base of the cavity, after pulling away slowly from the water surface, travels quite rapidly toward the missile. During this motion, no large bubbles are broken off and left in the wake. The cavity remains almost intact. There is some entrainment of air in the wake because of the instability of the flow at the base of the cavity but this leaves only a trail of very small bubbles.

Such behavior will be called a "base closure" in this report, even though no actual closure occurs, to distinguish it from other modes of cavity collapse. The change from point to base closure may be thought of as a displacement of the point closure back to the rear end of the cavity where it appears only as an acceleration of the base. Figure 8 shows that the same change from point to base closure occurs at higher  $F$  values, when we go from  $M=11$  to  $M=69$ .

Near  $M=69$ , as we go to still higher values of  $F$ , other changes occur. At the highest Froude number (Round 131) there is a point closure. At intermediate values of  $F$  another significant change occurs. During the base closure of Round 190 the cavity shortens but maintains a cigar-like shape. In Round 189 ( $F=444$ ), on the other hand, the cavity becomes very thin near the base and the closure is from the sides rather than from the base. There are other rounds in which a rather long section of the cavity (not necessarily at the base), collapses to a line almost at the same instant. These collapses will be called "line closures" in this report. Other striking examples of these closures will be given in figures 36 and 38, and it will be shown that these are the most violent of all observed cavity collapses.

The rounds with  $M$  values near 100 behave similarly to those just discussed. Those at  $M=125$  do also, and Round 142 has a very striking line closure.

Cavity Collapse. The type of cavity collapse is shown for various values of  $F$  and  $M$  on figure 17. Each point plotted on the figure represents a separate water entry, and the points are so placed on  $F$  versus  $M$  coordinate axes as to indicate the values of these quantities for each round. Point closures and base closures are shown by dots and circles, respectively. Line closures are indicated by crosses. The cross is drawn in a circle to indicate that the line closure is at the base of the cavity. A simple cross indicates that the closure would have been judged a point closure if it had occurred at a point and not along a line. The cavities indicated as having line closures were so judged because the observer felt that "the closure was almost simultaneous along a considerable portion of the cavity." An attempt was made to reduce the subjectivity of this evaluation by using a quantitative criterion, but this was not successful and was abandoned. The dashed line on figure 17 roughly divides the area into regions of point closures and base closures.

It will be seen that point closures occur predominantly in the "northwest" portion of the plot, and base closures in the "southeast" portion. This is in agreement with the observations made earlier regarding figure 8. It is not easy to explain why this collapse pattern is obtained, because of the large number of opposing influences. Collapse at a cross section of the cavity is favored by increased depth, and by lower missile speed at the point considered. Decreased pressure in the cavity due to increased speed of the inflowing air and, especially, to growth of the cavity after surface

closure, has roughly the same collapsing effect over all of the cavity. It appears probable that point closures at small values of  $M$  are due to the rapid deceleration with consequent small cavity-generating power for later portions of the trajectory. Point closures at higher  $F$  may be explained by the following argument. Consider two water entries, identical except for entry speed, and assume that the effect of gravity on the trajectories can be neglected. The speeds at two points (fixed in space) along the trajectories will have the same ratio for the two launchings if the drag coefficient is the same. Assume that the collapse time of a cavity cross section is proportional to the maximum radius, as it is approximately for a vapor-filled spherical cavity (ref. (9)), and that the maximum radius is approximately proportional to the missile speed (ref. (1)) at the time of generation. In going between the two trajectory points the higher-speed entry will suffer the greater absolute change of speed and accordingly the collapse time will decrease more. This tends to move the closure position forward for the higher-speed entry, as is observed.

The model tests under analysis were lighted by special incandescent bulbs immersed in the water. In a number of these tests, one to eight of the bulbs broke while the model was in flight. The motion pictures show that the breakage occurred immediately after cavity collapse, and generally after line closures. (Pressure measurements in the water have recently shown that maximum pressure occurs at cavity collapse.) Instances of lamp breakage are indicated in figure 17 by darker symbols. It will be seen that these are grouped about the region of line closure. This indicates that a pressure wave of maximum destructive effect, for a given missile shape, occurred at intermediate entry speeds rather than at the highest speeds where it might be expected.

In the vertical entries of steel spheres reported in reference (1), point closures always occurred except with  $\frac{1}{4}$ -inch spheres at low entry speeds, where the collapses were nearly base closures. As was mentioned earlier, the effective mass of a sphere is independent of its diameter and equals 2.28 times the specific gravity. For steel spheres  $M=17.7$ , and  $F$  was less than 100 for the entries of reference (1). No data from the present study contribute to the region below  $F=100$ , but the sphere data appear consistent with figure 17.

The Universal Curves. On figures 18 and 19 are plotted the universal curves of equation (4) for  $S/M$  versus  $T/M$  and  $V$  versus  $T/M$ . The lighter lines give the experimental values for the thirteen rounds of figure 8. The rather large

scatter is not caused by invalidity of the basic assumptions but principally by failure to correct the data completely. The rounds whose curves lie below the universal graphs had nose-flats which were 0.45 times the missile diameter. The use of equation (4) in plotting the universal graphs assumes sharp separation of the flow from the nose flat, and this is inherent in equation (1). Water entries of models with nose flat 0.45 times the body diameter showed some wetting of the nose behind the flat. The result of this is an increase of the drag coefficient. An increase of 11 percent in  $C_D$  would be enough to remove most of the scatter shown for these rounds, and such an increase is entirely reasonable. Strictly, in the present analysis, the effective nose-flat diameter should have been based on actual drag coefficients as already described. Measured drag coefficients were not available and the effect on cavity development is quite small. The data for Round 169 (fig. 8) lie well above both universal curves and are undoubtedly in error.

The curves of figures 18 and 19, in addition to furnishing obvious information relating the values of  $S$ ,  $T$ , and  $V$ , serve also in facilitating changes of variables. For example, data will be given in figures 25 and 26 to show the dependence of cavity length on the distance the missile has traveled. The corresponding relation between cavity length and time is easily obtained by use of the relation in figure 18.

#### ANALYSIS OF CAVITY DIMENSIONS AND EVENTS

In addition to qualitative studies such as those already described, quantitative analyses were made of a number of dimensions, times, and other quantities which help to define the cavity behavior. Some of these are of obvious importance in cavity analysis; others may have no apparent use. Some of the latter quantities were analyzed because the results were needed to facilitate other parts of the study. They have been included because of possible utility.

Two types of curves will be given. One type is the familiar presentation of the variation of a quantity, such as the length of the cavity, as a function of time or distance. On the other hand, single numbers associated with each entry (such as the maximum volume attained) are presented as contours; that is, as families of lines representing constant values of the quantity on coordinate axes which are the Froude number and effective mass.

Maximum Cavity Diameter. After the water entry of a missile the cavity that is generated will, at each instant, have a maximum diameter at some cross section and figure 8 shows that this is near the water surface until after pullaway. Also, during the whole of the cavity's development, there will be some overall maximum value of this diameter and this also is found quite close to the water surface. After a section of cavity is generated at any depth and the wall is moving outward, the speed of this wall decreases because of the expansion of the geometrical flow pattern. At or near the water surface, forces other than those due to this flow have little effect until after the cavity closes at the surface.

A contour plot of overall maximum cavity diameters in dimensionless units, given in figure 20, shows that there is almost no dependence of this maximum on  $M$ . This would be expected. The maximum diameter attained at any cavity cross section will depend on the missile speed at the time this portion of cavity is generated, but the subsequent deceleration of the missile (due to smallness of  $M$ ) affects the maximum diameter only very indirectly through the effect of surface closure. From figure 20 the extreme diameter varies about as the 0.7 power of the Froude number. The contours range over diameters between 8 and 35 times the diameter of the nose flat. Dashed lines on figure 20 and other graphs are used to indicate that the lines are rough approximations only.

The variation of maximum cavity diameter with time is shown in figures 21 and 22 for  $M=11$  and  $M=69$ , respectively. The maximum diameter increases until shortly after surface closure when it shares in the general cavity contraction. At all Froude numbers given on figure 21 for  $M=11$ , a deep closure occurs. At deep closure the maximum diameters suffer a discontinuous change from the maximum near the base end (upper end) of the cavity to the lesser diameter of the portion of the cavity which remains attached to the missile. The lower ends of these discontinuous decreases were inadequately determined and are not shown on figure 21. The graphs for  $F=200$ ,  $M=11$  and  $F=550$ ,  $M=69$  have no discontinuous portions although there are deep closures, because the portion of the cavity with maximum diameter remains attached to the missile at deep closure. Rounds with  $M=69$  and with  $F$  greater than 600 will have deep closures and discontinuities in the curves for maximum diameter.

Time of Pullaway. Figure 23 is a contour plot of the "time of pullaway"; that is, the time in dimensionless units

between water impact and the apparent separation of the cavity from the water surface.

The interpretation of time plots, such as figure 23, is complicated by the variation of the time unit when  $v_0$  changes (with  $F$ ). This may be shown strikingly as follows. Consider some event which requires the same actual time for all values of  $F$  and  $M$ . Such an invariant time is "the time which elapses while a missile travels a distance numerically equal to the entry speed,  $v_0$ , with a constant speed equal to  $v_0$ ." This is, of course, one fixed time unit, say one second. If contours of this invariant time interval (as defined between the quotation marks above) were plotted on  $F$ - $M$  coordinates, these contours would be parallel to the  $M$  axis, and the contour time labels would be proportional to the  $F$ -values at the contours, if  $d$  is constant. In other words, this invariant time is proportional to  $F$  in the dimensionless time units. Accordingly, the variation of time in fixed units may be regarded as the deviation from proportionality of the time-Froude number dependence in dimensionless units.

The contour patterns of figures 20 and 23 are very similar but this is only an indication that the quantities involved depend strongly on  $F$  and only slightly on  $M$ . This behavior will be observed for a number of cavity dimensions and times.

Pullaway requires that the cavity pressure be below atmospheric. Surface closure must occur first, and then a pressure drop in the expanding closed cavity. Surface closure could not be observed in the films of the present study and the accuracy of the pullaway times is rather low. For the vertical entry of spheres, reference (1) showed that the time from water impact to surface closure was constant (in the dimensionless units) to the accuracy of the determination. This leads to the conclusion that, for the conditions of reference (1), the dimensionless depth of the missile when surface closure occurs would always be the same if there were no deceleration after water entry.

For  $M=100$ , figure 23 gives the relation  $T_p = 0.75F - 120$ . There is a small increase of the time of pullaway in seconds also, as  $v_0$  alone increases. The data of reference (1) for the vertical entry of spheres gave a  $T_p$  value of approximately 8.4 for  $M=17.7$  and  $F$  between 20 and 100. The value of  $T_p$  increased with  $F$ , but only about 0.05 over the range of  $F$  values available. These data appear reasonably consistent with figure 23.

Cavity Length. Contours of the maximum length attained by the cavity after water entry are given in figure 24. The pattern is similar to that of figure 23, but there is an upturning of the contours at small values of  $M$  due to the greater deceleration suffered by these rounds.

At  $M=100$ , the maximum length is proportional to the Froude number until the length becomes about 300 nose-flat diameters in the region where the collapse type changes from base to point closure. At larger Froude numbers the dependence is again linear, but the rate of increase of cavity length is only about half as great as before.

On figures 25 and 26 curves of cavity length versus distance traveled are given for  $M=11$  and  $M=69$ , respectively. Before pullaway the cavity length equals the distance traveled and the graphs lie on a 45-degree line, which they leave at pullaway. It was because of the behavior of the curves relative to the 45-degree line that distance traveled was chosen as the abscissa rather than time, in figures 25 and 26. By using the universal curve for  $S/M$  versus  $T/M$  on figure 18, the graphs on figures 25 and 26 can be converted to curves of cavity length versus time. These are somewhat similar to the curves for cavity volume in figures 28 and 29, which will be discussed later.

For  $M=11$  (fig. 25) the Froude numbers range from 200 to 600 and all curves are similar. Point closures always occur. As  $F$  becomes greater, pullaway is later, and the cavity length is greater just before closure. The vertical straight lines on figure 25 represent the discontinuities in length at closure. The lower ends of these lines should show the length of the cavity which remains attached to the missile after point closure, but these are unspecified in figure 25. The lengths of the cavities which remain attached were found to vary considerably; many of the deep closures occurred between the fields of the two cameras and could not be seen, and many others were difficult to specify with accuracy. The behavior is quite different for  $M=69$  (fig. 26). Base closures occur at  $F$  values below about 500, and the length curves in this region have no straight portions after pullaway. At  $F=550$  (and above) a point closure occurs and the graph on figure 26 is similar to those on figure 25. The lengths shown on figure 26 for the attached cavity, after base or point closure, are of low accuracy.

Cavity Volume. The behavior shown in figure 27 for the maximum volume attained by the cavity is quite similar to that already seen for maximum length in figure 24. At  $M=100$

the volume increases as the 2.5 power of  $F$ , up to a maximum volume of  $2 \times 10^4 d^3$  and at higher values of  $F$ , drops to about the square. If there is a deep closure, it occurs after the time of maximum volume and its effects are not seen in the contour plot.

The variation of cavity volume with time is shown for  $M=11$  and  $M=69$  in figures 28 and 29, respectively. All of the curves given for  $M=11$  have a discontinuous drop in volume at deep closure. The lower ends of these vertical lines in figure 28 (the volume of the cavity left attached to the missile) were not determined with accuracy and are not given in the figure.

It was mentioned before that curves for cavity length versus time are somewhat similar to figures 28 and 29, but there is a significant difference when deep closure occurs. Usually, as shown on figure 25, the cavity length is still increasing when deep closure occurs; but cavity volume has gone considerably past its peak (fig. 28). This behavior of the cavity volume was discussed in reference (1). It is possible for the cavity length to be decreasing when deep closure occurs. In figure 26 the curve for  $F=550$  shows a closure when the length is at a maximum. This behavior was found for Round 193 and it will be discussed later in connection with figure 37.

The variation of volume change at deep closure is interesting. At  $M=11$  the change increases with Froude number. The curves for  $F=200$ ,  $M=11$  (fig. 28) and for  $F=550$ ,  $M=69$  (fig. 29) are quite similar but the cavity developments are not. These curves are approximately those of Round 169 on figure 12 and Round 193 on figure 37, respectively. The cavity of Round 169 hardly pulls away from the surface before deep closure, while that of Round 193 was moving away from the surface rapidly when the closure occurred.

Cavity Collapse. At some point in its history the cavity suffers a rapid and usually great decrease in length. This change may be actually discontinuous when a deep closure occurs, or only quite rapid, as in the case of a base closure. Usually the cavity is reduced to less than one-third of its former length, as may be seen from figure 8.

An attempt was made to obtain a contour map of the ratio of the lengths of the cavity segments divided by a point closure. This was not successful because of the difficulties in observing deep closure.

It is useful to be able to apply a single definition to the specification of the time of the collapse, independent of its type. The time when the cavity length is half the distance that the missile has traveled since water entry was chosen as suited to this purpose. This occurs very close to the time of maximum shortening rate, as is evident from figure 8.

Figure 30 gives a contour plot of the time after entry when the cavity length is half the distance traveled. The dependence on  $M$  is very slight. At  $M=100$ , the time is linearly dependent on  $F$  up to about  $F=1000$ . Figure 11a of reference (1) (NAVORD 1809) shows a linear dependence also for the vertical entry of spheres.

Contours for the "cavity length which is half the distance traveled" on figure 31, have the usual characteristics. There is a close similarity to the contours for maximum cavity length on figure 24. At  $M=100$  the dependence on  $F$  is again linear and the length is almost proportional to  $F$ , when  $F$  is small.

The Detached Bubble. Collapse of the cavity detaches a portion of the cavity and leaves it as a bubble in the wake in all cases except perfect base closures. Base closures leave a trail of small bubbles but these trails vary from heavy continuous clouds of minute bubbles to a light sprinkling of them. Collapse causes also a compressed cavity state with pressure above ambient. The residual bubble usually begins to enlarge immediately after detachment from the main bubble. Subsequently, it oscillates several times about its normal size. At first or second maximum its shape is usually roughly spherical. The minimum size is often obscured by bubble clouds caused by the collapse instability.

Although the present report is concerned primarily with the bubble which remains attached to the missile, the observation of the "residual bubble" and bubble trails in the wake are of so great interest and contain so much potential information concerning the flow processes, that some remarks and data will be included here pertaining to these phenomena. Various collapse behaviors are illustrated in the outline sketches of figures 32 to 38. Dashed lines indicate probable cavity boundaries which are obscured by bubble clouds. Some areas are cross-hatched to indicate that they are presumably bubble clouds and not large bubbles. Although the water-entry was always oblique to the water surface, the cavities are sketched as if the missile were

traveling directly up the page. The obliquity of the water surface is shown on a number of the figures by short oblique lines labeled WL. The line across the pages through the entry points is simply a reference line to show the distance traveled by the missile. The upper dashed line marks the edge of the frame of the motion picture.

Figures 32 to 34 show three point closures. Figure 32 (Round 208,  $M=6.4$ ,  $F=549$ ) shows a large residual bubble and a very small attached one. These are characteristic of large values of  $F$  and small values of  $M$ , respectively. Figures 33 and 34 show how the size of the residual bubble decreases as  $F$  becomes less.

In figure 35 (Round 148,  $M=95$ ,  $F=672$ ) decreased deceleration because of larger  $M$  results in a much longer cavity. Cavity outline A shows the point closure occurring near the edge of the frame and separating off a considerable amount of the cavity. Further compression has so reduced the volume at outline B that the cavity is lost in the bubble cloud. At the maximum of the rebound (outline C) a large bubble is seen again.

Figure 36 (Round 91,  $M=95$ ,  $F=591$ ) shows (outline A) a long narrow cavity segment cut off by a line closure. The cavity disappears in outline B, and becomes rather large again in rebound at outline C.

Figure 37 (Round 193) is similar to figure 36 but is included to show a frequently observed phenomenon. Initially the cavity pulls away from the water surface and moves rather rapidly with all the appearance of a base closure. Outline A shows, however, that a point closure occurred before the base reached the point of the closure. The cavity disappears in outline B and reappears in C, as before.

Figure 38 (Round 94) shows an almost perfect line closure at the base. A heavy bubble-cloud wake is left but there is no evidence of any discrete bubbles.

Rounds 180 and 190 on figures 13 and 15 are typical examples of base closures.

Contours showing volumes of the residual bubble are given in figure 39. The lower dashed line shows the approximate position of the boundary of the base-closure area below which no measurable bubbles are left behind. When the base closure is very rapid and approaches a line closure, one or more small bubbles usually show up on the rebound of the wake. These generally mark places where the missile tail struck the cavity wall and deformed it slightly.

Cavity Pressure. During the data analysis 23 closed cavities were observed whose shapes seemed to be changing very slowly and which might therefore be suitable for the estimation of cavity pressure. Rather surprisingly, they were distributed over the full ranges of values of  $P$  and  $M$ . Ambient pressures at these cavities ranged from 17.3 to 22.4 psi, corresponding to depths of 6 to 18 feet below the water surface. In general, the depth of the cavities was greater as the value of  $P$  was increased, since higher values of  $P$  usually meant that greater distances had to be traversed before the steady cavity phase was reached. On the other hand, there was little change of ambient pressure with  $M$ .

The pressure contour plot is given in figure 40. The rather low accuracy of the plot is indicated by the fact that only the two contours at highest cavity pressures (and lowest values of  $M$ ) were deemed definite enough to be represented by solid lines. These were better defined because the large deceleration at low values of  $M$  results in an earlier "almost-steady" phase. Cavities with  $M=11$  had an average  $\sigma$  of 0.14 and no cavities at higher  $M$  values had a  $\sigma$  value greater than 0.085. This means that the cavities at  $M=11$  were smaller. Also the instantaneous missile speed increased with  $M$ , from an average of 32 feet per second at  $M=11$  to 168 feet per second at the higher  $M$  values.

A comparison of cavity-pressure values obtained from the cavity diameter with those obtained from the cavity length, showed excellent agreement for  $M=11$  and considerably poorer agreement for larger  $M$  values. Values plotted preparatory to drawing pressure contours were considerably more consistent when the pressures were obtained from cavity volumes, than when the means of the values obtained from diameter and length were used.

The pressure contours of figure 40 will certainly depend on missile size. A missile with the same values of  $P$  and  $M$  as one of the models of the program being analyzed, but with 10 times the diameter, might be expected to have "almost-steady" cavities at 10 times the depth; that is, at 60 to 180 feet where the ambient pressures would be 2 to 4 times as great as for the smaller models.

The change of cavitation number with change of scale may be relatively small.

## RECAPITULATION AND CONCLUSIONS

In Chapter 1 it was shown that one may reasonably expect to correlate water-entry cavity data with only three experimental parameters: a Froude number, an effective mass, and the angle of entry. In Chapter 2 this correlation was applied to motion-picture records of a water-entry model program. The result was a number of curves and contour plots showing how each of various cavity dimensions or event times depend on the experimental parameters. In addition, estimates were made of cavity pressures by a method described in Chapter 1.

It is felt that the data presented in this report serve several purposes:

- a. they indicate that the theory is reasonably applicable to experimental data,
- b. the lack of obvious contradictions lends credence to the theory,
- c. they show that under the limitations set down it appears possible to present a systematic set of data for the water-entry cavity, and
- d. the cavity data as presented are available to assist in predicting hydroballistic behavior after water entry.

On the other hand, the following limitations of the content of this report should be recognized:

- a. the application to experimental data has not verified the correlation theory because of limitations on the experimental conditions. For example, all missiles with  $M=69$  had substantially the same nose-flat diameter (with  $d/D=0.5$ ) and the same missile mass. Data are needed over several values of  $d$  with values of mass chosen so that  $M$  is unchanged,
- b. the data presented are less accurate than that which could be obtained from an experimental program designed specifically to secure these data,
- c. data do not extend over the whole region of practical importance. In fact, the most important region for missiles is probably for  $F < 200$ , and almost no data for this region are given in this report,
- d. present data generally extend only to about the time of cavity collapse; that is, to deep closure or base closure.

NOLTR 63-264

There is great need for data throughout the later stage during which the small cavity is undergoing attrition.

It is recommended that a further program be carried out to remove these limitations and to verify the correlation theory presented in this report.

REFERENCES

- (1) May, A., "Vertical Entry of Missiles into Water," J. Appl. Phys. 23, 1362 (1952). Also NavOrd Report 1809 (1951)
- (2) Waugh, J. G., and Stubstad, G. W., "Water-Entry Cavity Modeling," Part 1. Vertical Cavities; Part 2. Oblique Cavities," NOTS NavOrd Report 5365 (1957)
- (3) May, A., "A Study of the Water-Entry Cavity," Proceedings of the Eighth Midwestern Mechanics Conference, Pergamon Press, New York (in press)
- (4) Levy, J., "On Modeling the Oblique Entry into Water of Air-Launched Missiles," Cal. Tech. Report E-12.19 (1956)
- (5) Richardson, E. G., "The Impact of a Solid on a Liquid Surface," Proc. Phys. Soc. (London) 61, 352 (1948)
- (6) Reichardt, H., "The Laws of Cavitation Bubbles at Axially Symmetrical Bodies in a Flow," Ministry of Aircraft Production, Transl. No. 766 (1945)
- (7) Rouse, H. and McNown, J. S., "Cavitation and Pressure Distribution - Head Forms at Zero Angle of Yaw," State University of Iowa Studies in English, Bull. 32 (1948)
- (8) Eisenberg, P. and Pond, H. L., "Water Tunnel Investigations of Steady State Cavities," DTMB Report 668 (1948)
- (9) Birkhoff, G. and Zarantonello, E. H., Jets, Wakes, and Cavities, Academic Press, Inc., New York (1957)

Table 1

## EXPERIMENTAL DATA FOR ROUNDS REDUCED

Round No.	Body Dia. Inches	Nose Dia. Inches	Q <sub>0</sub> Degrees	V <sub>0</sub> ft/sec	M	P
153	1.570	1.570	60	453	11.0	221
81	1.570	1.570	70	895	11.6	436
157	1.570	1.570	60	555	11.0	270
168	1.570	1.570	45	543	11.0	265
169	1.570	1.570	45	595	11.0	290
158	1.570	1.570	60	751	11.0	365
159	1.570	1.570	60	898	11.0	437
55	1.570	1.570	45	1003	11.6	494
172	1.570	1.570	45	1125	11.0	548
104	1.570	1.256	60	613	24.5	334
103	1.570	1.256	60	873	24.5	476
61	1.570	1.099	45	970	36.7	564
47	1.570	1.099	45	940	36.7	547
59	1.570	0.942	45	633	53.4	407
106	1.570	0.942	60	634	51.1	399
69	1.570	0.942	70	831	55.1	523
82	1.570	0.942	70	924	51.1	581
111	1.570	0.785	60	746	49.8	514
64	1.570	0.942	70	932	53.4	586
56	1.570	0.942	45	991	53.4	623
190	1.570	0.864	47	321	68.7	211
178	1.570	0.864	47	444	68.9	291
192	1.570	0.864	47	548	68.7	360
180	1.570	0.864	47	604	68.7	397
189	1.570	0.864	47	675	68.7	444
95	1.570	0.864	60	887	71.6	583
193	1.570	0.864	47	832	68.7	547
98	1.570	0.864	60	889	71.6	584
112	1.570	0.864	60	961	71.6	631

Table 1 (Con't)

Round No.	Body Dia. Inches	Nose Dia. Inches	$\phi_o$ Degrees	$v_o$ ft/sec	M	R
216	0.963	0.482	47	630	74.1	544
131	0.963	0.482	60	1597	74.2	596
205	1.570	0.774	47	599	99.7	394
105	1.570	0.785	60	616	94.6	425
58	1.570	0.785	45	656	94.6	425
228	1.570	0.785	47	904	92.9	623
91	1.570	0.785	70	857	95.3	591
70	1.570	0.785	70	888	94.6	612
49	1.570	0.785	45	953	94.7	657
63	1.570	0.785	70	946	94.6	652
90	1.570	0.785	70	1087	94.6	750
183	0.963	0.433	47	558	104.6	507
124	0.963	0.433	60	1163	104.7	1057
126	0.963	0.433	60	1053	104.6	957
109	0.963	0.433	60	1256	104.6	1142
137	0.963	0.433	60	1206	104.6	1096
107	0.963	0.433	60	1600	104.6	1455
186	1.570	0.707	47	337	125.3	245
184	1.570	0.707	47	426	125.3	309
187	1.570	0.707	47	547	125.3	397
188	1.570	0.707	47	611	125.3	444
162	1.570	0.707	47	871	125.7	633
123	1.570	0.707	60	991	124.8	720
134	1.570	0.707	60	908	125.5	659
142	1.570	0.707	60	898	125.7	652
161	1.570	0.707	47	875	130.4	636
160	1.570	0.707	60	1088	130.7	790
155	1.570	0.707	60	1062	135.2	771
182	1.570	0.628	47	584	182.2	450
165	1.570	0.628	60	865	177.5	666

Table 1 (Con't)

Round No.	Body Dia. Inches	Nose Dia. Inches	$\theta$ Degrees	$v_0$ ft/sec	$\mu$	$R$
216	0.963	0.482	47	630	74.1	544
131	0.963	0.482	60	1597	74.3	599
205	1.570	0.774	47	599	99.7	394
105	1.570	0.785	60	616	94.6	425
58	1.570	0.785	45	656	94.6	425
228	1.570	0.785	47	904	92.9	623
91	1.570	0.785	70	857	95.3	591
70	1.570	0.785	70	888	94.6	612
49	1.570	0.785	45	953	94.7	657
63	1.570	0.785	70	946	94.6	652
90	1.570	0.785	70	1087	94.6	750
183	0.963	0.433	47	558	104.6	507
124	0.963	0.433	60	1163	104.7	1057
126	0.963	0.433	60	1053	104.6	957
109	0.963	0.433	60	1256	104.6	1142
137	0.963	0.433	60	1206	104.6	1096
107	0.963	0.433	60	1600	104.6	1455
186	1.570	0.707	47	337	125.3	245
184	1.570	0.707	47	426	125.3	309
187	1.570	0.707	47	547	125.3	397
188	1.570	0.707	47	611	125.3	444
162	1.570	0.707	47	871	125.7	633
123	1.570	0.707	60	991	124.8	720
134	1.570	0.707	60	908	125.5	659
142	1.570	0.707	60	898	125.7	652
161	1.570	0.707	47	875	130.4	636
160	1.570	0.707	60	1088	130.7	790
155	1.570	0.707	60	1062	135.2	771
182	1.570	0.628	47	584	182.2	450
165	1.570	0.628	60	865	177.5	666

NOLTR 63-264

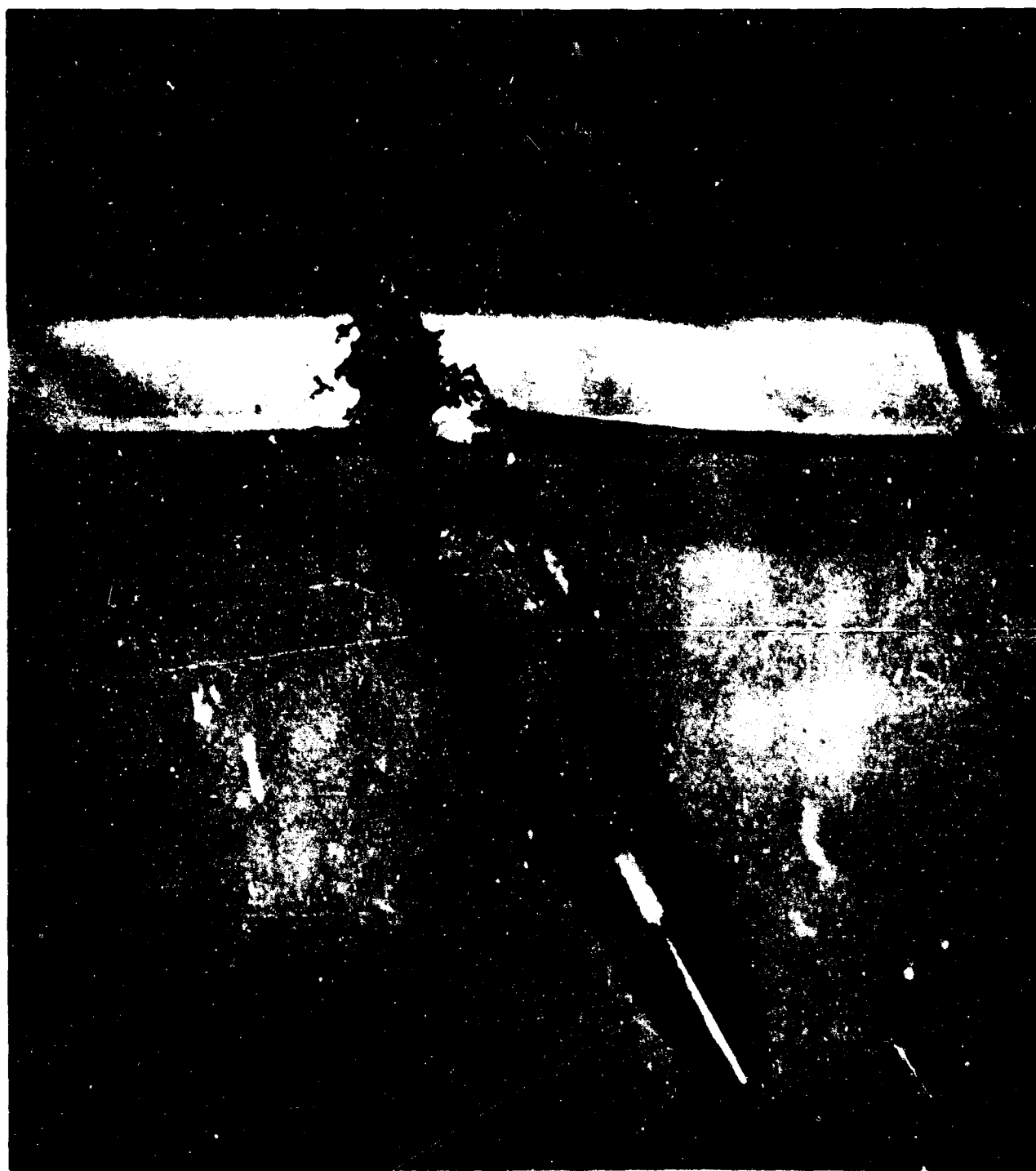


FIG. 1 WATER ENTRY OF RIGHT CYLINDER

NOLTR 63-264



FIG. 2 CAVITY WITH "ALMOST STEADY" FLOW

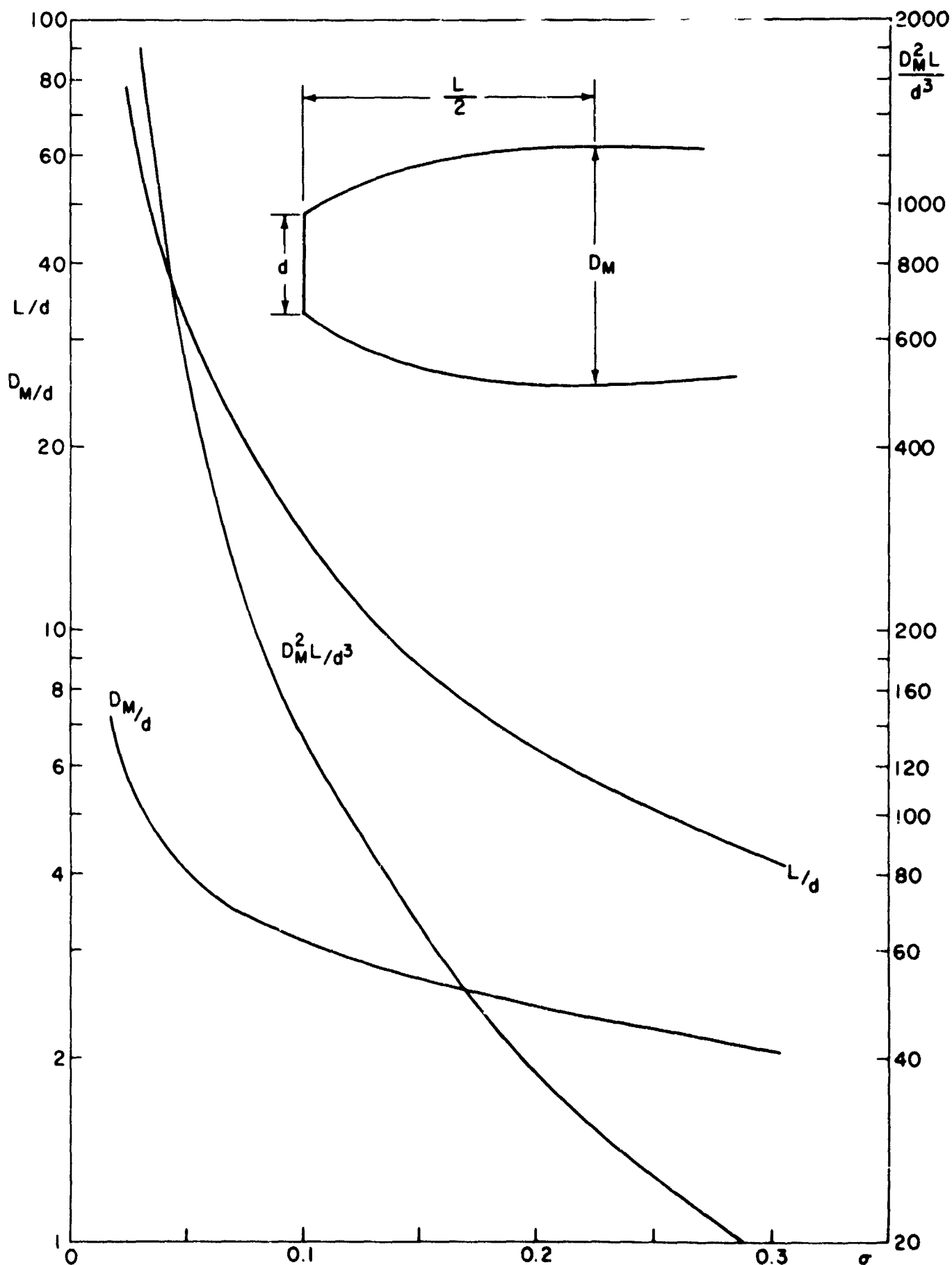


FIG. 3 VARIATIONS OF DIMENSIONS OF STEADY CAVITY WITH CAVITATION NUMBER

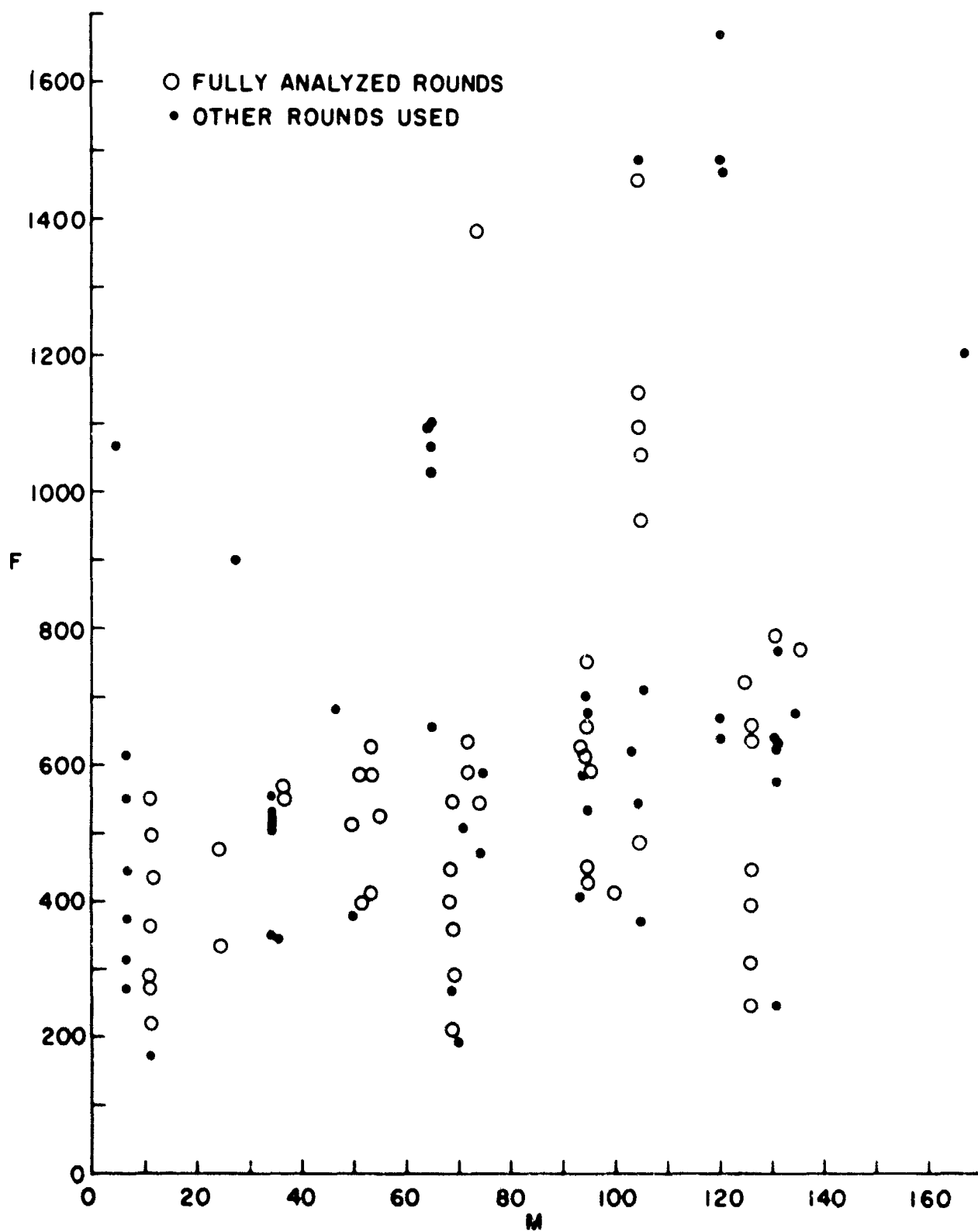


FIG. 4 EXPERIMENTAL PARAMETERS OF AVAILABLE WATER-ENTRY TESTS

NOLTR 63-264

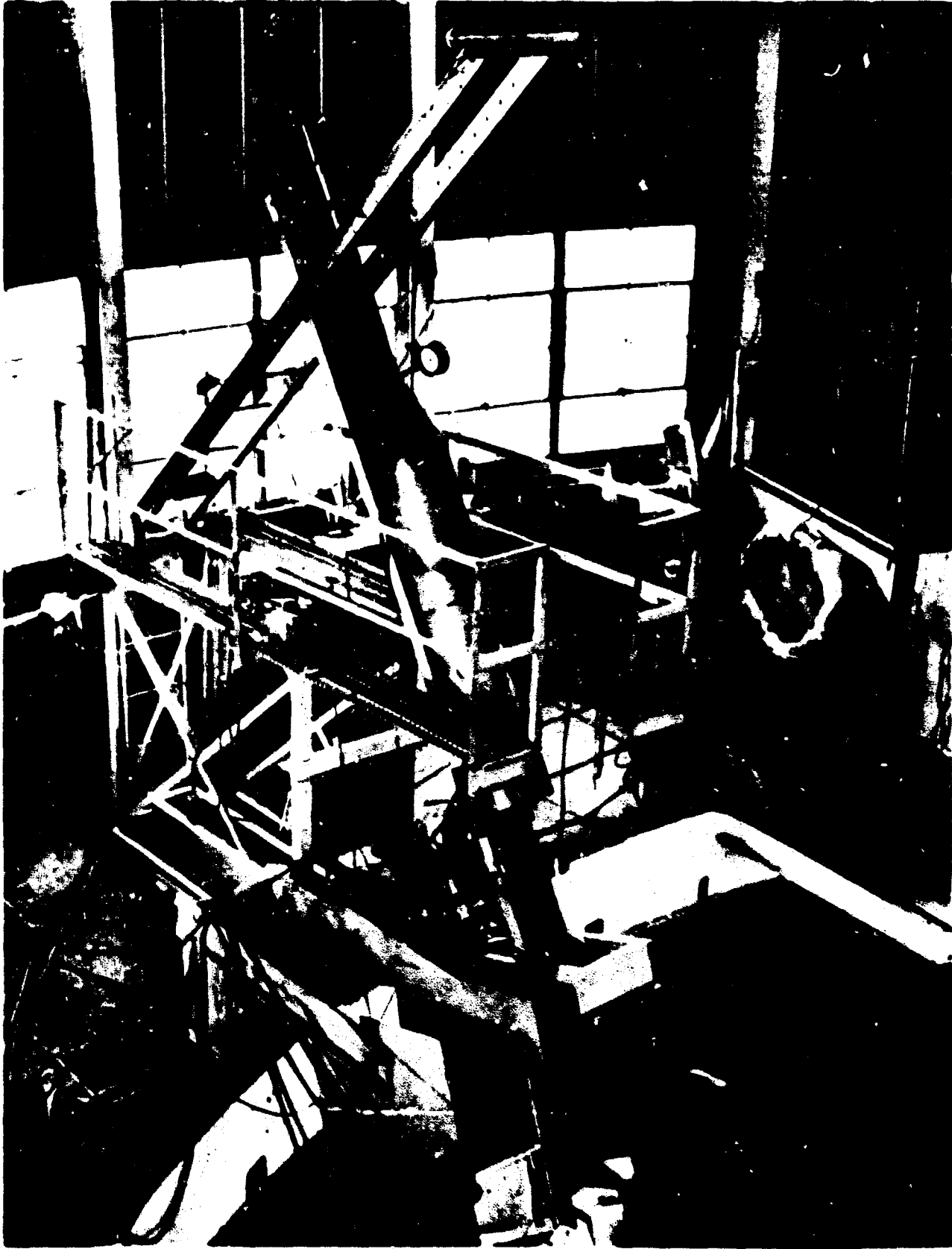


FIG 5 GUN MOUNT

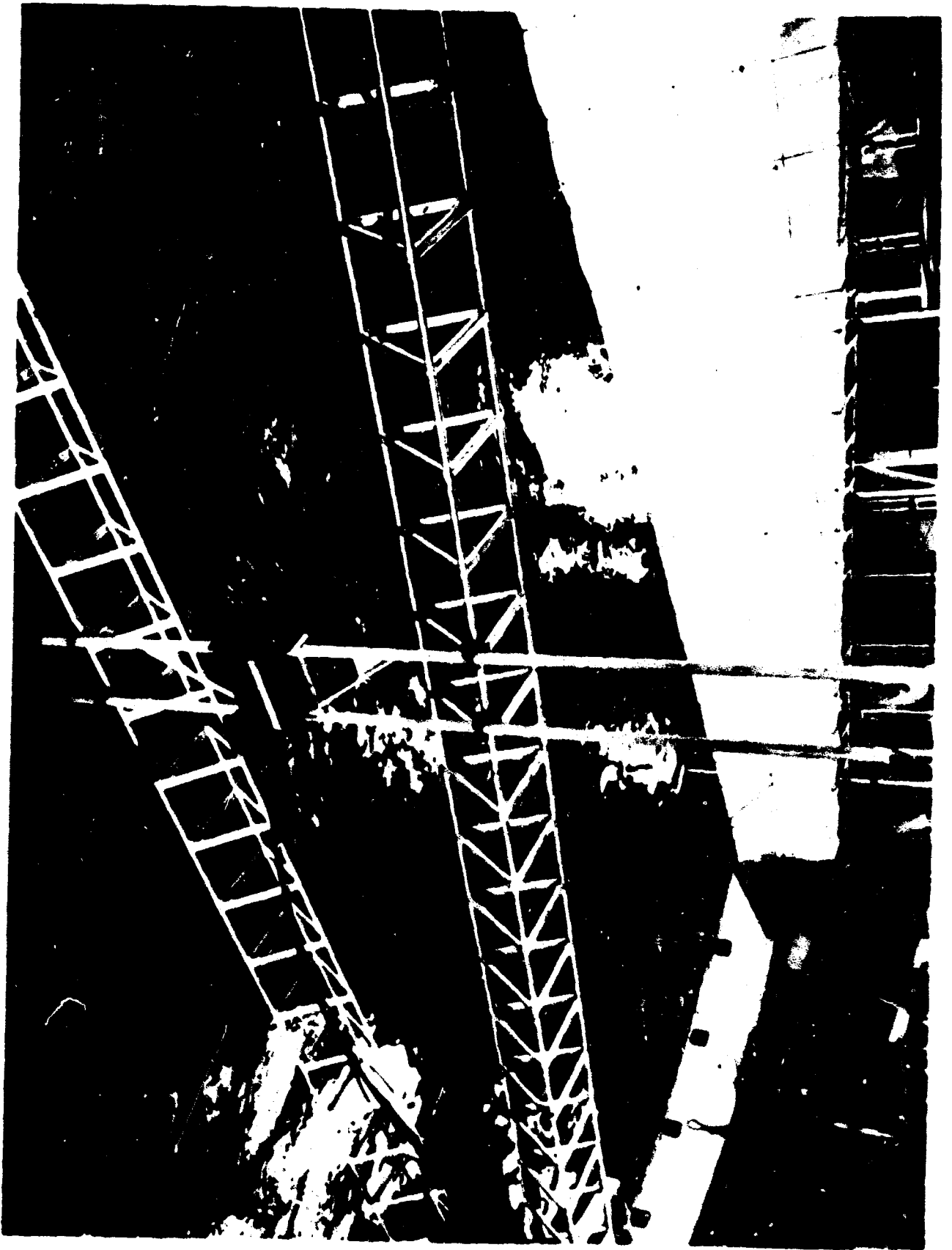
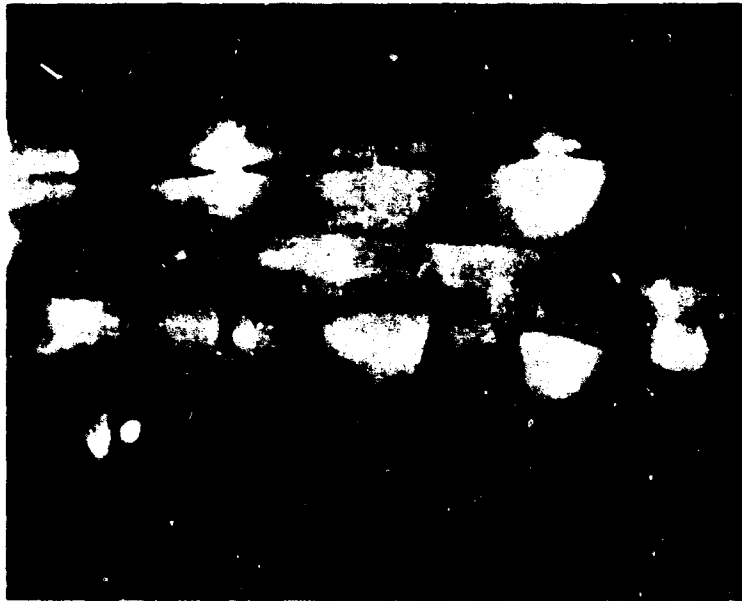


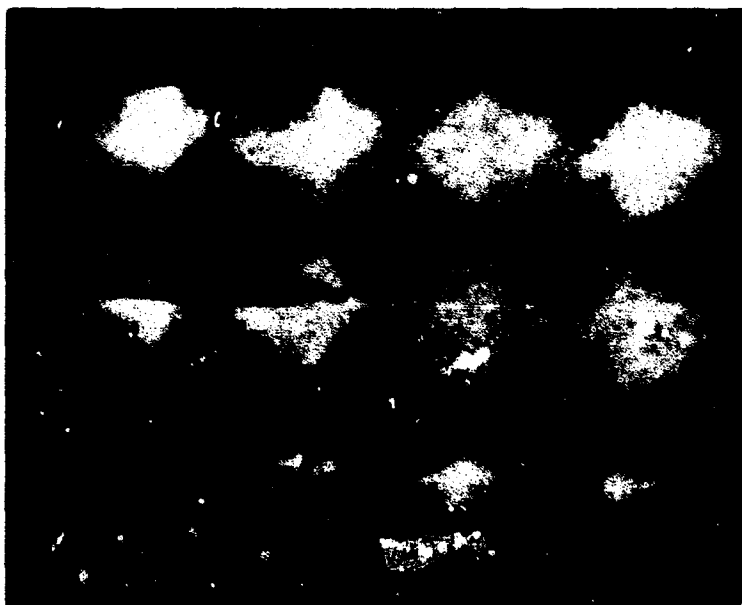
FIG 6 ARRANGEMENT OF CAMERAS AND LIGHTS

NOLTR 63-264

NOLTR 63-264



PHOTOGRAPH FROM FIRST CAMERA



PHOTOGRAPH FROM SECOND CAMERA

FIG. 7 PHOTOGRAPHS OF WATER-ENTRY CAVITY

NOLTR 63-264

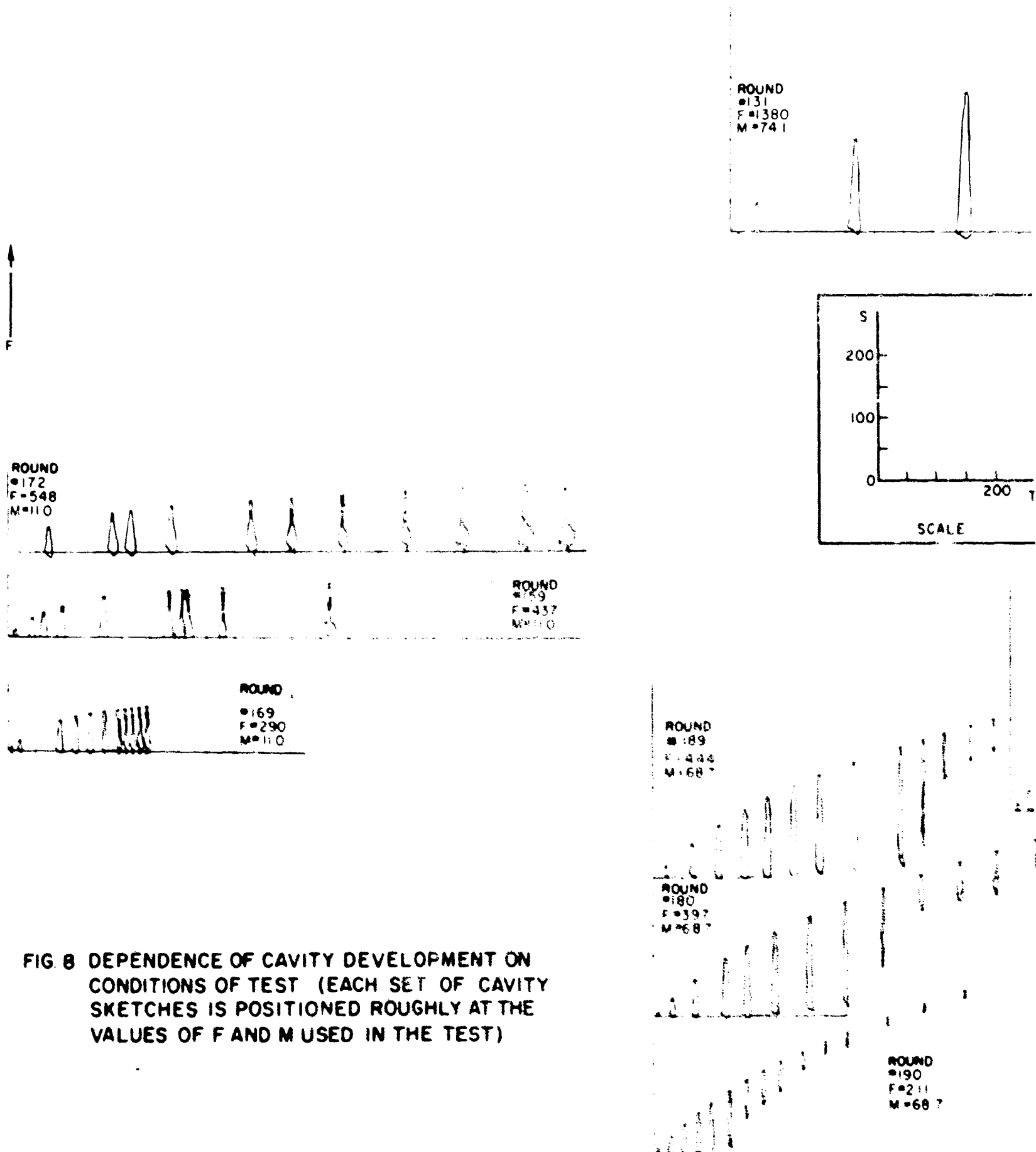
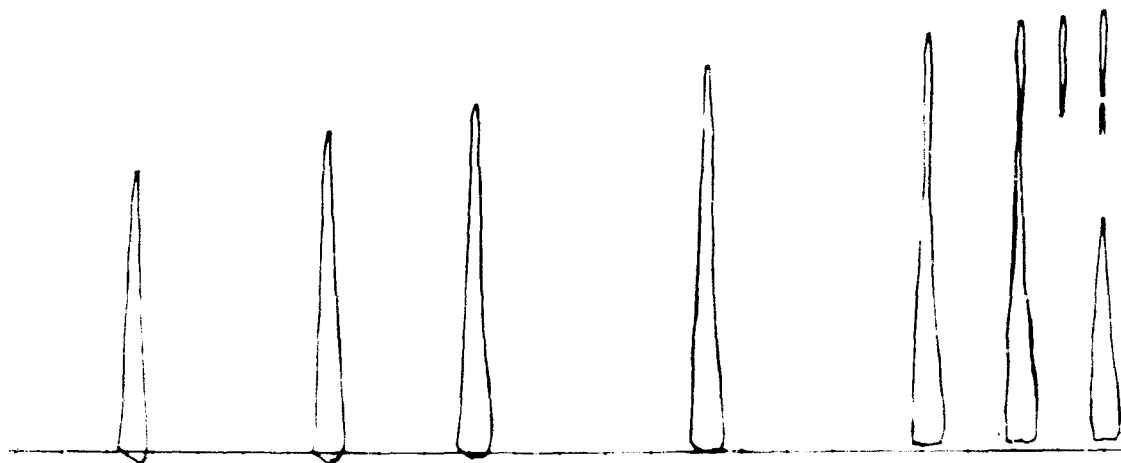
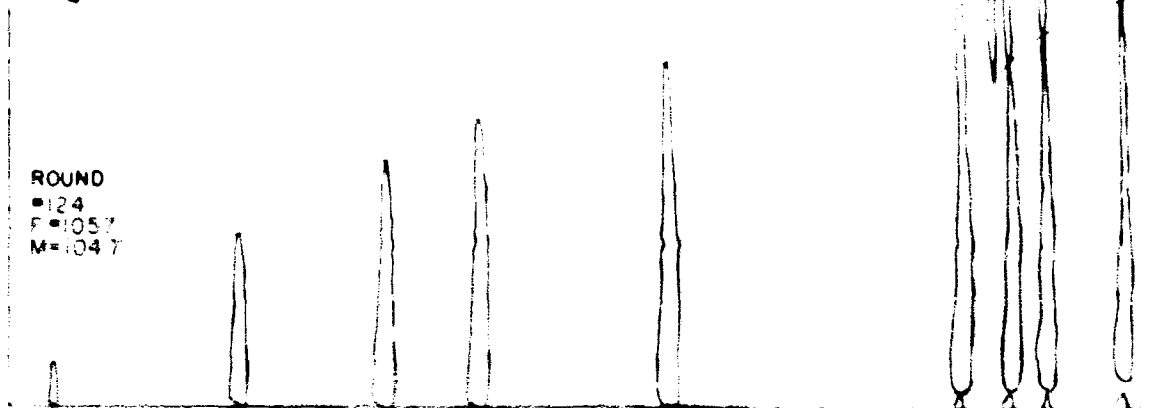


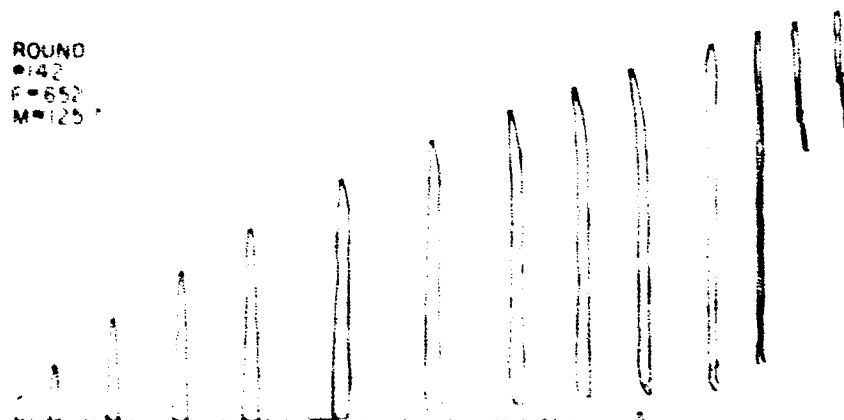
FIG. 8 DEPENDENCE OF CAVITY DEVELOPMENT ON CONDITIONS OF TEST (EACH SET OF CAVITY SKETCHES IS POSITIONED ROUGHLY AT THE VALUES OF F AND M USED IN THE TEST)



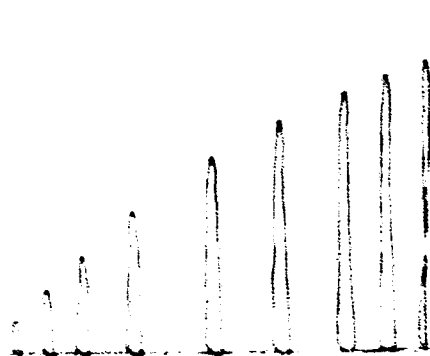
ROUND  
#124  
F=105.7  
M=104.7



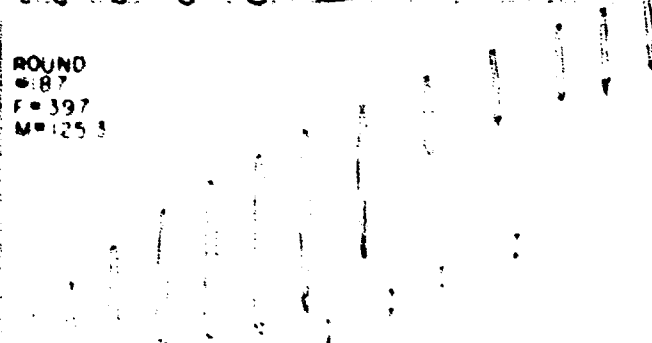
ROUND  
#142  
F=652  
M=125.7



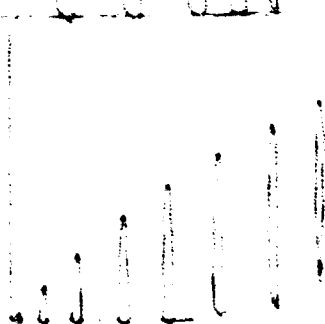
ROUND  
#228  
F=623  
M=92.9



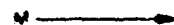
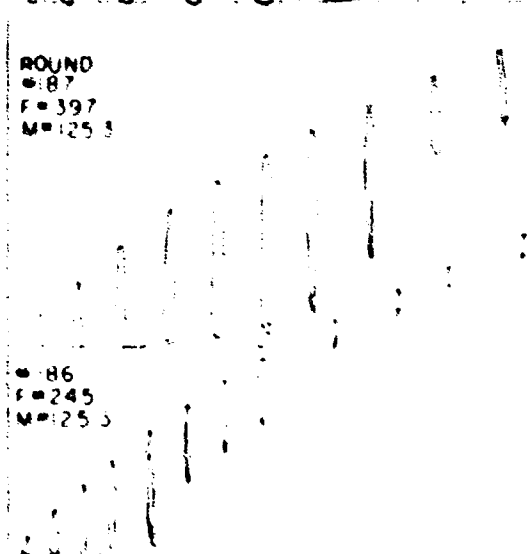
ROUND  
#187  
F=397  
M=125.3



ROUND  
#205  
F=415.1  
M=99.7



ROUND  
#186  
F=245  
M=125.3



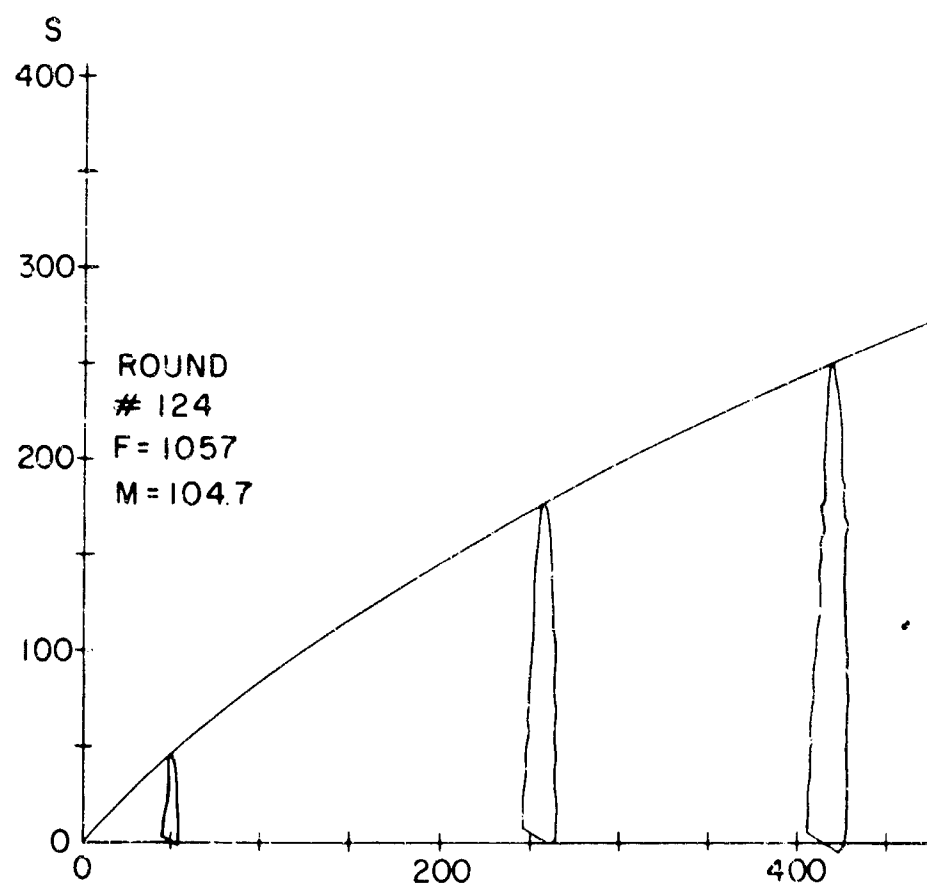
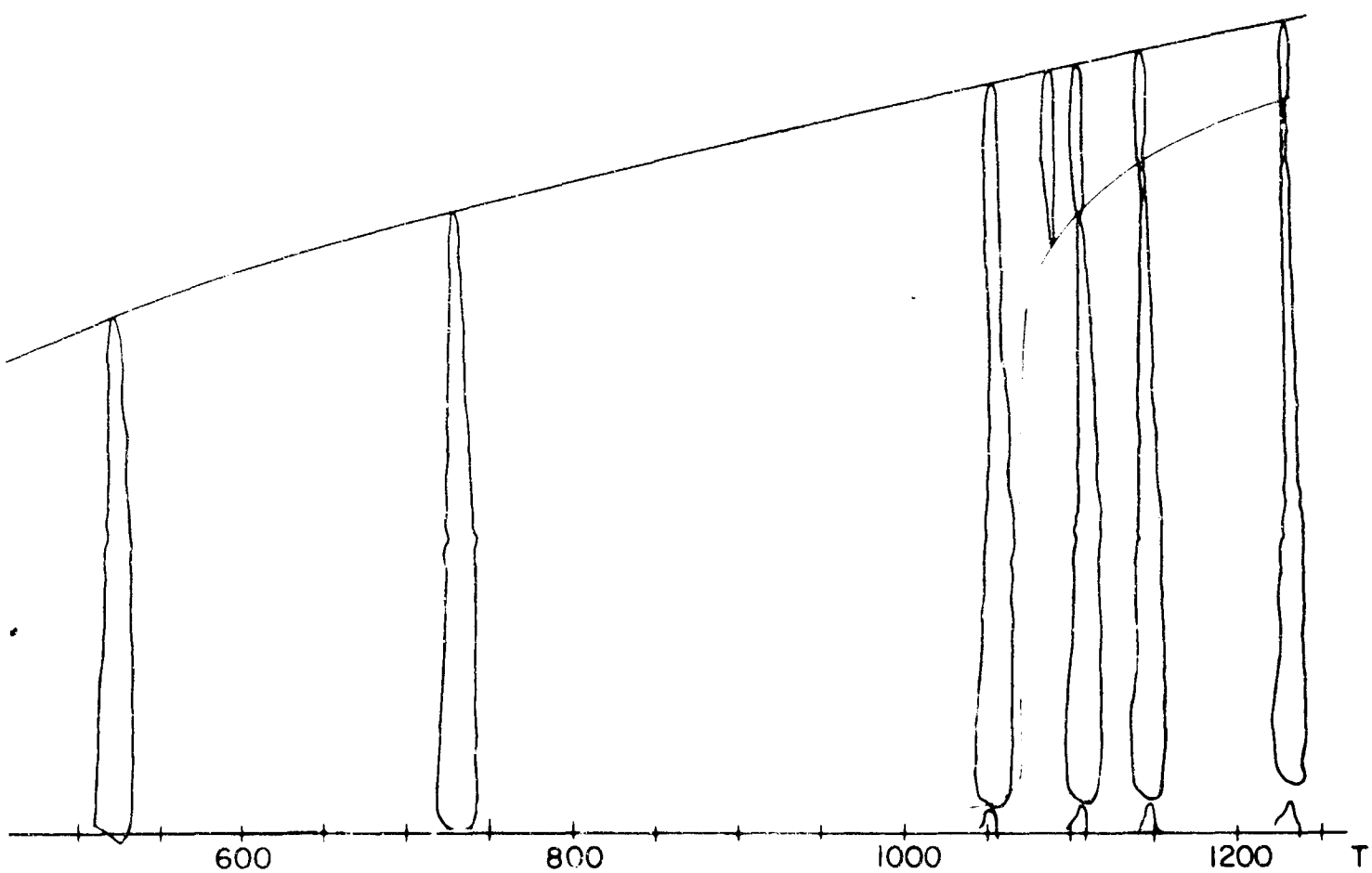


FIG 9 CAVITY DEVELOPMENT-R



ROUND 124

NOLTR 63-264

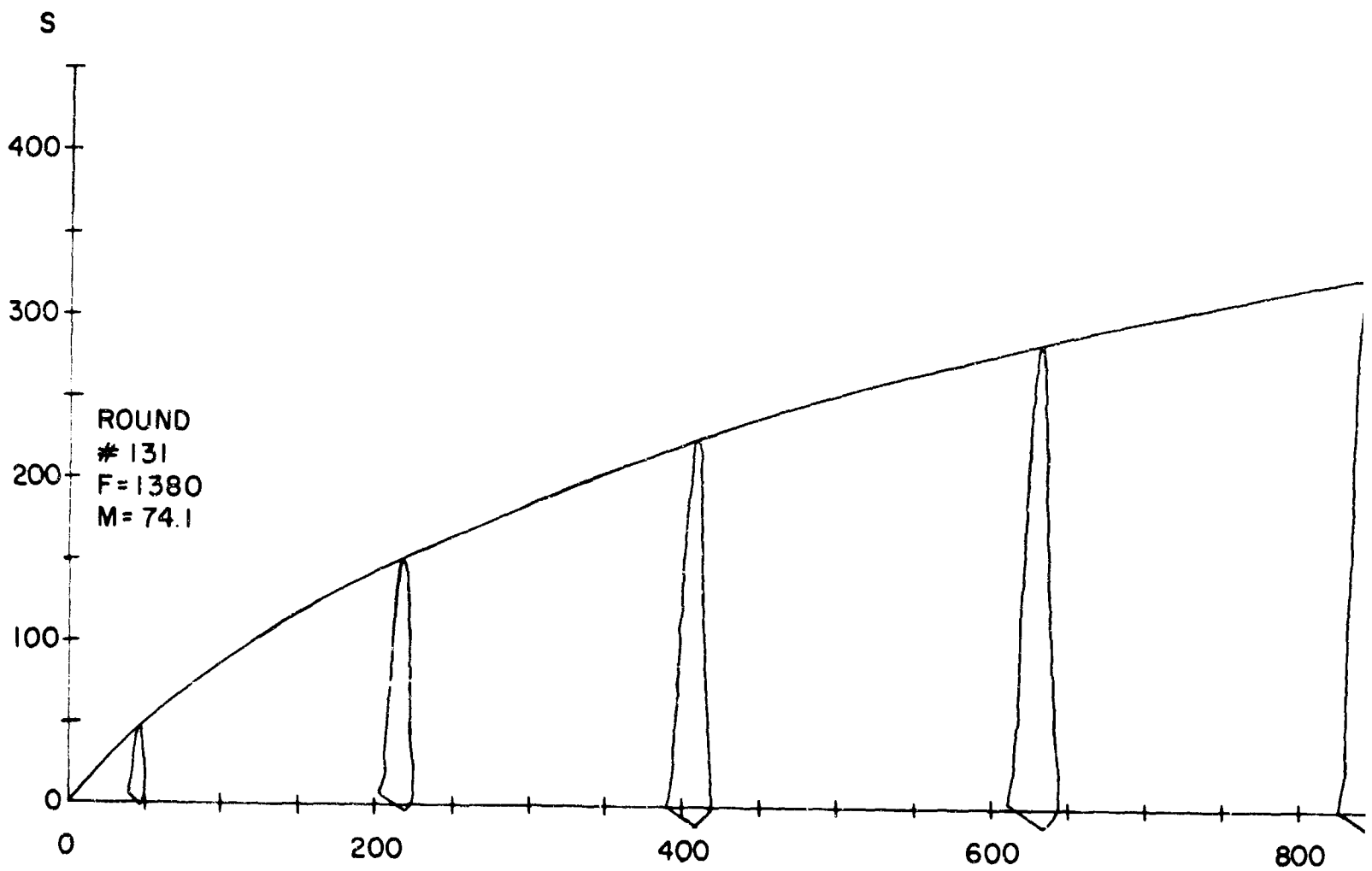
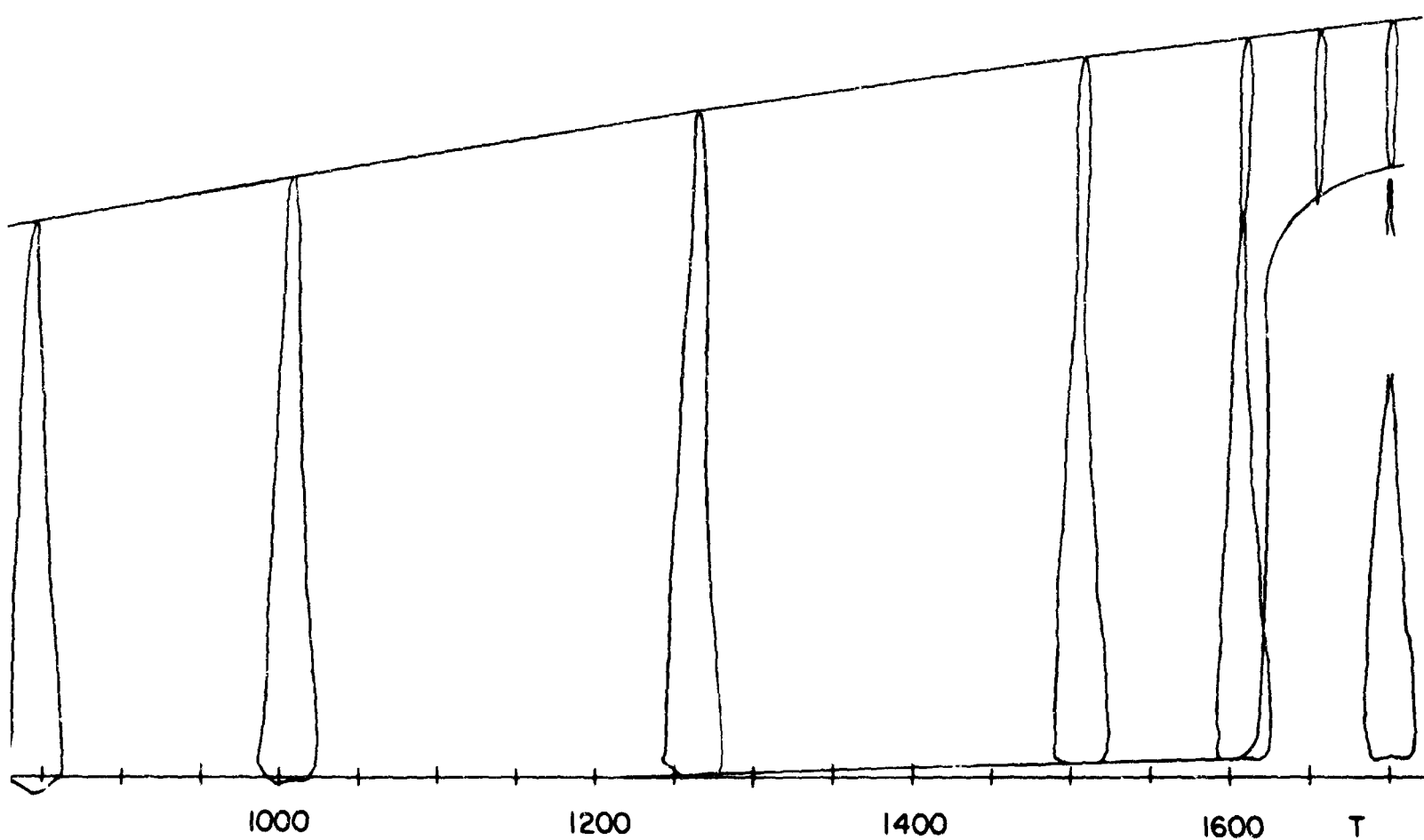
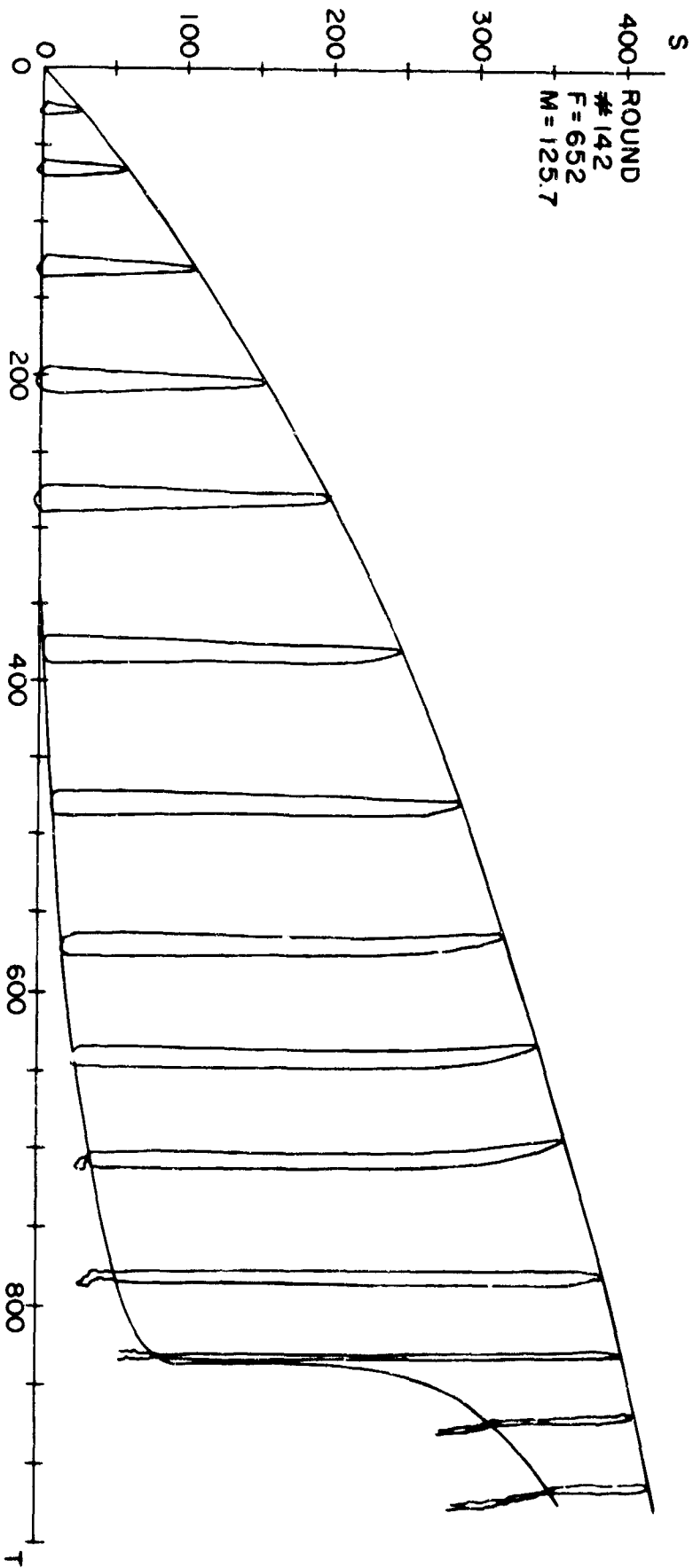


FIG. 10 CAVITY DEVELOPMENT—ROUND 131





NOLTR 63-264

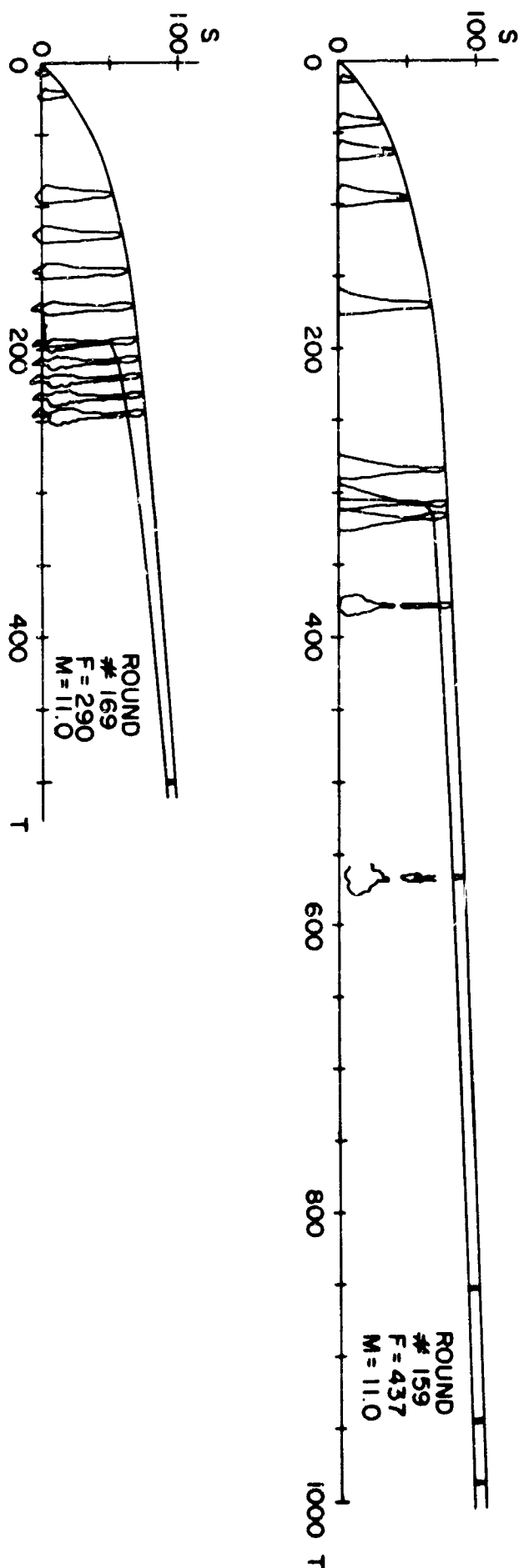


FIG. 12 CAVITY DEVELOPMENT - ROUNDS 159 AND 169

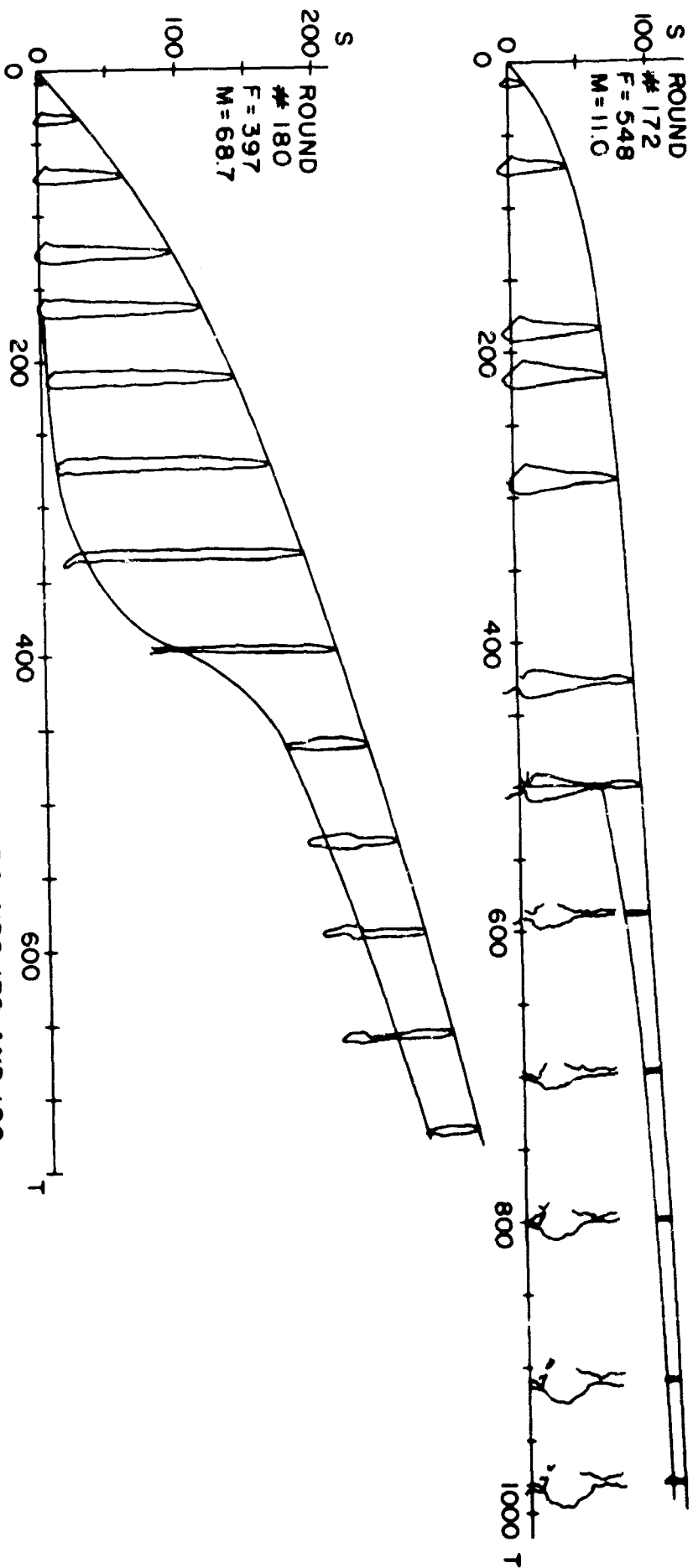


FIG. 13 CAVITY DEVELOPMENT-ROUNDS 172 AND 180

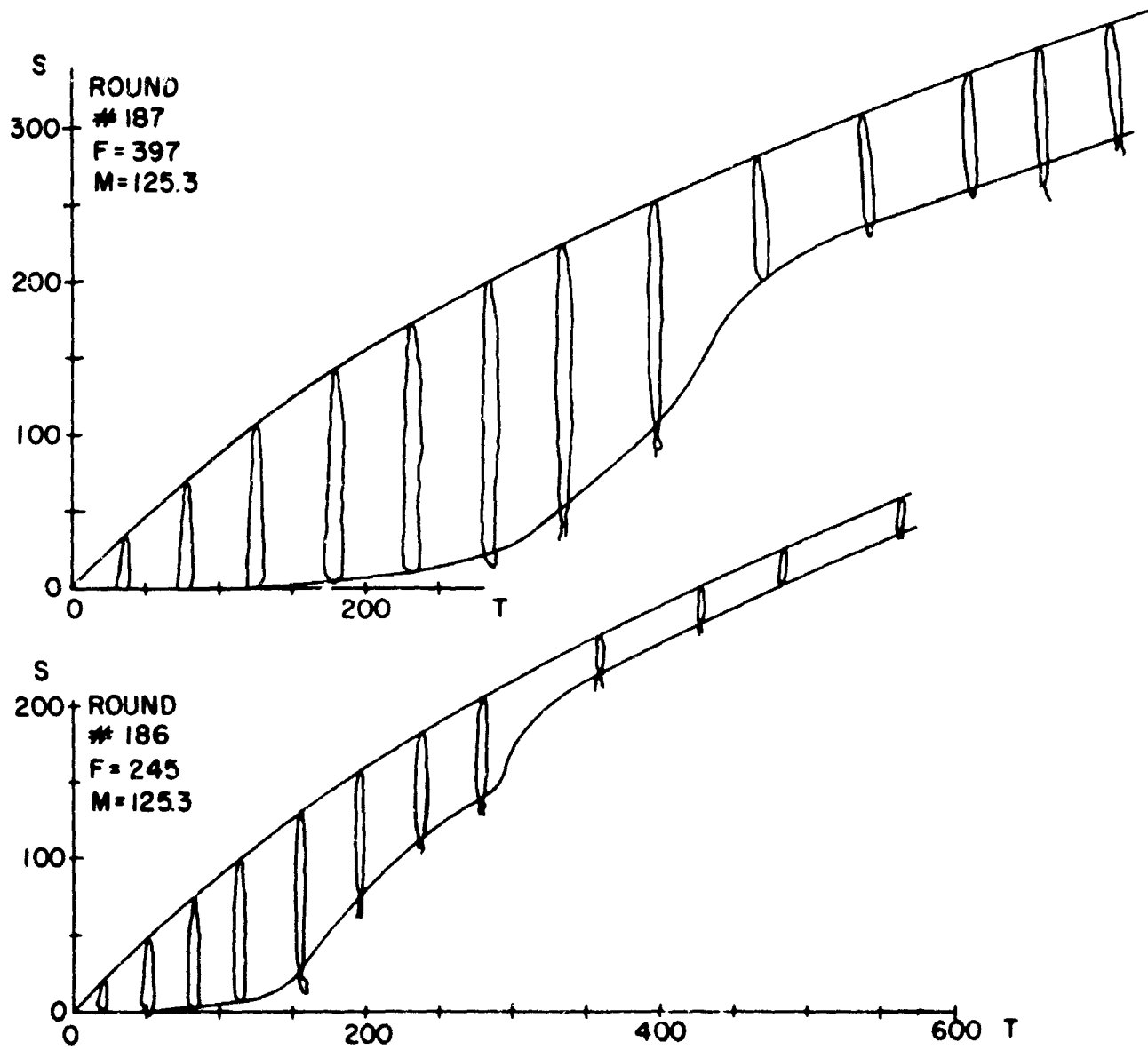


FIG. 14 CAVITY DEVELOPMENT-ROUNDS 186 AND 187

NOLTR 63-264

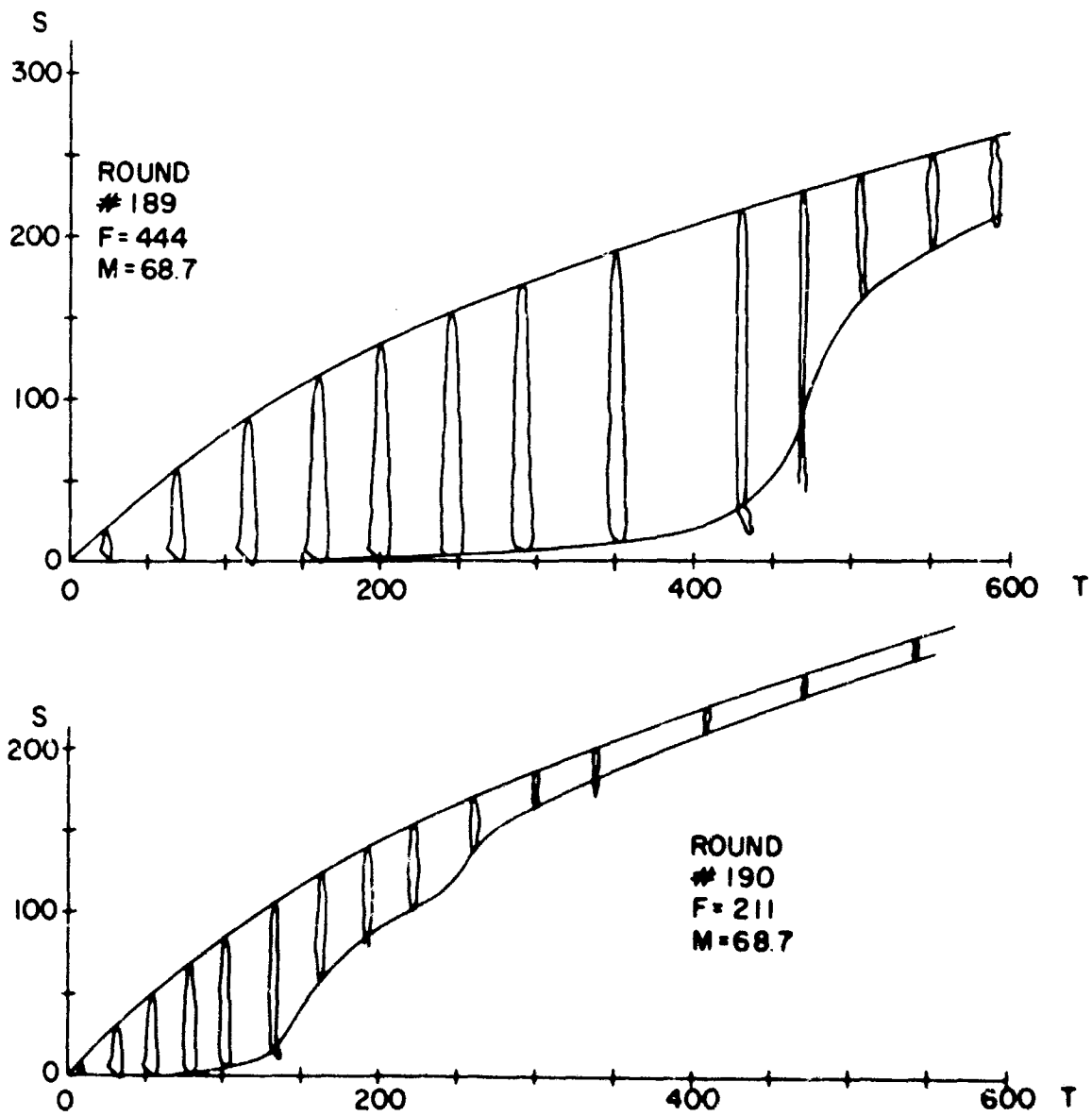


FIG 15 CAVITY DEVELOPMENT — ROUNDS 189 AND 190

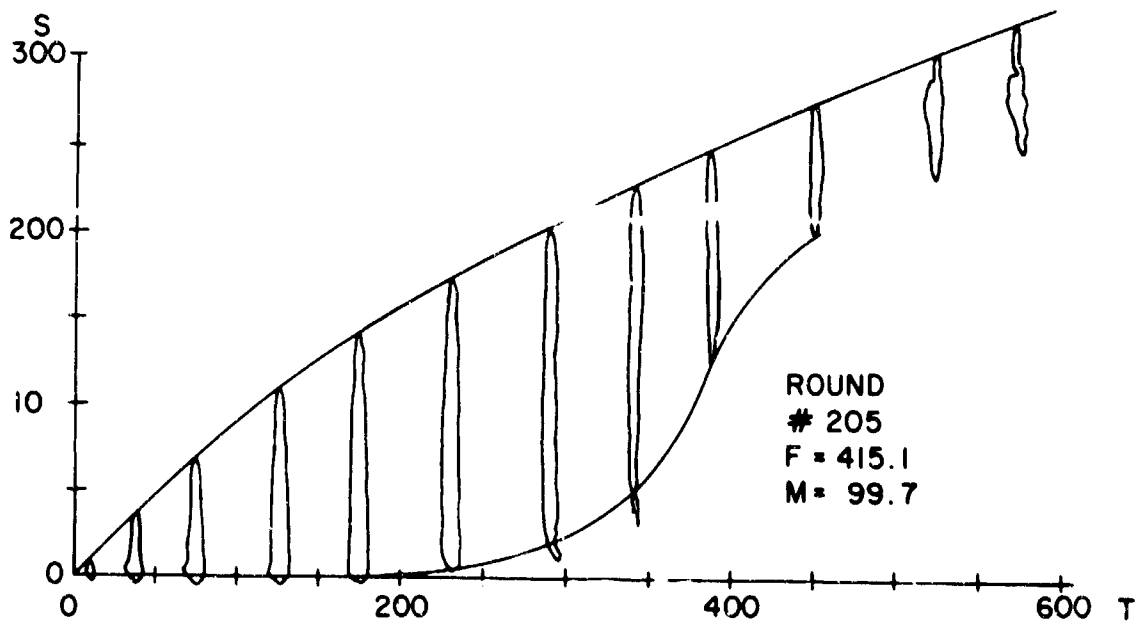
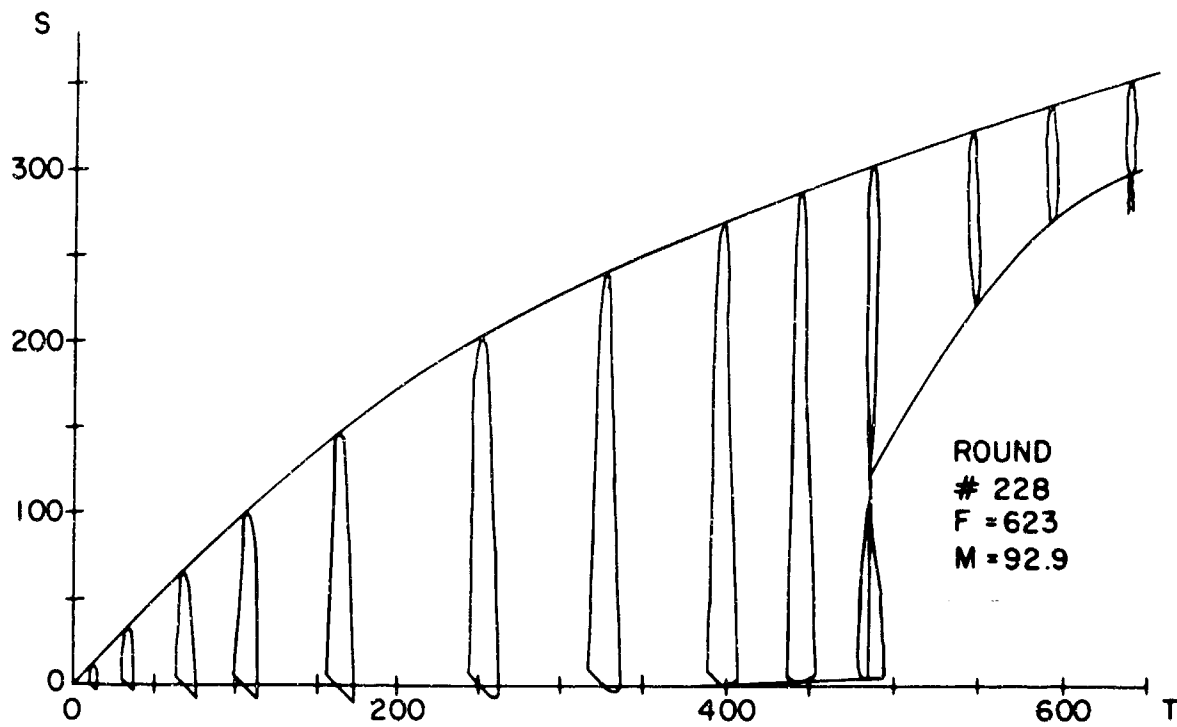


FIG. 16 CAVITY DEVELOPMENT — ROUNDS 205 AND 228

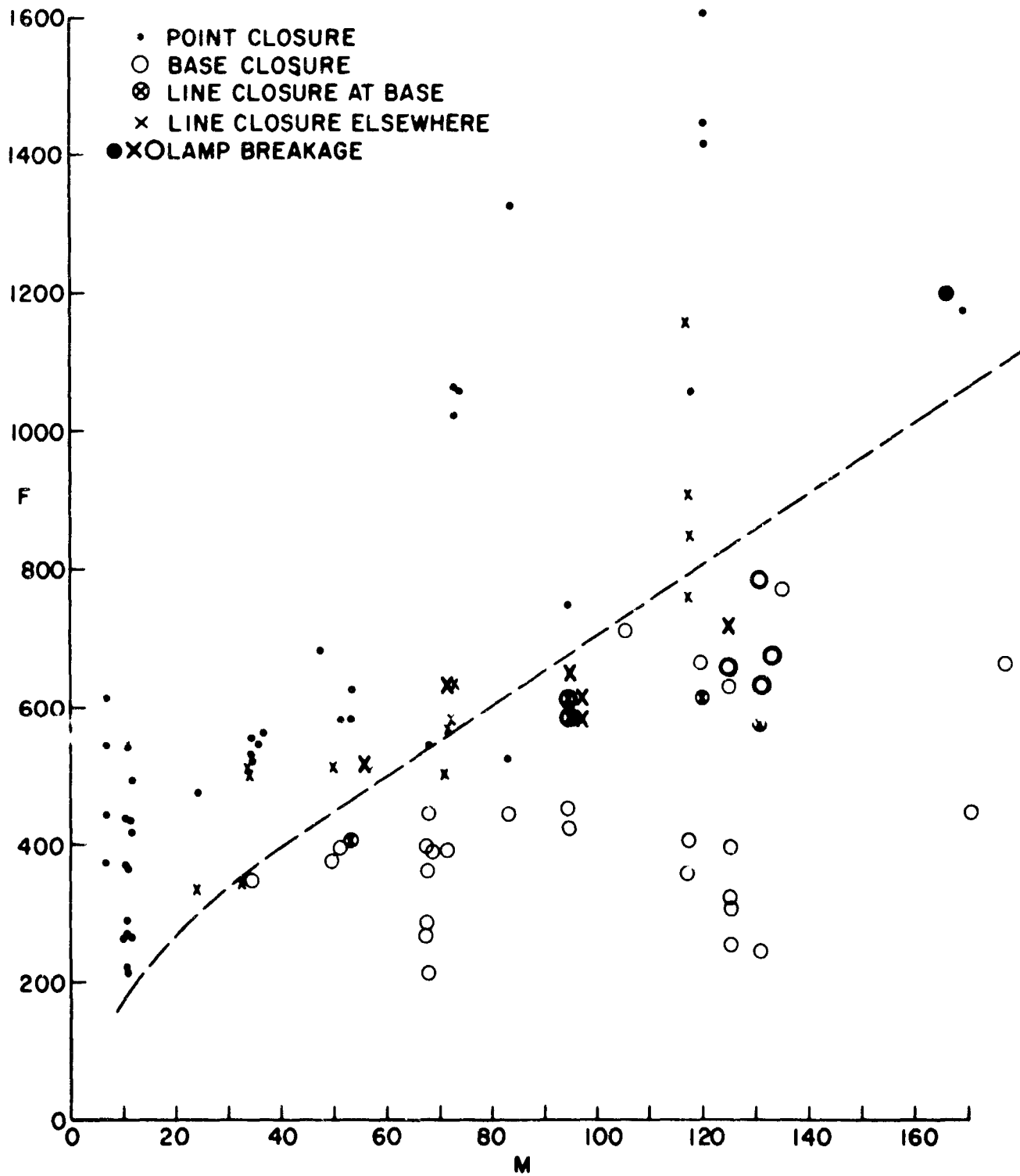


FIG. 17 TYPE OF CAVITY COLLAPSE

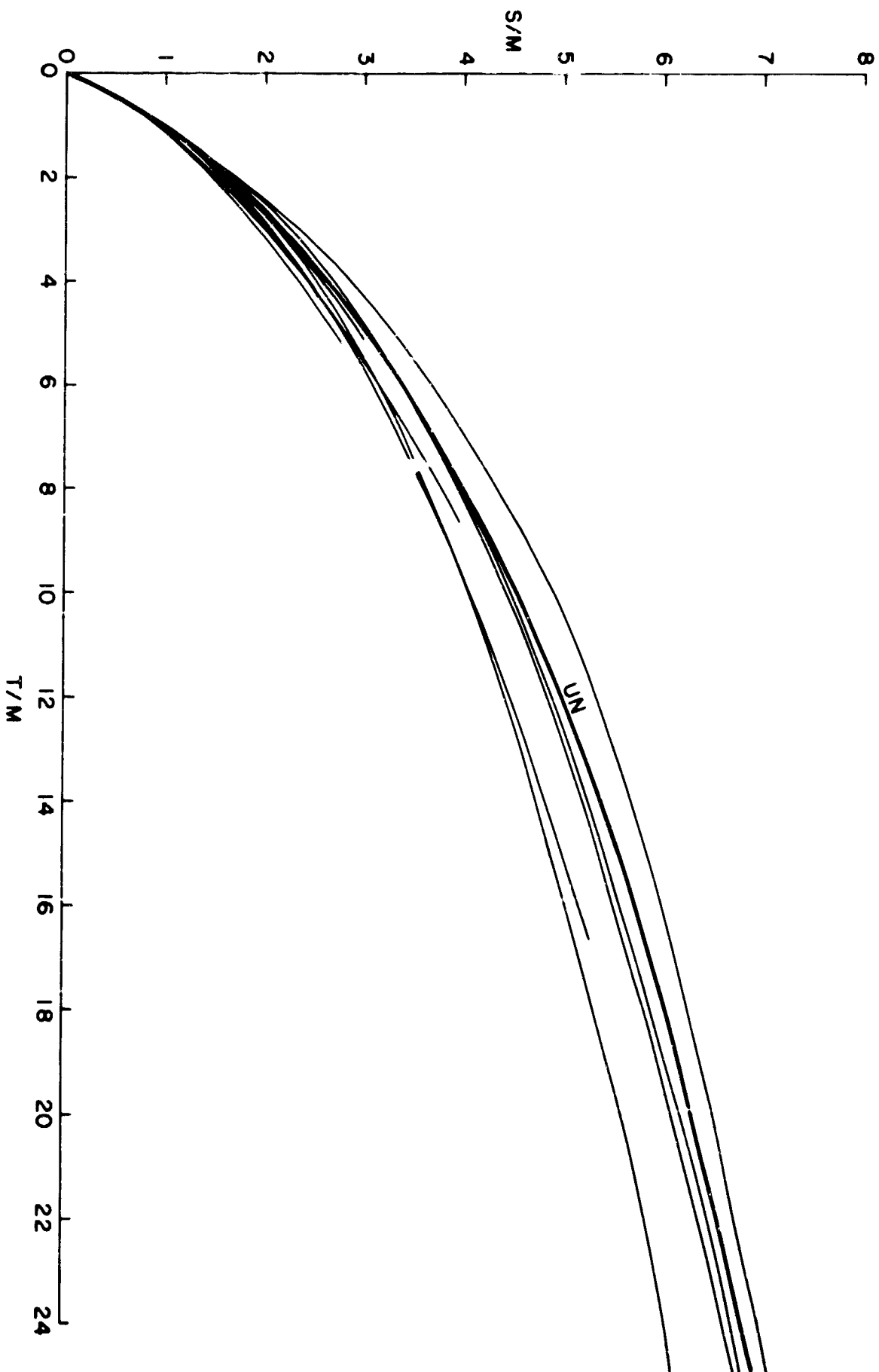


FIG. 18 THE "UNIVERSAL" S/M VERSUS T/M GRAPH

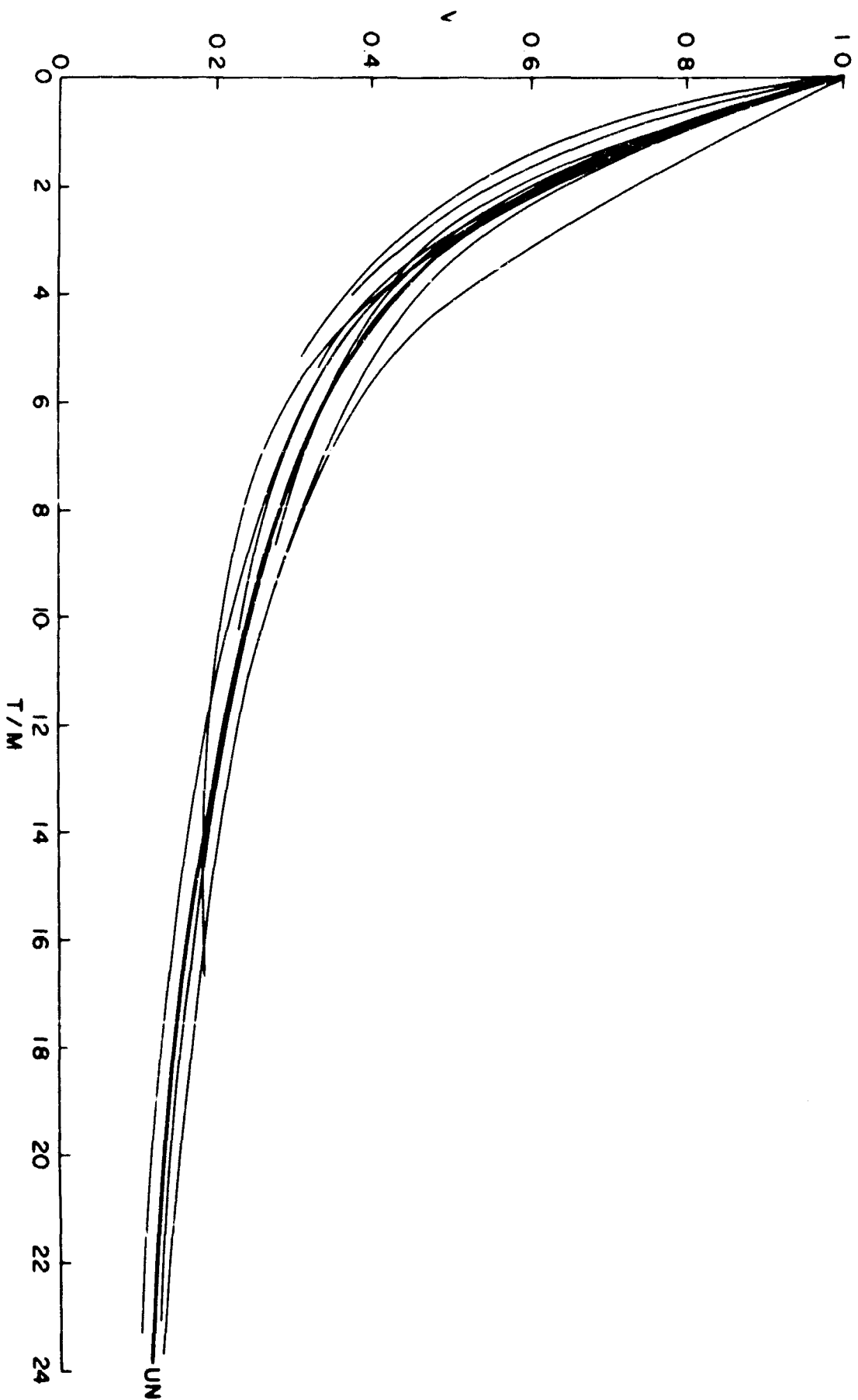


FIG. 19 THE "UNIVERSAL"  $v$  VERSUS  $T/M$  GRAPH

NOLTR 63-264

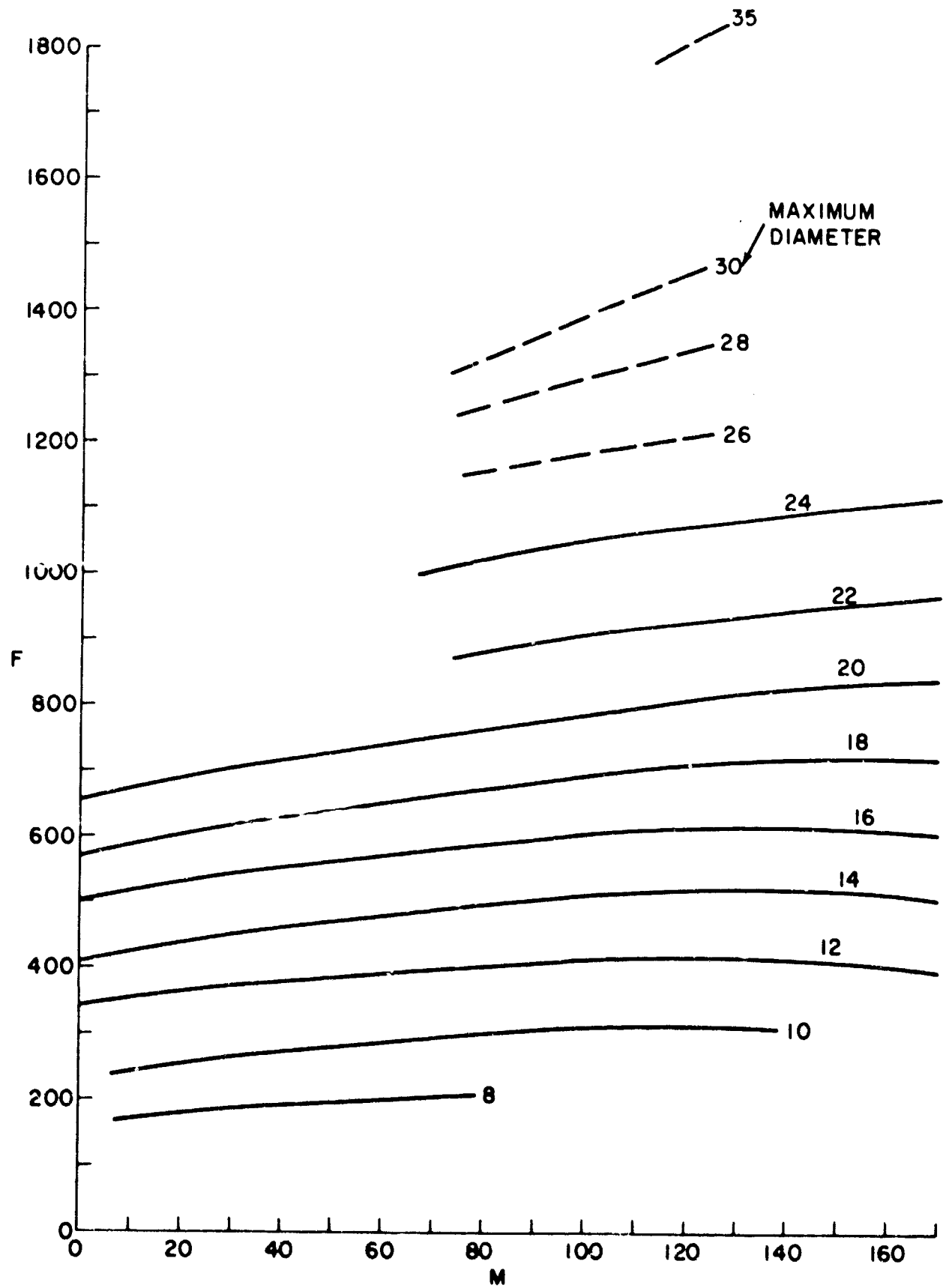


FIG. 20 CONTOURS OF MAXIMUM CAVITY DIAMETER

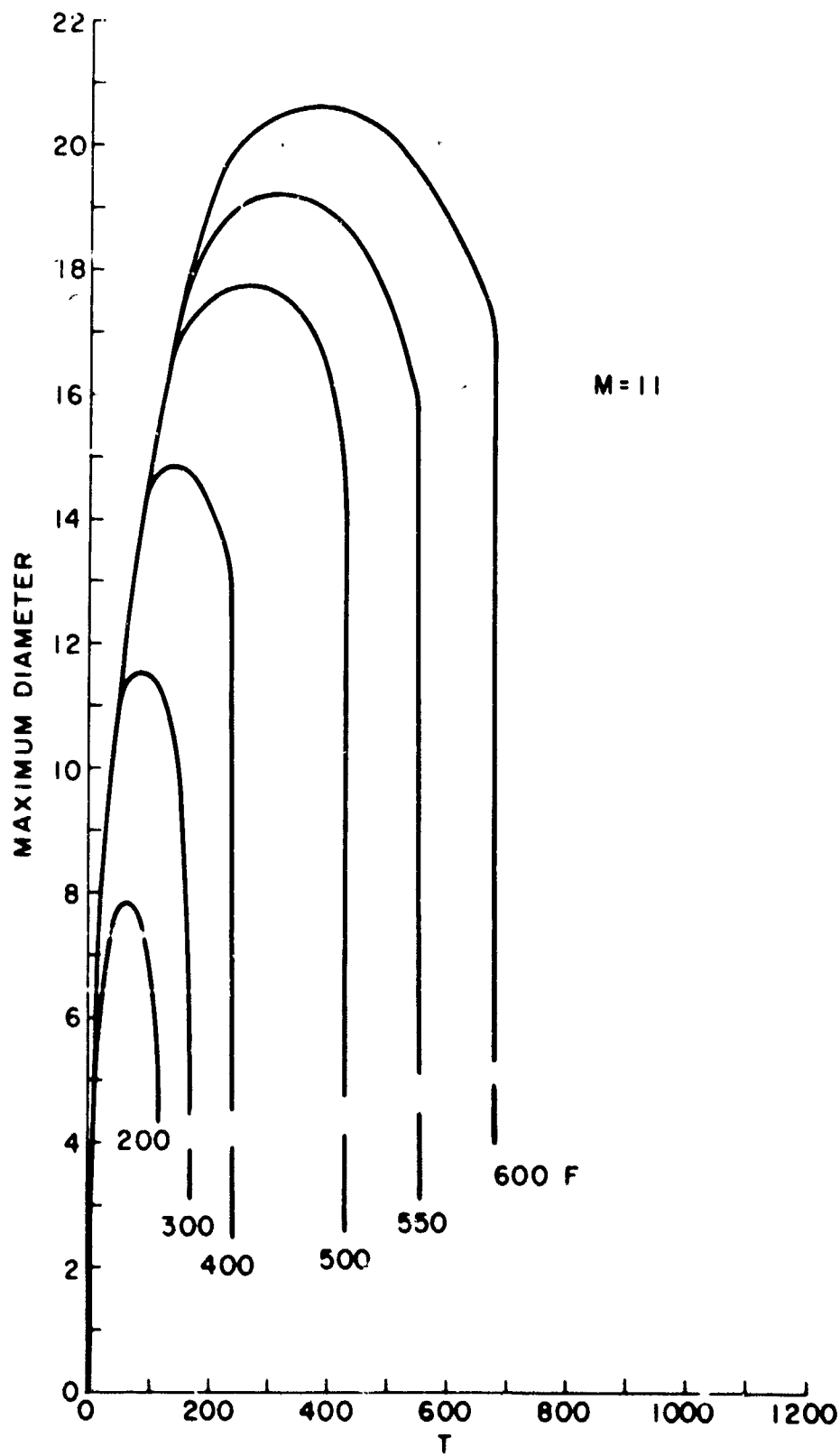


FIG. 21 VARIATION OF CAVITY DIAMETER AFTER ENTRY (M = 11)

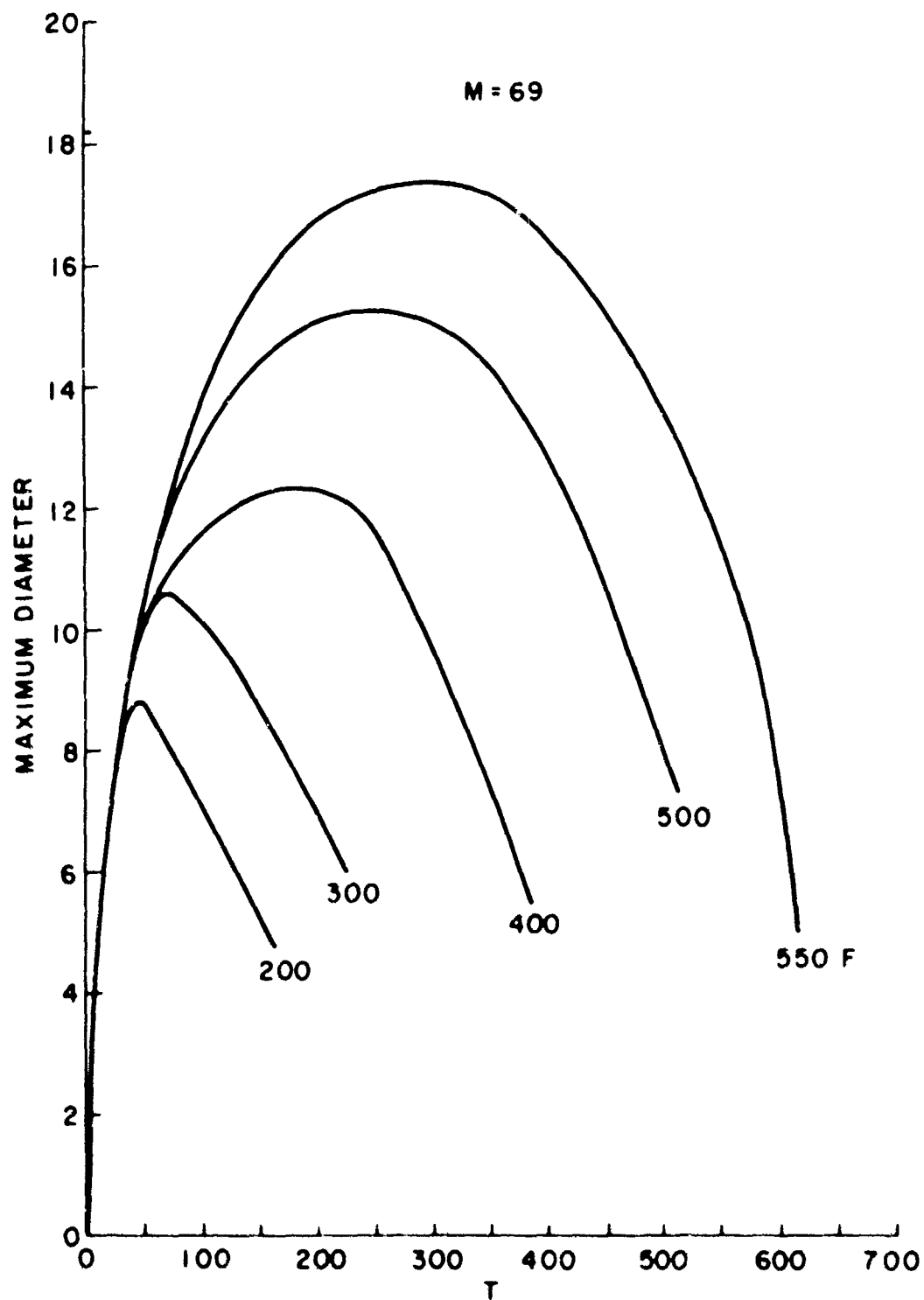


FIG. 22 VARIATION OF CAVITY DIAMETER AFTER ENTRY (M=69)

NOLTR 63-264

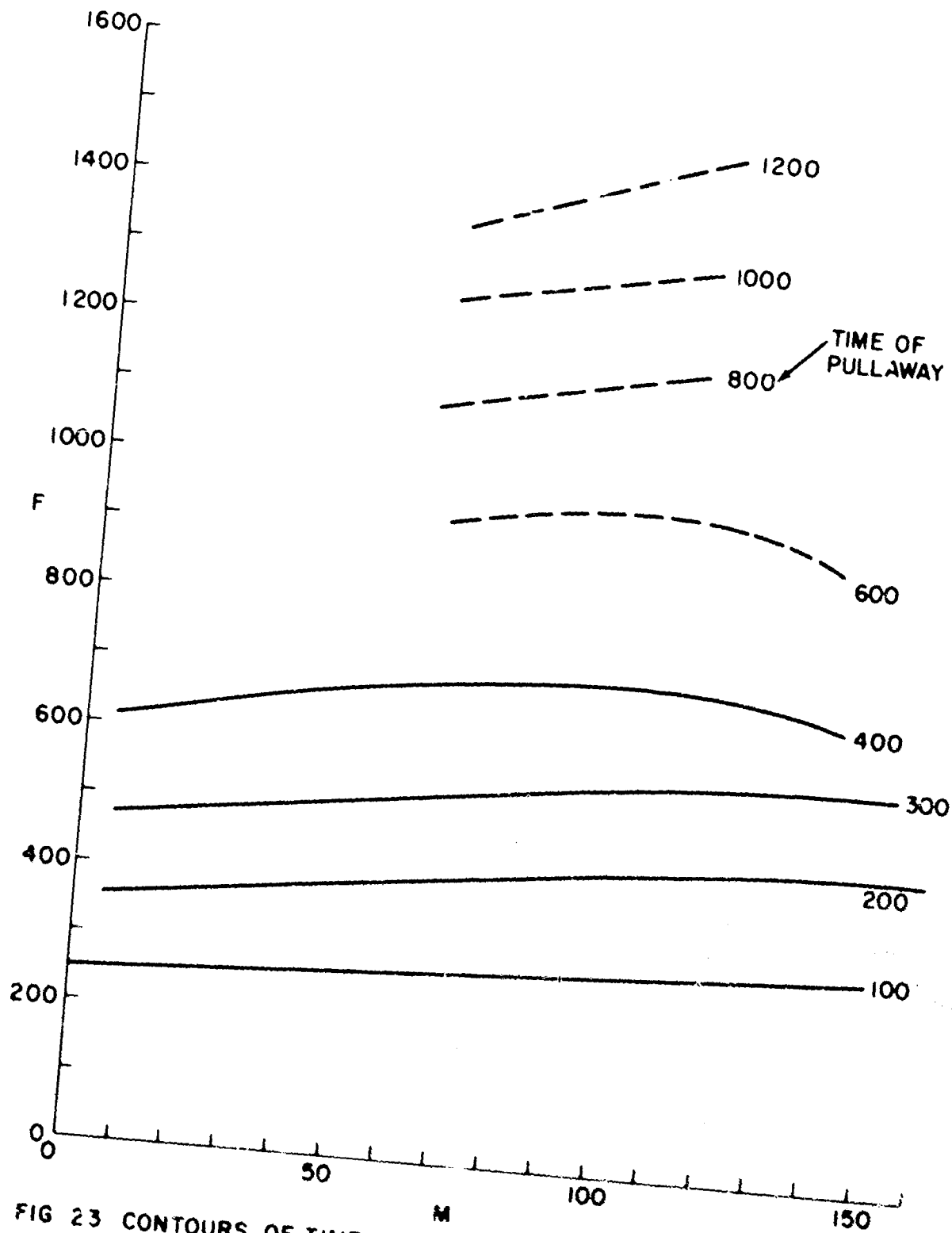


FIG 23 CONTOURS OF TIME OF PULLAWAY OF CAVITY FROM WATER SURFACE (TIMES ARE MEASURED FROM WATER IMPACT)

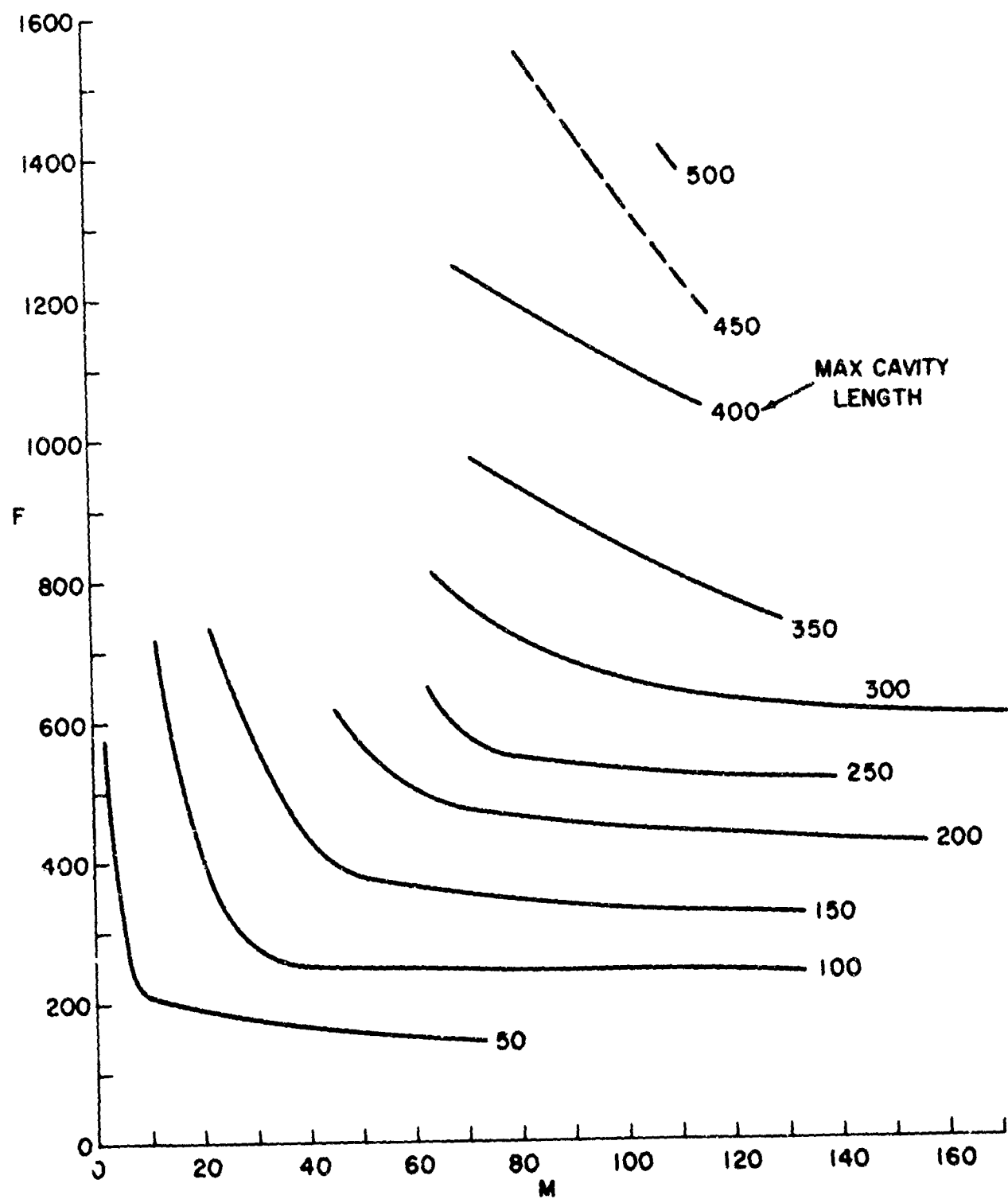


FIG. 24 CONTOURS OF MAXIMUM CAVITY LENGTH

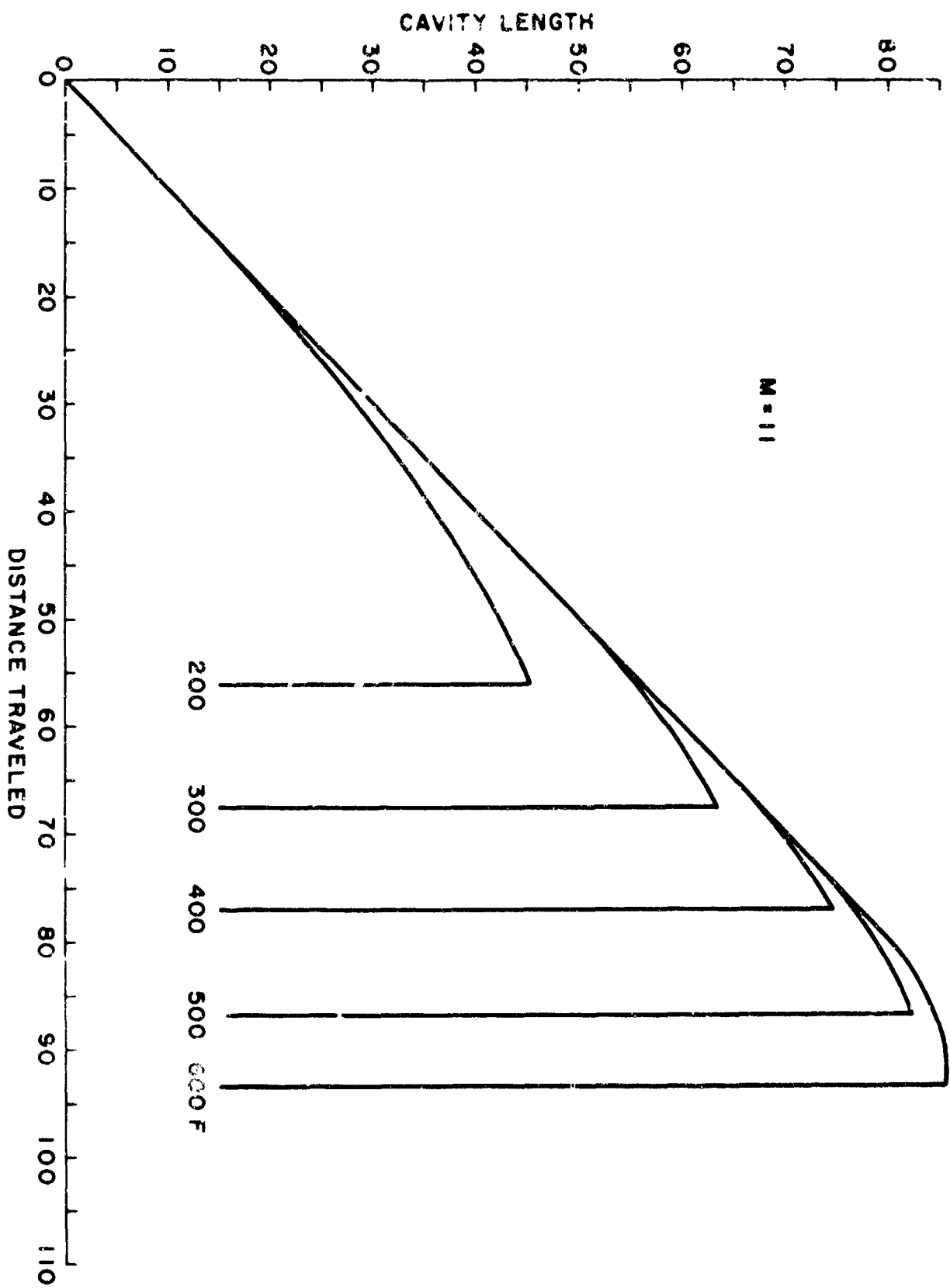


FIG. 25 VARIATION OF CAVITY LENGTH AFTER ENTRY ( $M=11$ )

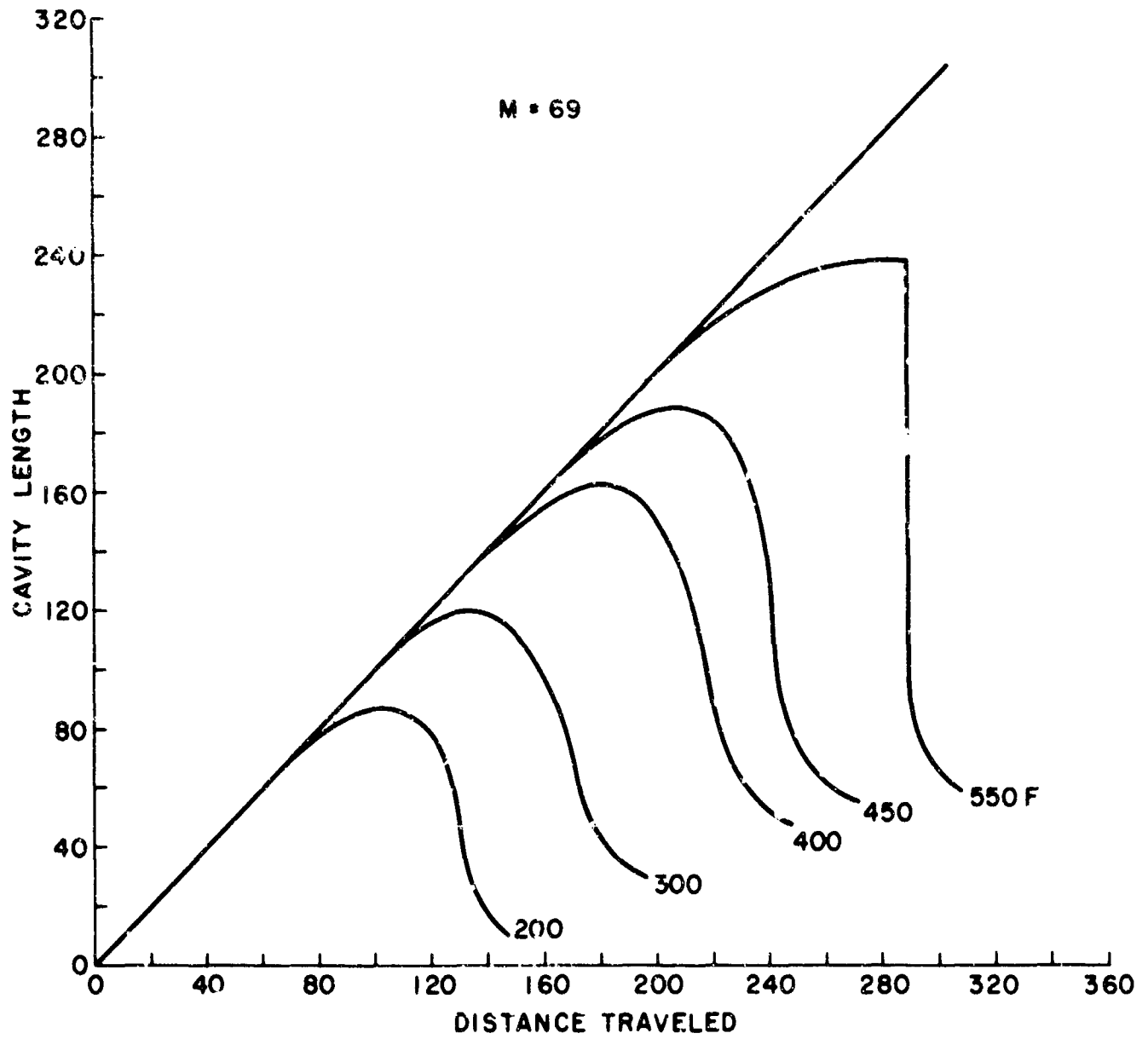


FIG. 26 VARIATION OF CAVITY LENGTH AFTER ENTRY ( $M = 69$ )

NOLTR 63-264

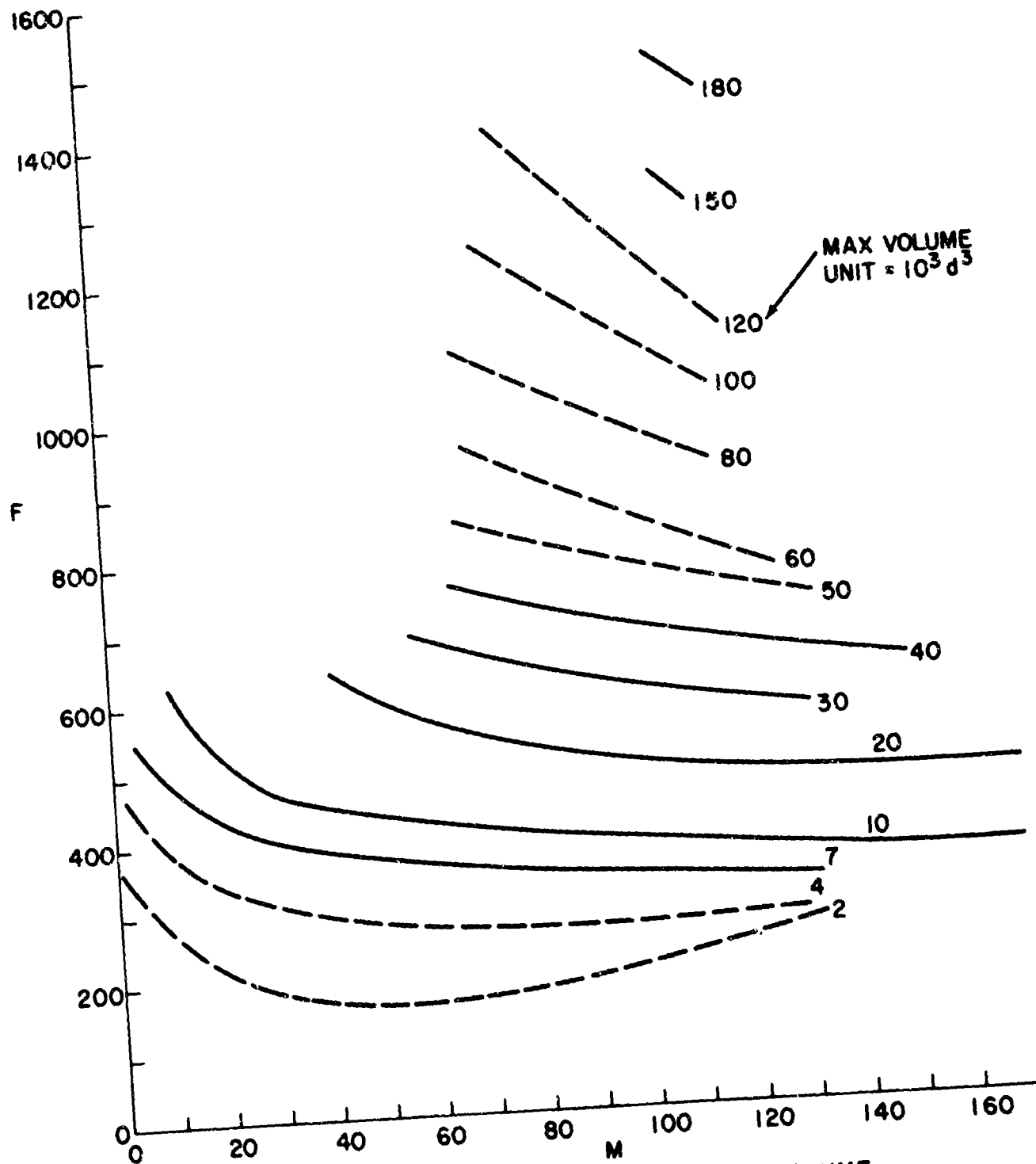


FIG. 27 CONTOURS OF MAXIMUM CAVITY VOLUME

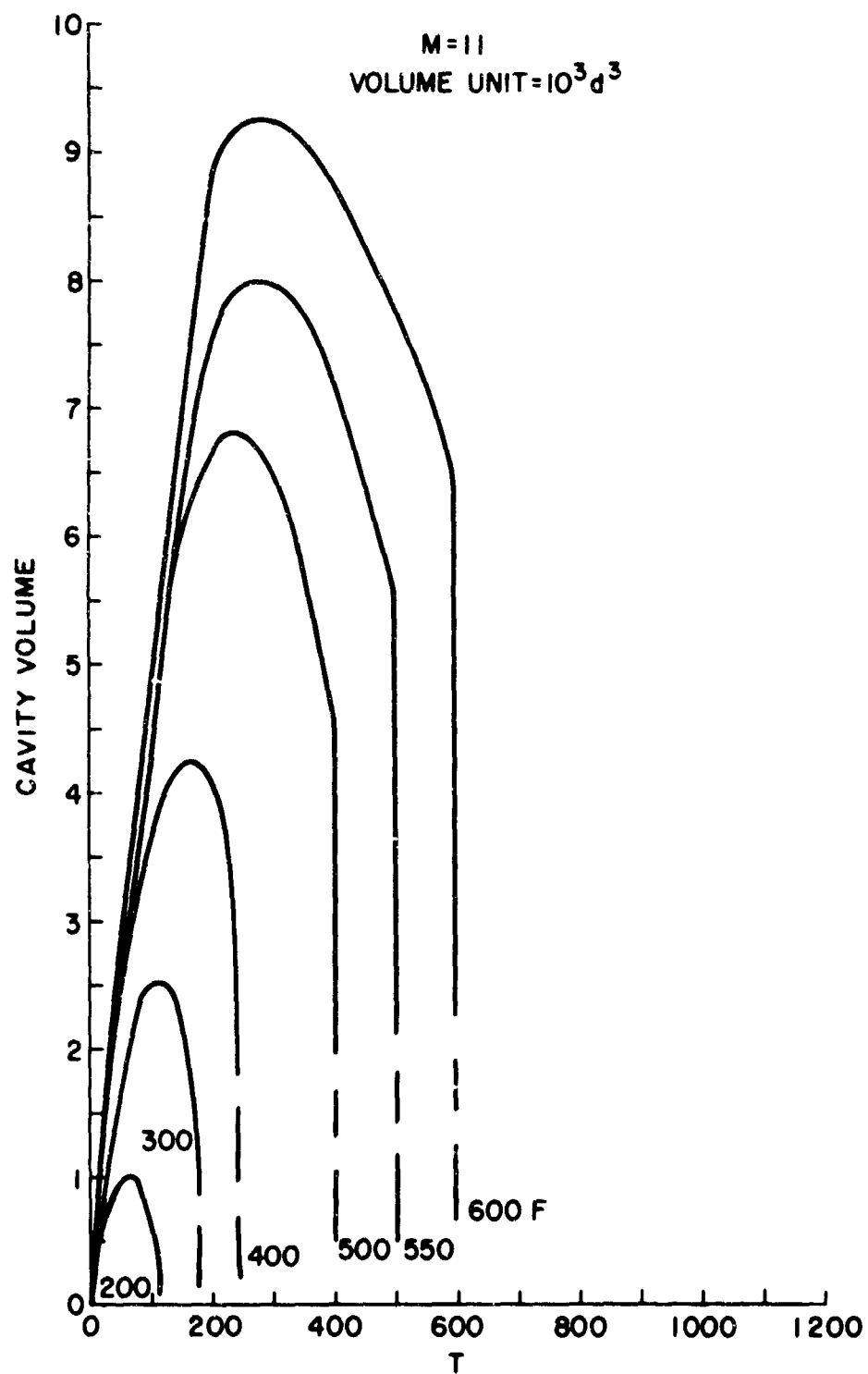


FIG. 28 VARIATION OF CAVITY VOLUME AFTER ENTRY ( $M=11$ )

NOLTR 63-264

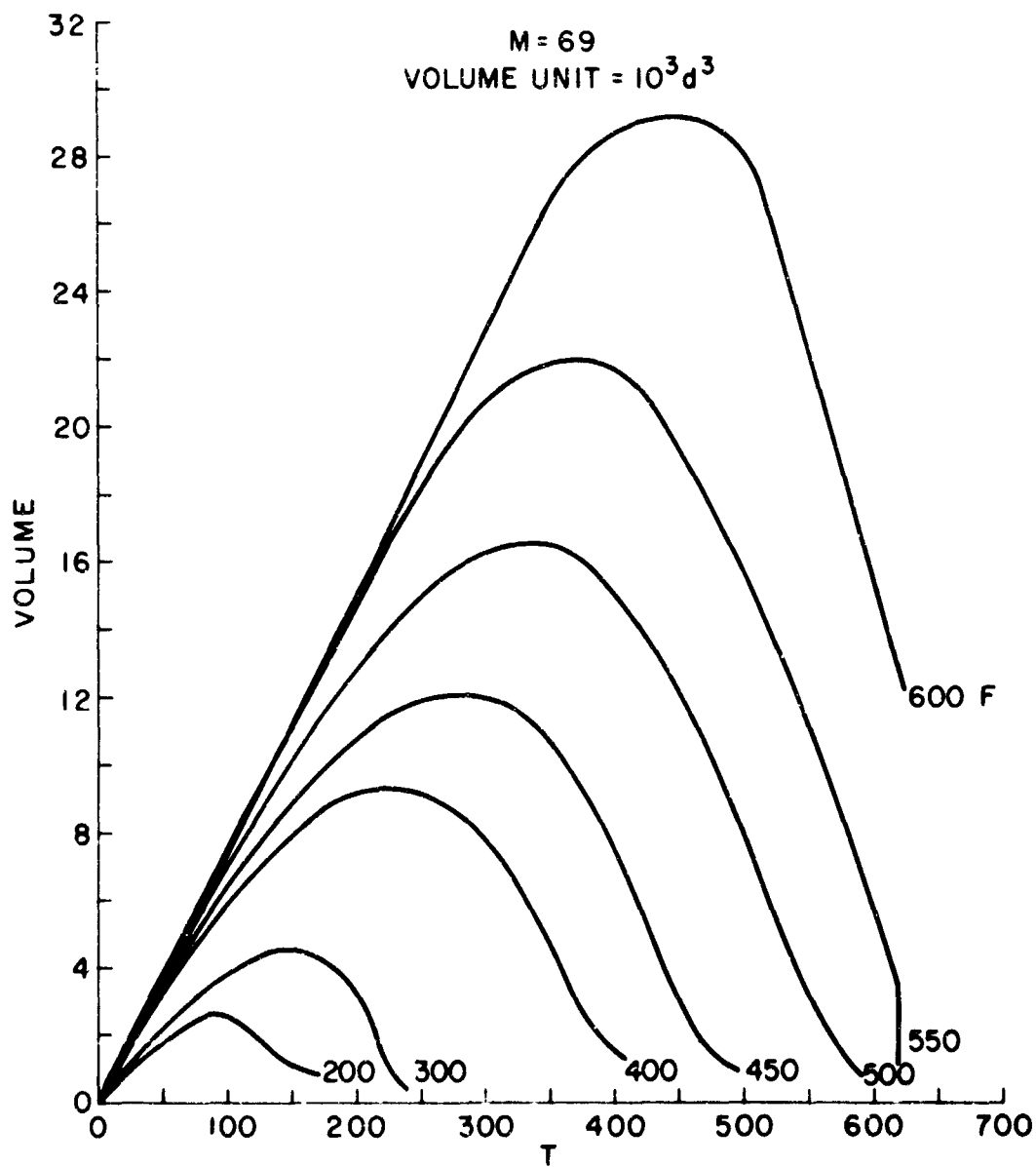


FIG. 29 VARIATION OF CAVITY VOLUME AFTER ENTRY (M = 69)

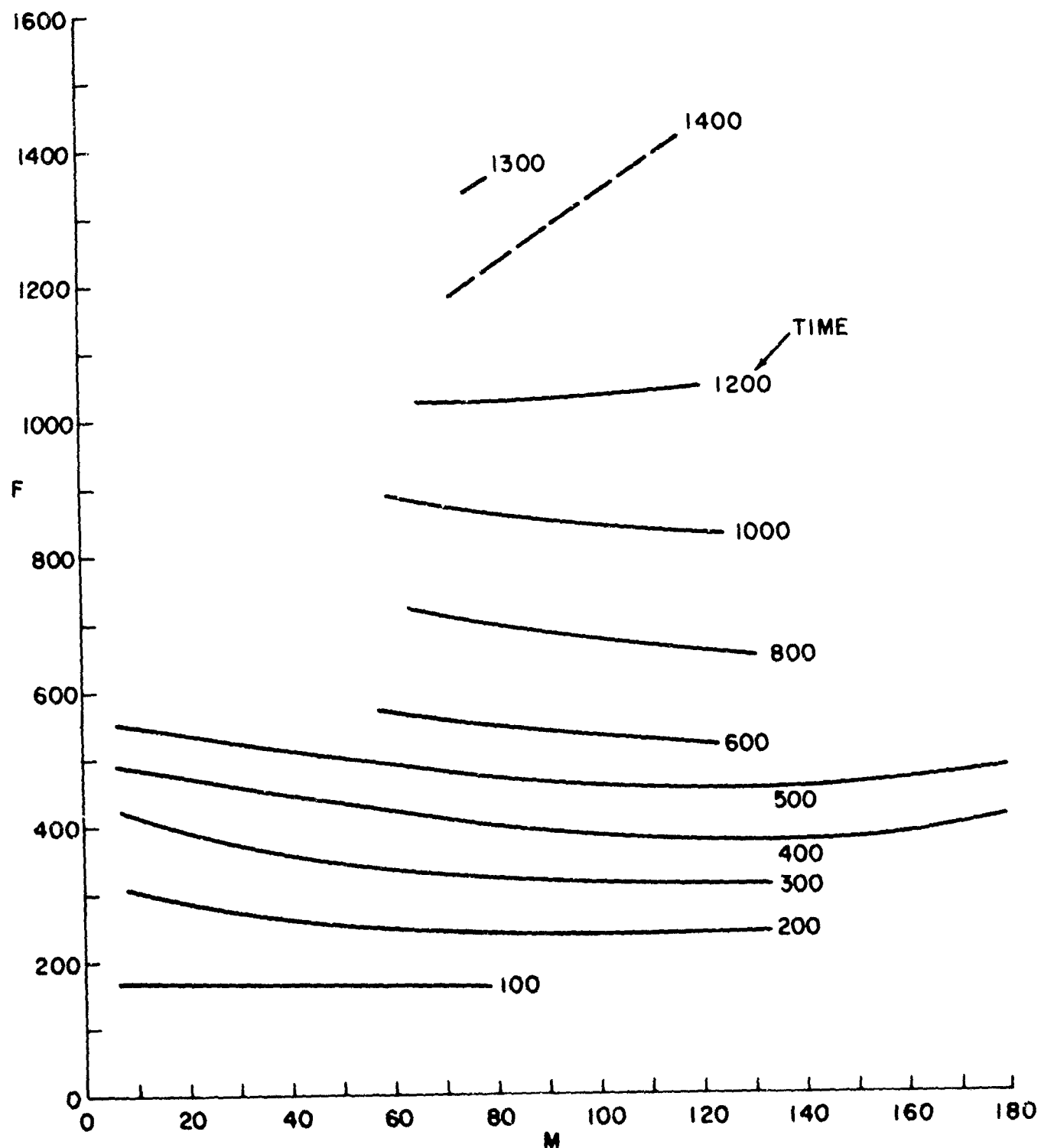


FIG. 30 CONTOURS OF TIME AFTER ENTRY WHEN CAVITY LENGTH IS HALF THE DISTANCE TRAVELED

NOLTR 63-264

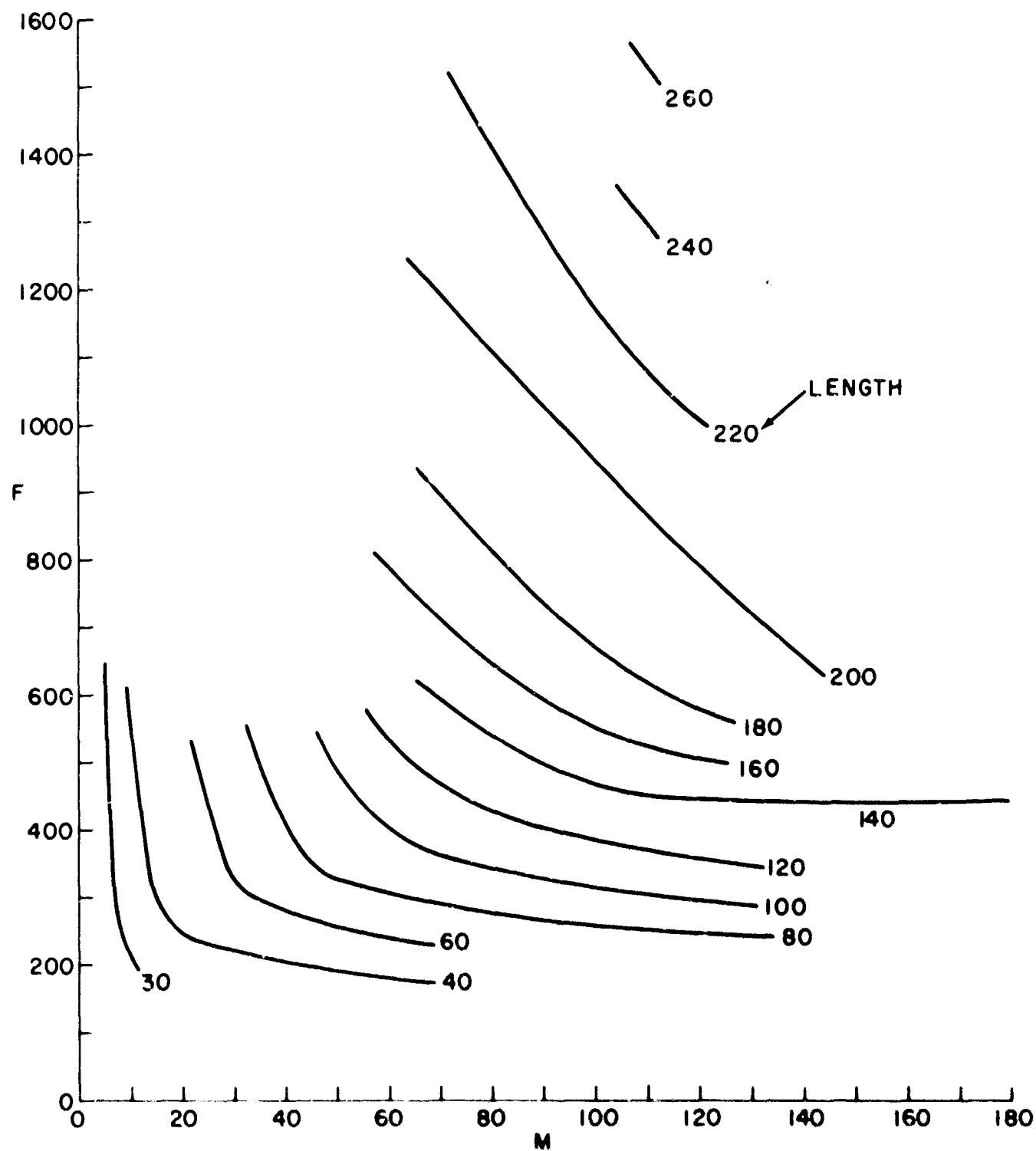


FIG 31 CONTOURS OF CAVITY LENGTH WHICH IS HALF THE DISTANCE TRAVELED

ROUND  
# 208  
M = 6.4  
F = 549

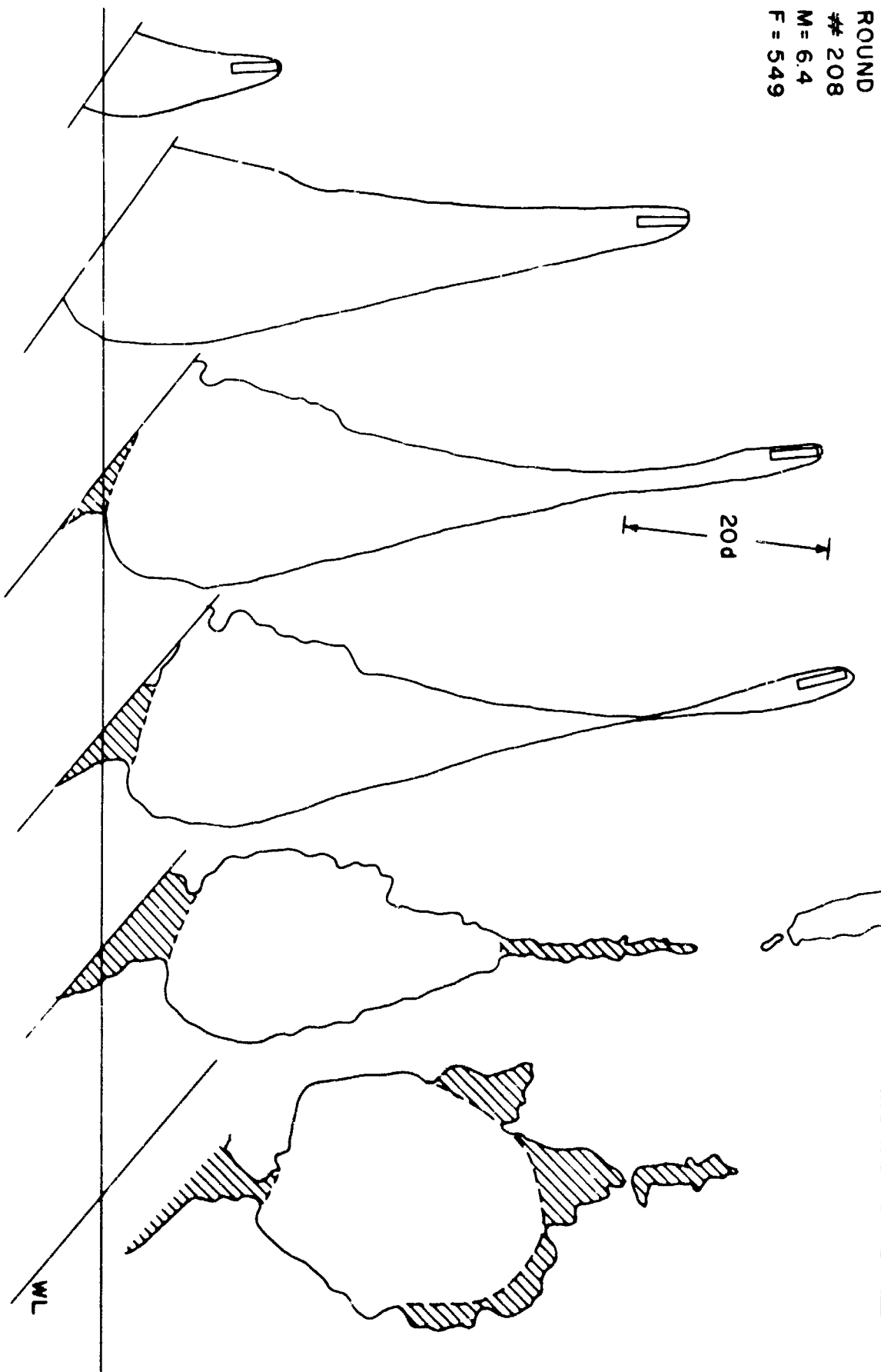


FIG 32 SKETCHES FROM ROUND 208

NOLTR 63-264

ROUND  
# 158  
M = 11.0  
F = 365

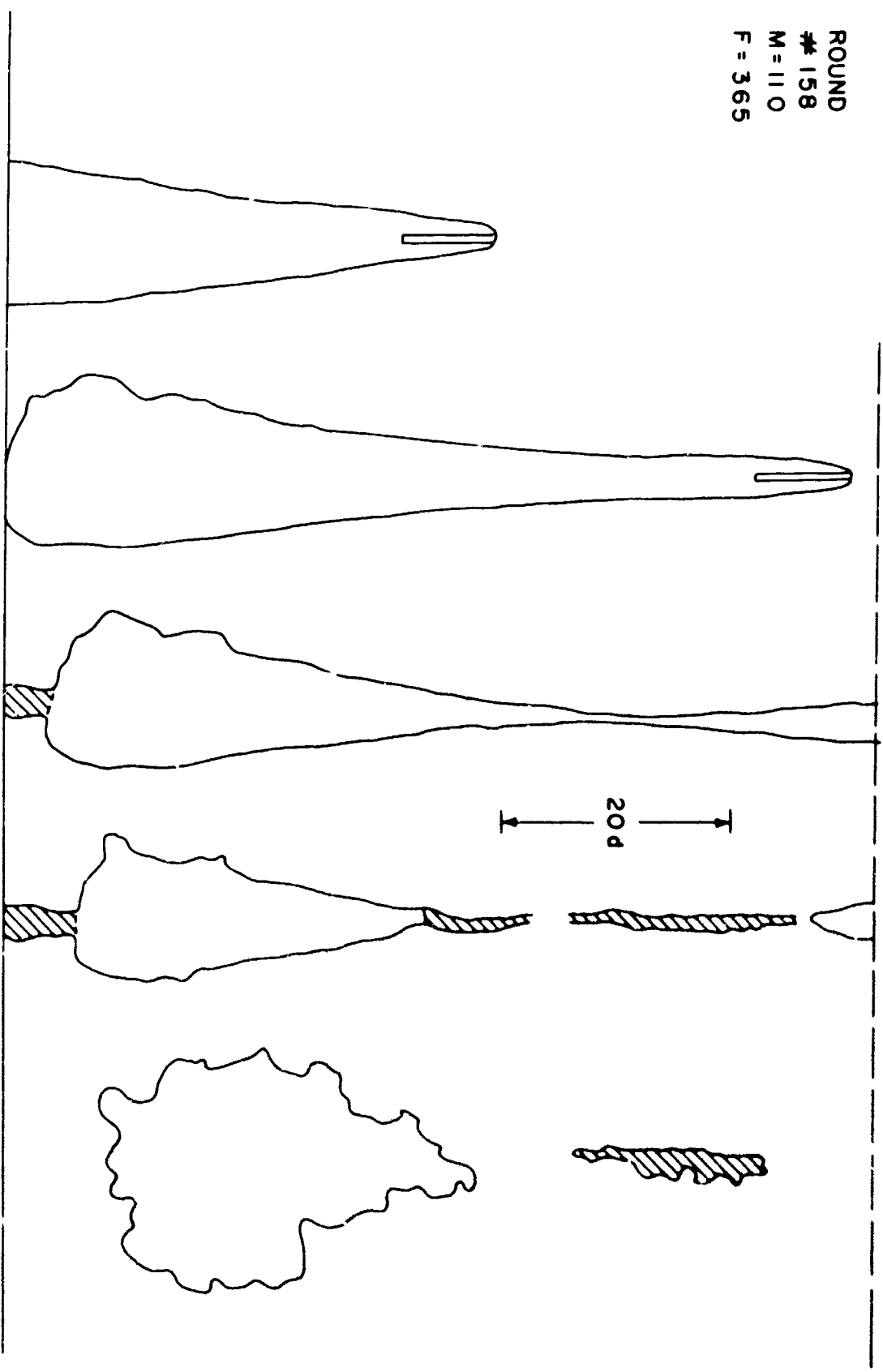


FIG. 33 SKETCHES FROM ROUND 158

ROUND  
# 156  
M = 11.0  
F = 216

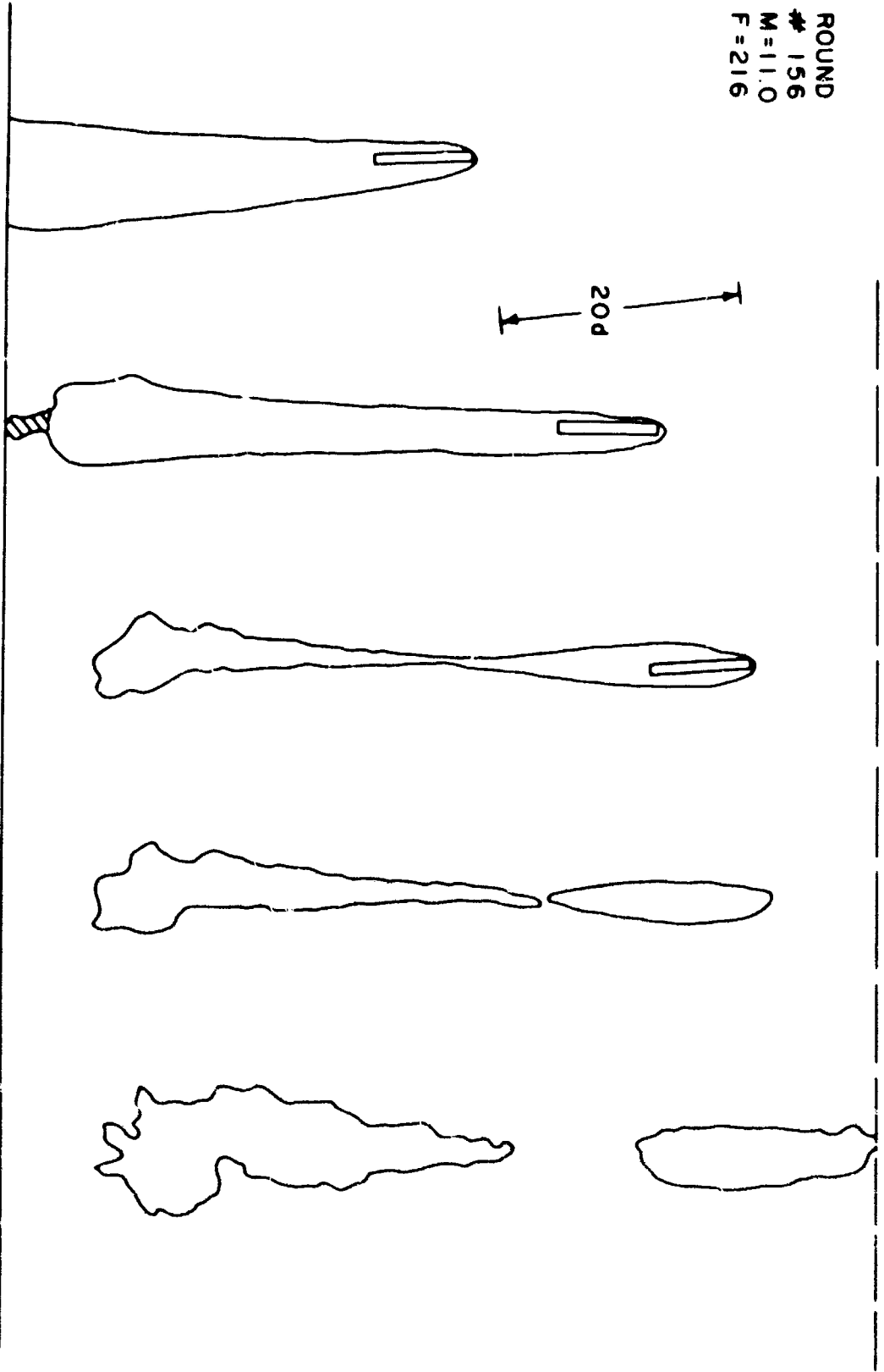


FIG 34 SKETCHES FROM ROUND 156

ROUND  
# 148  
M=95  
F=672

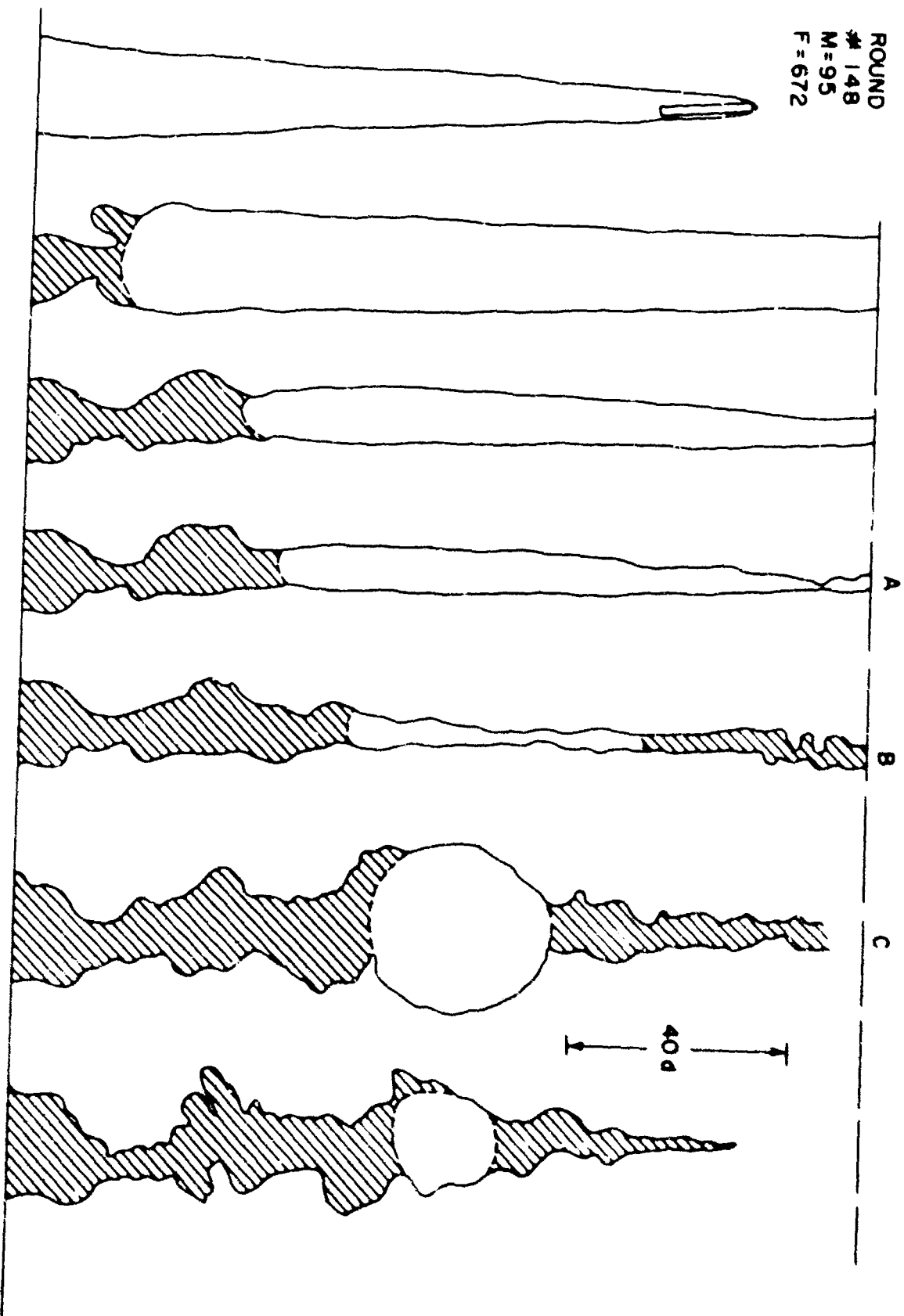


FIG 35 SKETCHES FROM ROUND 148

ROUND  
# 9.  
M = 95.0  
F = 591

40 d

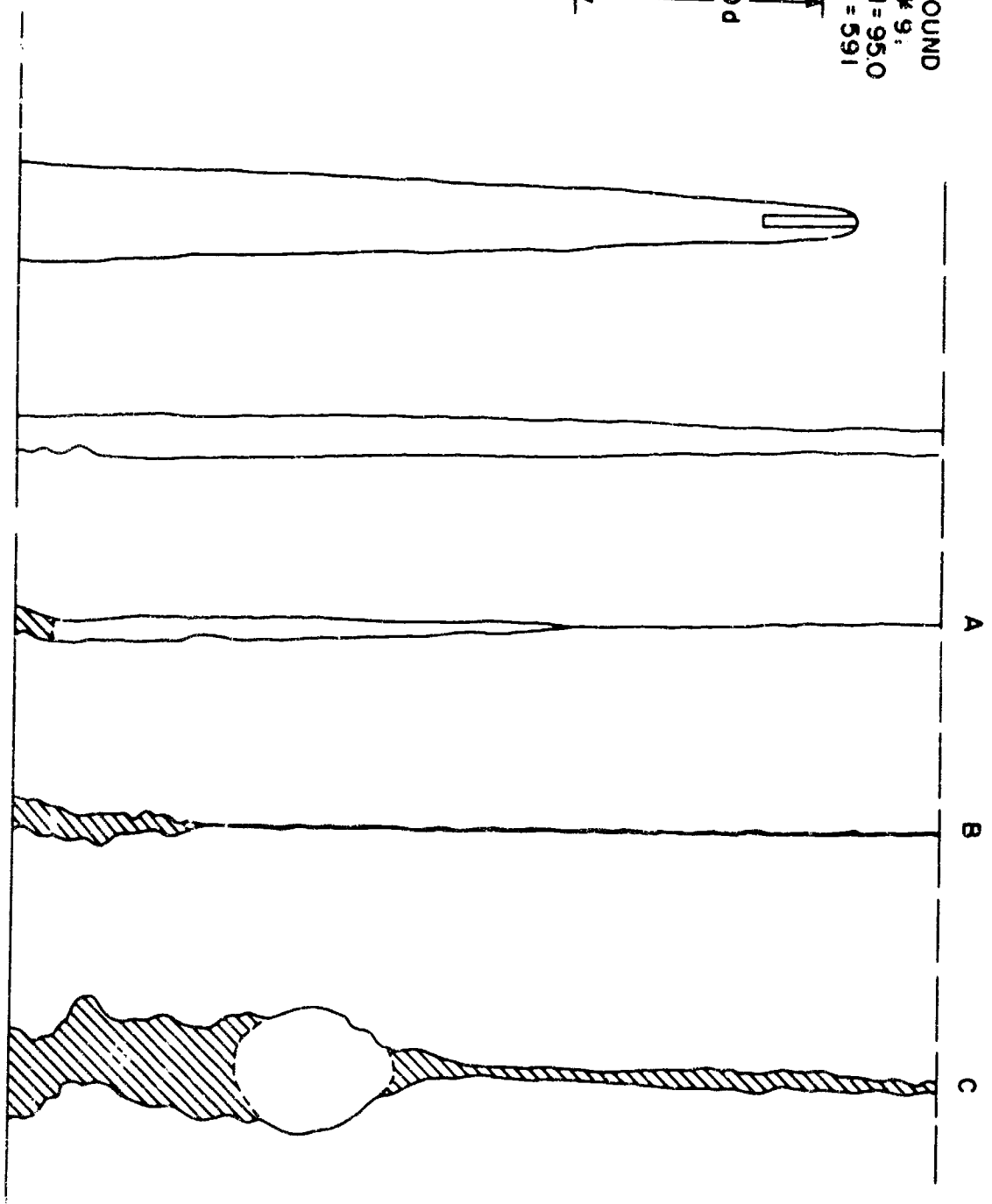
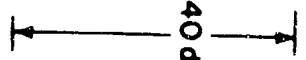


FIG 36 SKETCHES FROM ROUND 91

ROUND  
# 193  
M = 68.7  
F = 54.7

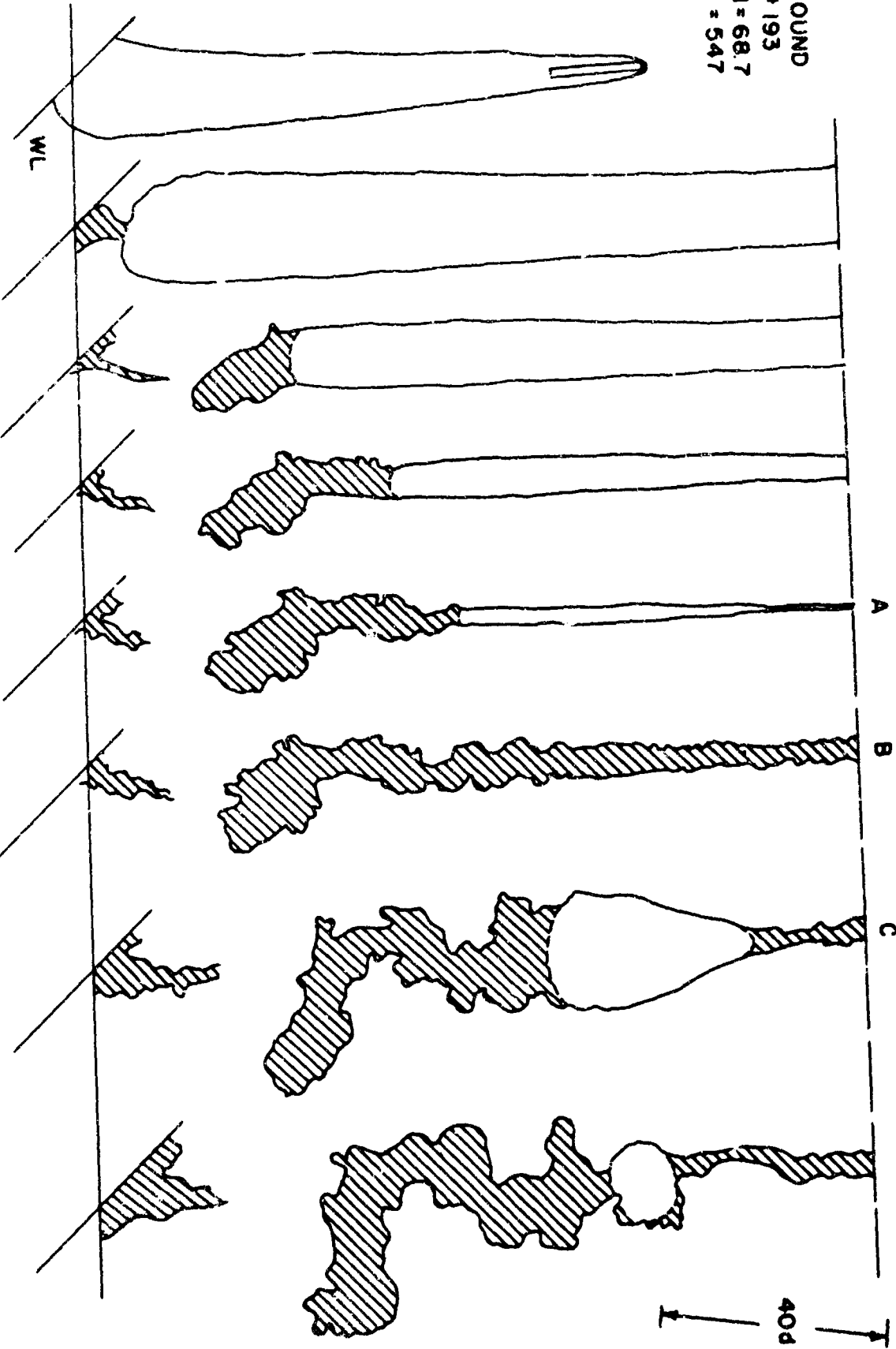


FIG. 37 SKETCHES FROM ROUND 193

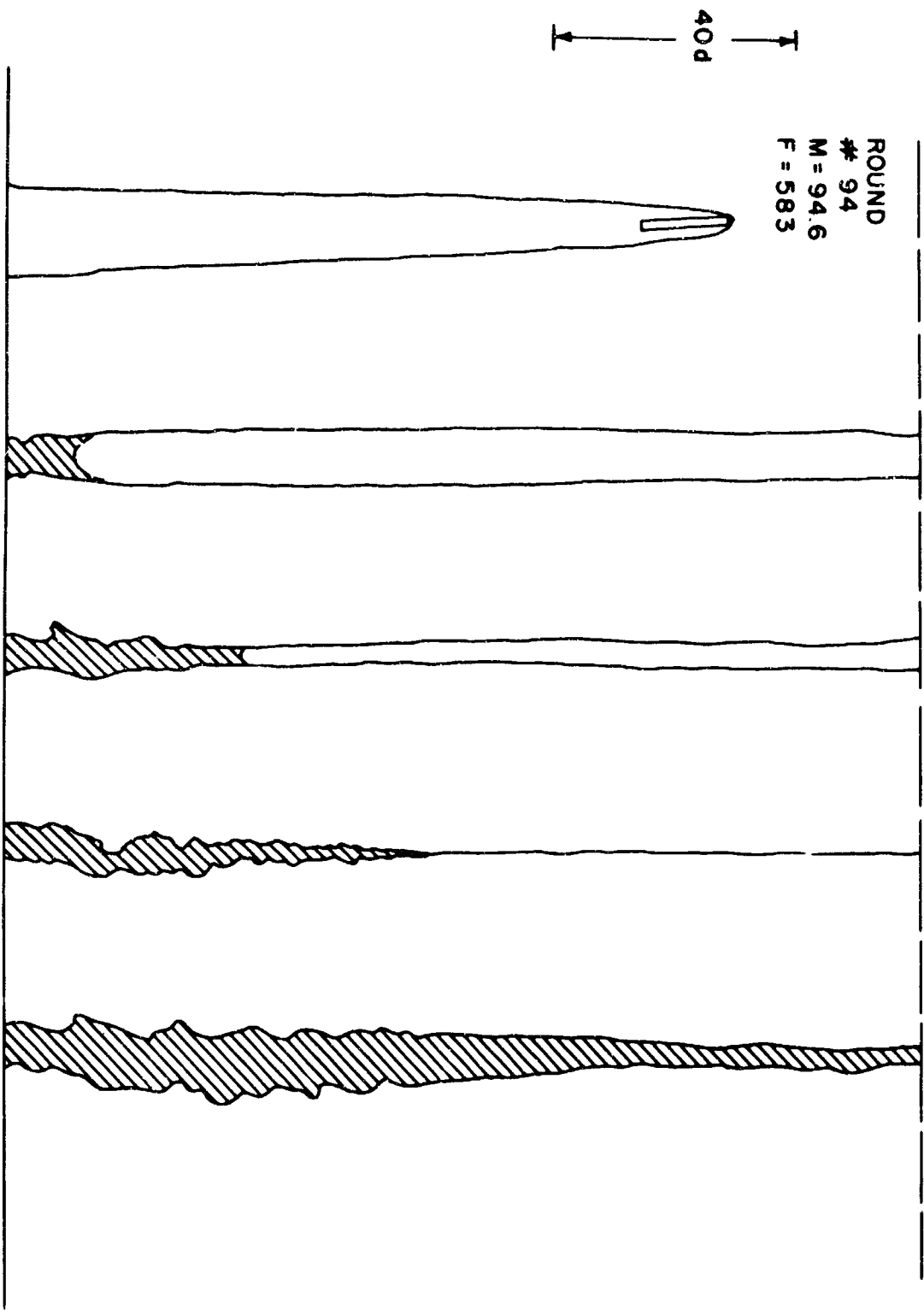
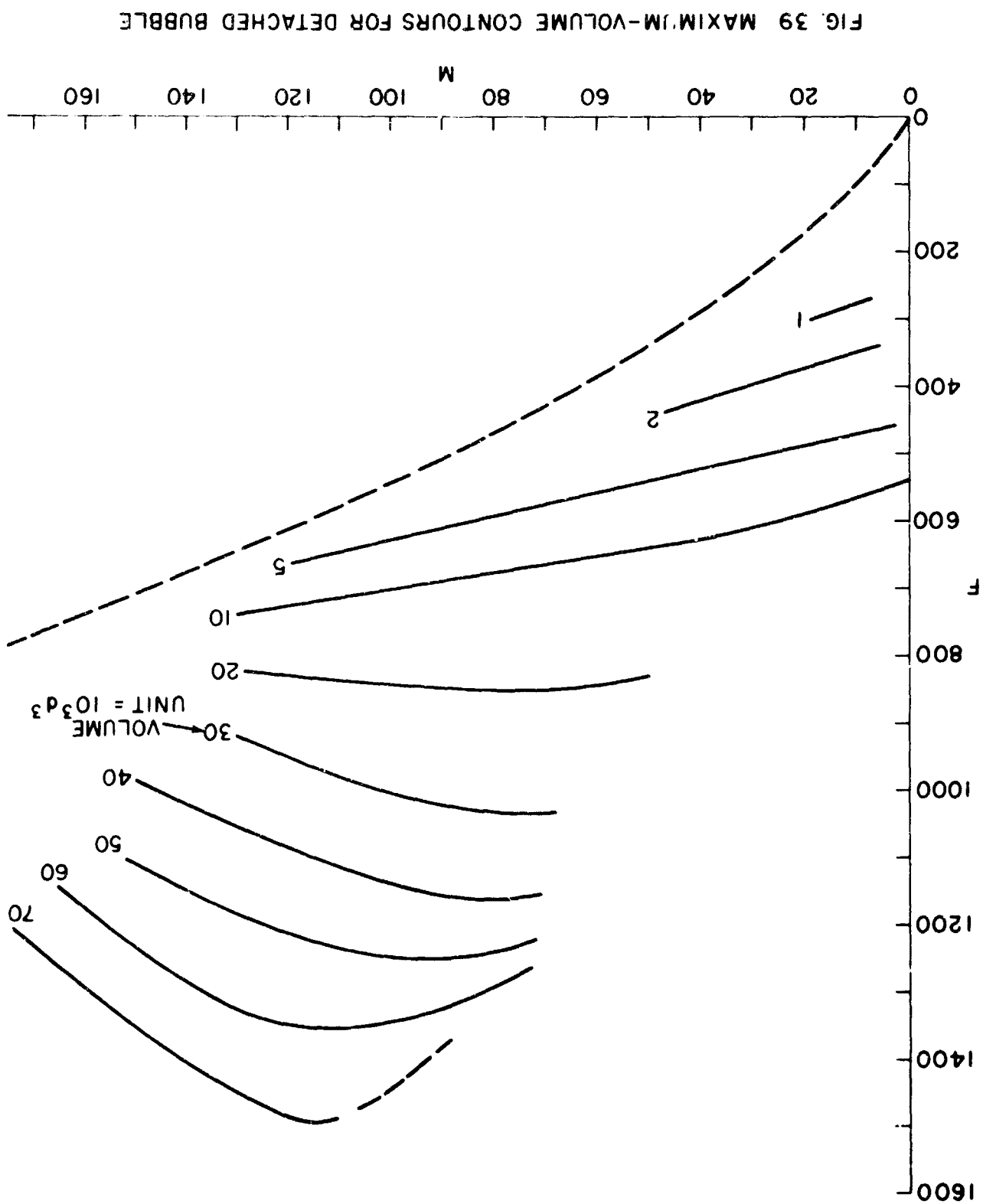


FIG. 38 SKETCHES FROM ROUND 94



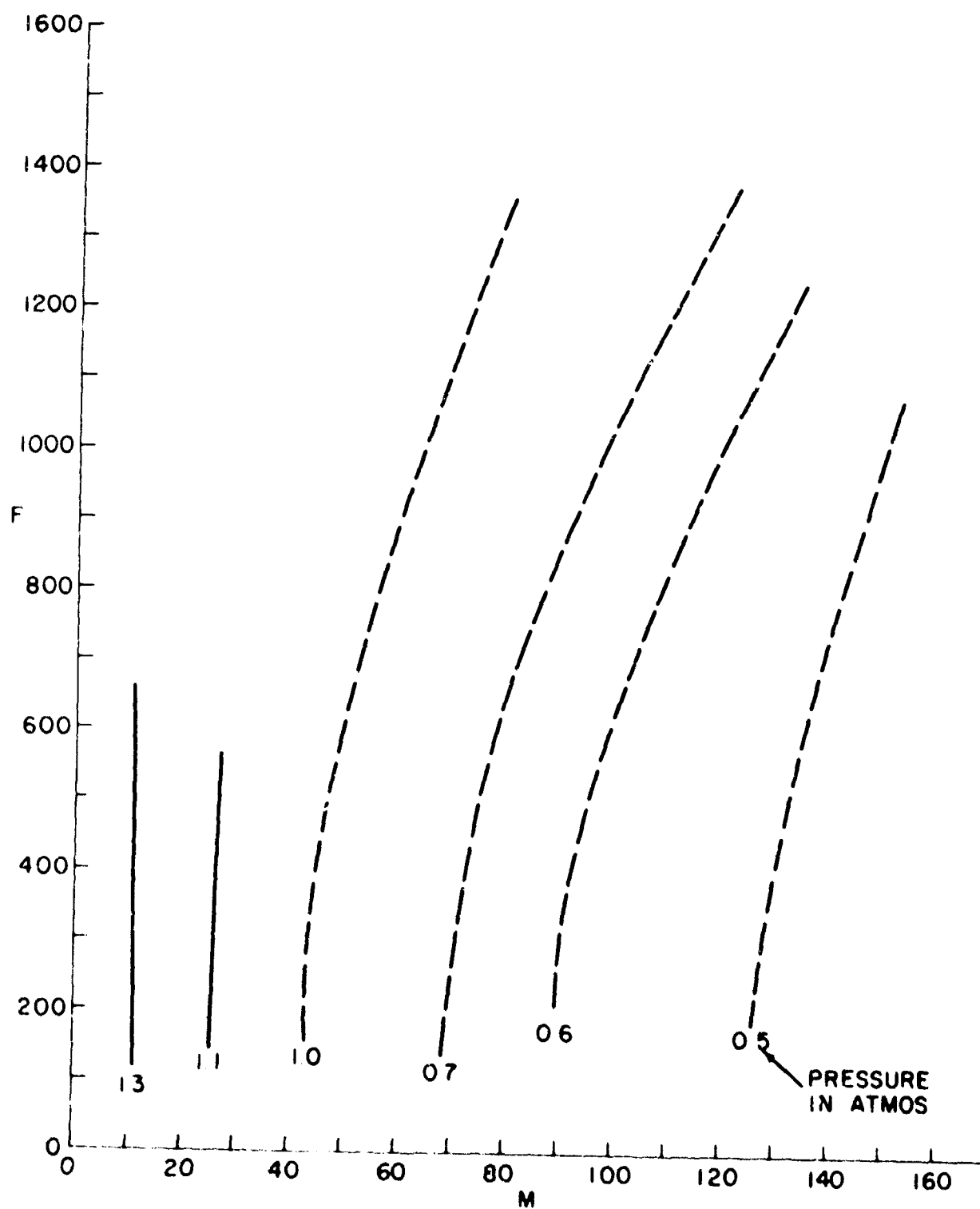


FIG 40 PRESSURE CONTOURS FOR "ALMOST STEADY" CAVITIES

NOLTR 63-264

DISTRIBUTION

	Copies
Chief, Bureau of Naval Weapons Department of the Navy Washington, D. C. 20360 Attn: Library, DLI-3	4
RRRE-4	1
RUTO	1
RUTO-32	1
RMMO	1
Defense Documentation Center Cameron Station Alexandria, Virginia	20
Chief, Bureau of Ships Department of the Navy Washington, D. C. 20360 Attn: Library	1
Chief, Office of Naval Research Department of the Navy Washington, D. C. 20360 Attn: Dr. W. L. Haberman	1
Fluid Dynamics Branch	1
David W. Taylor Model Basin Washington, D. C. 20490 Attn: Mr. Paul Granville	1
Mr. G. J. Franz	1
Library	1
National Academy of Sciences National Research Council 2101 Constitution Avenue, N. W. Washington 25, D. C.	1
Director of Research National Aeronautics and Space Administration 1512 H Street, N. W. Washington, D. C.	1
Director National Aeronautics and Space Administration Goddard Space Flight Laboratory Greenbelt, Maryland Attn: Library	1

NOLTR 63-264

Copies

Director  
National Aeronautics and Space Administration  
Langley Field, Virginia  
Attn: Library

1

Director  
Ames Research Laboratory  
National Aeronautics and Space Administration  
Moffett Field, California  
Attn: Library

1

Director  
Lewis Research Center  
National Aeronautics and Space Administration  
2100 Brookpark Road  
Cleveland, Ohio  
Attn: Library

1

National Bureau of Standards  
Fluid Mechanics Section  
Washington, D. C.  
Attn: Dr. G. B. Schubauer

1

National Science Foundation  
Washington, D. C.  
Attn: Dr. J. H. McMillen

1

U. S. Naval Academy  
Annapolis, Maryland  
Attn: Library

1

U. S. Naval Air Development Center  
Johnsville, Pennsylvania  
Attn: Library

1

Commander  
U. S. Naval Ordnance Test Station  
3203 E. Foothill Boulevard  
Pasadena 8, California  
Attn: Messrs. Lang or Fabula (Code P5015)  
Mr. Waugh (Code P8074)  
Mr. Brooks (Code P8040)

1

1

1

Commander  
U. S. Naval Ordnance Test Station  
China Lake, California  
Attn: Mr. H. Kelly (Code 40606)

1

NOLTR 63-264

	Copies
Superintendent U. S. Naval Postgraduate School Monterey, California Attn: Library	1
U. S. Naval Research Laboratory Washington, D. C. 20390 Attn: Library	1
U. S. Naval Underwater Ordnance Station Newport, Rhode Island Attn: Mr. R. J. Grady	1
U. S. Naval Weapons Laboratory Dahlgren, Virginia Attn: Dr. A. V. Hershey	1
U. S. Navy Electronics Laboratory San Diego, California Attn: Library	1
Hydrographer U. S. Navy Hydrographic Office Washington, D. C.	1
U. S. Navy Underwater Sound Laboratory Fort Trumbull New London, Connecticut Attn: Library	1
University of California Berkeley 4, California Attn: Professor J. V. Wehausen	1
Director Scripps Institute of Oceanography University of California La Jolla, California Attn: Library	1
California Institute of Technology Pasadena, California Attn: Dr. A. T. Ellis, Hydrodynamics Laboratory Mr. T. Kiceniuk, Hydrodynamics Laboratory Professor M. S. Plesset, Division of Engineering Professor T. Y. Wu	1 1 1 1
Carnegie Institute of Technology Pittsburgh 12, Pennsylvania Attn: Department of Civil Engineering	1

NOLTR 63-264

	Copies
The Catholic University of America Washington, D. C. 20017 Attn: Dr. Chang, Mechanical Engineering Department	1
Department of Civil Engineering University of Colorado Boulder, Colorado	1
Colorado State University Fort Collins, Colorado Attn: Civil Engineering Hydraulics Laboratory	1
Georgia Institute of Technology Atlanta, Georgia Attn: Hydraulics Laboratory	1
Department of Theoretical and Applied Mechanics College of Engineering University of Illinois Urbana, Illinois Attn: Dr. J. M. Robertson	1
Iowa Institute of Hydraulic Research State University of Iowa Iowa City, Iowa Attn: Professor H. Rouse	1
The Johns Hopkins University Baltimore 18, Maryland Attn: Professor F. H. Clauser	1
Director Applied Physics Laboratory The Johns Hopkins University 8621 Georgia Avenue Silver Spring, Maryland Attn Library	1
University of Kansas Lawrence, Kansas Attn: Department of Engineering Mechanics	1
University of Maryland College Park, Maryland Mechanical Engineering Department Attn: Dr. C. L. Sayre	1
Hydrodynamics Laboratory Massachusetts Institute of Technology Cambridge 39, Massachusetts Attn: Professor A. T. Ippen	1

NOLTR 63-264

Copies

University of Michigan  
Ann Arbor, Michigan  
Attn: Professor V. L. Streeter

1

Director  
St. Anthony Falls Hydraulic Laboratory  
University of Minnesota  
Minneapolis 14, Minnesota  
Attn: Professor L. G. Straub

1

University of Nebraska  
Lincoln 8, Nebraska  
Attn: Hydraulics Laboratory

1

The Technological Institute  
Northwestern University  
Evanston, Illinois

1

Director  
Ordnance Research Laboratory  
Pennsylvania State University  
University Park, Pennsylvania  
Attn: Dr. G. F. Wislicenus

1

Director  
Southwest Research Institute  
Department of Mechanical Sciences  
San Antonio 6, Texas  
Attn: Library

1

Stanford University  
Stanford, California  
Attn: Department of Civil Engineering  
Professor E. Y. Hsu

1

1

Stevens Institute of Technology  
Davidson Laboratory  
Hoboken, New Jersey  
Attn: Mr. Anthony Suarez  
Mr. Albert Strumpf  
Mr. J. P. Breslin

1

1

1

Director  
Woods Hole Oceanographic Institute  
Woods Hole, Massachusetts  
Attn: Library

1

Director  
Alden Hydraulic Laboratory  
Worcester Polytechnic Institute  
Worcester 9, Massachusetts  
Attn: Professor L. J. Hooper  
Professor Lawrence C. Neale

1

1

**Copies**

Aerojet General Corporation 6352 Irwindale Avenue Azusa, California Attn: Mr. J. Levy	1
AIResearch Manufacturing Company 9851 Sepulveda Boulevard Los Angeles 45, California Attn: Mr. Blaine R. Parkin	1
Allegheny Ballistics Laboratory Hercules Powder Company Cumberland, Maryland Attn: Captain N. J. Kleiss	1
Hydrodynamics Laboratory Convair San Diego 12, California Attn: Mr. R. H. Oversmith Mr. R. M. Hopkins	1 1
Grumman Aircraft Corporation Bethpage, Long Island, New York Attn: Mr. Giuseppe Avallone	1
Hydronautics, Inc. Pindell School Road Howard County Laurel, Maryland Attn: Mr. P. Eisenberg Mr. M. P. Tulin	1 1
Lockheed Missiles and Space Company Sunnyvale, California Attn: Mr. R. W. Kermeen	1
Missile Development Division North American Aviation, Inc. Downey, California Attn: Library	1
Oceanics, Inc. Plainview, Long Island, New York Attn: Dr. Paul Kaplan	1
Technical Research Group, Inc. 2 Aerial Way Syosset, New York	1
Therm Advanced Research Division Therm, Inc. Ithaca, New York	1

NOLTR 63-264

Copies

Sandia Corporation  
Albuquerque, New Mexico  
Attn: W. V. Hereford, Division 7215

1

Aerospace Corporation  
P.O. Box 95085  
Los Angeles 45, California 90045  
Attn: Dr. J. S. Whittier

1

<p>Naval Ordnance Laboratory, White Oak, Md. (NOL technical report 63-264) A STUDY OF THE WATER-ENTRY CAVITY, by Albert May and William R. Hoover. 4 Dec. 1963. 26p. illus., tables. (Ballistics research report 121) BuWeps task RRRE-04-022-002.</p> <p style="text-align: center;">UNCLASSIFIED</p> <p>For missiles producing clean cavities after water entry the cavity development is shown by theory to depend significantly only on: entry angle; an effective mass; and a Froude number based on the nose-flat diameter. A method is outlined for estimating pressures in closed, almost-steady cavities, from cavity geometry.</p>	<ol style="list-style-type: none"> <li>1. Missiles - water entry</li> <li>2. Missiles, underwater - Cavitation</li> <li>I. Title</li> <li>II. May, Albert</li> <li>III. Hoover, William R., Jr. author</li> <li>IV. Series</li> <li>V. Project</li> </ol> <p>Abstract card is unclassified.</p>	<p>Naval Ordnance Laboratory, White Oak, Md. (NOL technical report 63-264) A STUDY OF THE WATER-ENTRY CAVITY, by Albert May and William R. Hoover. 4 Dec. 1963. 26p. illus., tables. (Ballistics research report 121) BuWeps task RRRE-04-022-002.</p> <p style="text-align: center;">UNCLASSIFIED</p> <p>For missiles producing clean cavities after water entry the cavity development is shown by theory to depend significantly only on: entry angle; an effective mass; and a Froude number based on the nose-flat diameter. A method is outlined for estimating pressures in closed, almost-steady cavities, from cavity geometry.</p>	<ol style="list-style-type: none"> <li>1. Missiles - water entry</li> <li>2. Missiles, underwater - Cavitation</li> <li>I. Title</li> <li>II. May, Albert</li> <li>III. Hoover, William R., Jr. author</li> <li>IV. Series</li> <li>V. Project</li> </ol> <p>Abstract card is unclassified.</p>
<p>Naval Ordnance Laboratory, White Oak, Md. (NOL technical report 63-264) A STUDY OF THE WATER-ENTRY CAVITY, by Albert May and William R. Hoover. 4 Dec. 1963. 26p. illus., tables. (Ballistics research report 121) BuWeps task RRRE-04-022-002.</p> <p style="text-align: center;">UNCLASSIFIED</p> <p>For missiles producing clean cavities after water entry the cavity development is shown by theory to depend significantly only on: entry angle; an effective mass; and a Froude number based on the nose-flat diameter. A method is outlined for estimating pressures in closed, almost-steady cavities, from cavity geometry.</p>	<ol style="list-style-type: none"> <li>1. Missiles - water entry</li> <li>2. Missiles, underwater - Cavitation</li> <li>I. Title</li> <li>II. May, Albert</li> <li>III. Hoover, William R., Jr. author</li> <li>IV. Series</li> <li>V. Project</li> </ol> <p>Abstract card is unclassified.</p>	<p>Naval Ordnance Laboratory, White Oak, Md. (NOL technical report 63-264) A STUDY OF THE WATER-ENTRY CAVITY, by Albert May and William R. Hoover. 4 Dec. 1963. 26p. illus., tables. (Ballistics research report 121) BuWeps task RRRE-04-022-002.</p> <p style="text-align: center;">UNCLASSIFIED</p> <p>For missiles producing clean cavities after water entry the cavity development is shown by theory to depend significantly only on: entry angle; an effective mass; and a Froude number based on the nose-flat diameter. A method is outlined for estimating pressures in closed, almost-steady cavities, from cavity geometry.</p>	<ol style="list-style-type: none"> <li>1. Missiles - water entry</li> <li>2. Missiles, underwater - Cavitation</li> <li>I. Title</li> <li>II. May, Albert</li> <li>III. Hoover, William R., Jr. author</li> <li>IV. Series</li> <li>V. Project</li> </ol> <p>Abstract card is unclassified.</p>

UNCLASSIFIED

Security Classification

DOCUMENT CONTROL DATA - R&D		
(Security Classification of title, body of abstract and indexing annotation must be entered when the overall report is classified)		
1. ORIGINATING ACTIVITY (Corporate author) U. S. Naval Ordnance Laboratory White Oak, Silver Spring, Maryland		2a. REPORT SECURITY CLASSIFICATION UNCLASSIFIED
		2b. GROUP N/A
3. REPORT TITLE A STUDY OF THE WATER-ENTRY CAVITY		
4. DESCRIPTIVE NOTES (Type of report and inclusive dates) N/A		
5. AUTHOR(S) (Last name, first name, initial) May, Albert and Hoover, William R.		
6. REPORT DATE 4 December 1963	7a. TOTAL NO. OF PAGES 73 pages	7b. NO. OF REFS 9
8a. CONTRACT OR GRANT NO.	9a. ORIGINATOR'S REPORT NUMBER(S) NOLTR 63-264	
b. PROJECT NO. WEPTASK RRRE 04-022-002		
c.	9b. OTHER REPORT NO(S) (Any other numbers that may be assigned this report)	
d.	Ballistics research report 121	
10. AVAILABILITY/LIMITATION NOTICES Released to DDC without restriction.		
11. SUPPLEMENTARY NOTES N/A	12. SPONSORING MILITARY ACTIVITY Bureau of Naval Weapons	
13. ABSTRACT For missiles producing clean cavities after water entry the cavity development is shown by theory to depend significantly on: entry angle, an effective mass, and a Froude number based on the nose-flat diameter. A method is outlined for estimating pressures in closed, almost-steady cavities, from cavity geometry.  Data from application of these methods to water-entry records of models are given. Influence of effective mass was small. The pressures in steady cavities were estimated as 0.5 to 1.3 atmospheres.		

UNCLASSIFIED  
Security Classification

14. KEY WORDS	LINK A		LINK B		LINK C	
	ROLE	WT	ROLE	WT	ROLE	WT
WATER-ENTRY CAVITY SCALING OBLIQUE ENTRY MODEL ANALYSIS						

**INSTRUCTIONS**

1. **ORIGINATING ACTIVITY:** Enter the name and address of the contractor, subcontractor, grantee, Department of Defense activity or other organization (*corporate author*) issuing the report.

2a. **REPORT SECURITY CLASSIFICATION:** Enter the overall security classification of the report. Indicate whether "Restricted Data" is included. Marking is to be in accordance with appropriate security regulations.

2b. **GROUP:** Automatic downgrading is specified in DoD Directive 5200.10 and Armed Forces Industrial Manual. Enter the group number. Also, when applicable, show that optional markings have been used for Group 3 and Group 4 as authorized.

3. **REPORT TITLE:** Enter the complete report title in all capital letters. Titles in all cases should be unclassified. If a meaningful title cannot be selected without classification, show title classification in all capitals in parenthesis immediately following the title.

4. **DESCRIPTIVE NOTES:** If appropriate, enter the type of report, e.g., interim, progress, summary, annual, or final. Give the inclusive dates when a specific reporting period is covered.

5. **AUTHOR(S):** Enter the name(s) of author(s) as shown on or in the report. Enter last name, first name, middle initial. If military, show rank and branch of service. The name of the principal author is an absolute minimum requirement.

6. **REPORT DATE:** Enter the date of the report as day, month, year, or month, year. If more than one date appears on the report, use date of publication.

7a. **TOTAL NUMBER OF PAGES:** The total page count should follow normal pagination procedures, i.e., enter the number of pages containing information.

7b. **NUMBER OF REFERENCES:** Enter the total number of references cited in the report.

8a. **CONTRACT OR GRANT NUMBER:** If appropriate, enter the applicable number of the contract or grant under which the report was written.

8b, & 8c, & 8d. **PROJECT NUMBER:** Enter the appropriate military department identification, such as project number, subproject number, system numbers, task number, etc.

9a. **ORIGINATOR'S REPORT NUMBER(S):** Enter the official report number by which the document will be identified and controlled by the originating activity. This number must be unique to this report.

9b. **OTHER REPORT NUMBER(S):** If the report has been assigned any other report numbers (either by the originator or by the sponsor), also enter this number(s).

10. **AVAILABILITY/LIMITATION NOTICES:** Enter any limitations on further dissemination of the report, other than those imposed by security classification, using standard statements such as:

- (1) "Qualified requesters may obtain copies of this report from DDC."
- (2) "Foreign announcement and dissemination of this report by DDC is not authorized."
- (3) "U. S. Government agencies may obtain copies of this report directly from DDC. Other qualified DDC users shall request through \_\_\_\_\_."
- (4) "U. S. military agencies may obtain copies of this report directly from DDC. Other qualified users shall request through \_\_\_\_\_."
- (5) "All distribution of this report is controlled. Qualified DDC users shall request through \_\_\_\_\_."

If the report has been furnished to the Office of Technical Services, Department of Commerce, for sale to the public, indicate this fact and enter the price, if known.

11. **SUPPLEMENTARY NOTES:** Use for additional explanatory notes.

12. **SPONSORING MILITARY ACTIVITY:** Enter the name of the departmental project office or laboratory sponsoring (paying for) the research and development. Include address.

13. **ABSTRACT:** Enter an abstract giving a brief and factual summary of the document indicative of the report, even though it may also appear elsewhere in the body of the technical report. If additional space is required, a continuation sheet shall be attached.

It is highly desirable that the abstract of classified reports be unclassified. Each paragraph of the abstract shall end with an indication of the military security classification of the information in the paragraph, represented as (TS), (S), (C), or (U).

There is no limitation on the length of the abstract. However, the suggested length is from 150 to 225 words.

14. **KEY WORDS:** Key words are technically meaningful terms or short phrases that characterize a report and may be used as index entries for cataloging the report. Key words must be selected so that no security classification is required. Identifiers, such as equipment model designation, trade name, military project code name, geographic location, may be used as key words but will be followed by an indication of technical context. The assignment of links, roles, and weights is optional.

UNCLASSIFIED

Security Classification